DTIC FILE COPY

AFOSR-TR· 90 0728

②

Three-Dimensional Structure Of Boundary Layers In Transition to Turbulence

Thorwald Herbert
Department of Mechanical Engineering
& Department of Aeronautical and Astronautical Engineering

DTIC
S ELECTE D
JUN 2 6 1990
D

U.S. Air Force
Air Force Office of Scientific Research
Bolling Air Force Base, D.C. 20332

Approved for public release;
distribution unlimited.

DISTRIBUTION STATEMENT A
Approved for public release;
Distribution Unlimited

March 1990

90 06 25 194

6c. ADDRESS (City, State, and ZIP Code)	7b. ADDRESS (City, State, and ZIP Code)
Department of Mechanical Engineering Ohio State University Columbus, OH 43212-1194	BUILDING 410 BOLLING AFB, DC 20332-6448

8a. NAME OF FUNDING / SPONSORING ORGANIZATION AFOSR/NA	8b. OFFICE SYMBOL (If applicable) AFOSR/NA	9. PROCUREMENT INSTRUMENT IDENTIFICATION NUMBER AFOSR 88-0186

8c. ADDRESS (City, State, and ZIP Code)	10. SOURCE OF FUNDING NUMBERS			
BUILDING 410 BOLLING AFB, DC 20332-6448	PROGRAM ELEMENT NO. 61102F	PROJECT NO 2307	TASK NO A1	WORK UNIT ACCESSION NO.

11. TITLE (Include Security Classification)

(U) Three-Dimensional Structure of Boundary Layers in Transition to Turbulence

12. PERSONAL AUTHOR(S)
Thorwald Herbert

13a. TYPE OF REPORT Final	13b. TIME COVERED FROM APR 88 TO MAR 89	14. DATE OF REPORT (Year, Month, Day) MAR 1989	15. PAGE COUNT 160

16. SUPPLEMENTARY NOTATION

17.	COSATI CODES		18. SUBJECT TERMS (Continue on reverse if necessary and identify by block number)
FIELD	GROUP	SUB-GROUP	> Transition, Boundary Layers, Stability

19. ABSTRACT (Continue on reverse if necessary and identify by block number)

A spectral code for linear stability analysis has been developed that allows easy adaptation to a large variety of basic flows and stability equations. This code is the basis for extensions to analyze secondary and nonlinear stability in parallel and nonparallel flows. Improved numerical techniques have been developed to reduce the computational demand of secondary instability studies. A new approach to convective instability analysis in nonparallel flows on the basis of parabolized stability equations has been developed for incompressible and compressible flows. Encouraging results have been obtained in the areas of linear, nonlinear, and secondary instability. The code appears as a viable alternative to DNS codes that allows transition simulations at a small fraction of the computational cost.

20. DISTRIBUTION / AVAILABILITY OF ABSTRACT ☐ UNCLASSIFIED/UNLIMITED ☒ SAME AS RPT. ☐ DTIC USERS	21. ABSTRACT SECURITY CLASSIFICATION UNCLASSIFIED
22a. NAME OF RESPONSIBLE INDIVIDUAL JAMES M MCMICHAEL	22b. TELEPHONE (Include Area Code) 202-767-4936 22c. OFFICE SYMBOL AFOSR/NA

Three-Dimensional Structure Of Boundary Layers In Transition to Turbulence

Thorwald Herbert
Department of Mechanical Engineering
& Department of Aeronautical and Astronautical Engineering

March 1990

TABLE OF CONTENTS

Summary

Our research program aims at developing and applying theoretical, numerical, and graphical tools for the quantitative description and deeper understanding of the transition phenomena and at relating transition phenomena to the processes in the viscous sublayer of turbulent flow. Toward these goals, a spectral code for linear stability analysis has been developed that allows easy adaptation to a large variety of basic flows and stability equations. This code is the basis for extensions to analyze secondary and nonlinear stability in parallel and nonparallel flows. Improved numerical techniques have been developed to reduce the computational demand of secondary instability studies. A new approach to convective instability analysis in nonparallel flows on the basis of parabolized stability equations (PSE) has been developed for incompressible and compressible flows. Encouraging results have been obtained in the areas of linear, nonlinear, and secondary instability. The PSE code appears as a viable alternative to DNS codes that allows transition simulations at a small fraction of the computational cost.

1. Objectives

Our research program aims at developing and applying theoretical, numerical, and graphical tools for the quantitative description and deeper understanding of the transition phenomena and at relating transition phenomena to the processes in the viscous sublayer of turbulent flow. In detail, the program aims at the following topics ·

(1) The effect of nonparallelism and TS amplitude growth on secondary instability.

(2) Secondary instability of longitudinal vortices in parallel and nonparallel flows.

(3) Secondary instability of oblique waves in boundary layers.

(4) Perturbation analysis of nonlinear interactions between competing modes of secondary instability. Interaction between 2D and 3D fields in the breakdown stage.

(5) Analysis of numerical transition simulations and three-dimensional threshold states.

The first-year effort focused on items (1) - (3), (4a, 2D-3D interaction), and (5b, threshold states).

2. Achievements

The variety of basic stability problems related to our studies spawned major efforts to develop stability codes on a common basis of program modules. These efforts were supported by the regrettable loss of a considerable part of my software and data (via unreadable tapes) when I had to return the workstations previously used (and on loan to OSU) to VPI & SU.

A second major effort was to attract students and to prepare them for this research program - an effort that was not fully successful. Instead of the planned simultaneous attack on a variety of problems, we have concentrated on the most promising areas and achieved progress in particular with a new approach to boundary layer transition based on parabolized equations. A more detailed report is given in the following

2.1. The Stability Code "Linear.x"

We have developed a stability code named "linear.x" that is sufficiently generic to allow analysis of incompressible and compressible stability problems. The code is highly modular such that different numerical methods can be implemented. The standard version uses single-domain spectral methods to solve the boundary-value problem directly. This choice, though not most efficient in terms of computer time, permits obtaining spectra of eigenvalues or single eigenvalues and eigenfunctions. Optionally, the program produces tables of eigenvalues and curves (e.g. neutral curves) in one coordinate plane of a three-dimensional parameter space.

Various built-in transformations account for shifted and/or stretched, semi-infinite, and infinite domains. Normally, the boundary conditions are satisfied in the end points of the physical domain, without artificial domain truncation. For single eigenmodes in semi-infinite domains, the asymptotic properties can be incorporated with this approach. In infinite domains, incorporation of asymptotic properties requires the use of two-domain or

multi-domain methods that have been implemented in a new version of the code. Account for the asymptotic properties is convenient or even indispensable when dealing with modes that slowly decay such as TS waves or Görtler vortices of small wavenumber. The use of multi-domain spectral methods in general increases the resolution for critical layers away from the boundaries such as the neighborhood of the generalized inflection point at high Mach numbers. As an alternative to the spectral approach, the compact finite-difference scheme of Malik (1988) has been implemented in a separate version of the code.

The code is void of any particular physical stability problem. The stability problem is condensed into four insert files that are included at compile time and can be prepared without any change to the stability code. The first of these insert files defines array sizes and contains the number of collocation points and the characteristics of the stability equations, such as the number of variables, constants, and parameters and the order of differentiation. The second file contains declarations of complex variables. The third file provides the basic flow for the stability analysis by direct calculation or reading from existing files. The last file defines the coefficients of the system of stability equations and their derivatives with respect to the parameters. This file can be produced by manual derivation of the equations or by using symbolic manipulators (Macsyma, Mathematica).

The operation of the batch version of the stability code is controlled by two files the first of which defines boundary conditions, domain transformations for the spectral method, and constants. The second input file controls the tasks to be performed and provides the relevant parameter values. An interactive version of the code has been developed and is under continuous development as the primary tool for our research. The interactive version is menu driven and provides output in form of text and color graphics. This more efficient research code to analyze spectra and the properties of eigenfunctions, and to monitor the results of traverses in the parameter space graphically was necessary to better grasp the content of the output and to shorten the multi-level procedure of obtaining plots locally, while the computations are performed on the Cray.

The interactive version of "linear.x" is the basis for other codes that implement the perturbation analysis of nonlinear modes and mode interactions, Floquet analysis of secondary instability, and the local stability properties in nonparallel flows.

The batch version of the stability code has been documented and an introduction to its use will appear in the proceedings of the NASA/ICASE Workshop on Stability and Transition. A preprint of this paper is contained in Appendix A.

The insert files for the stability code have been produced and tested for the most common stability problems in incompressible flows. Available basic flows are boundary layers (flat plate, curved wall, Falkner-Skan, rotating disk, Falkner-Skan-Cook), plane and circular Couette and Poiseuille flows, and mixing layer. Compressible basic flows available in consistent format are similarity solutions for boundary layers (plane and axisymmetric), the viscous normal shock, and the compressible plane Couette flow.

The code and selected insert files have been distributed to students, various colleagues, and participants in the NASA/ICASE Workshop on Stability and Transition. At

this Workshop, I was member of the panel on "Theory of Stability and Transition." The position paper submitted for the proceedings (Appendix B) reflects some of the work under this grant.

2.2. Perturbation Analysis of Nonlinear Secondary Instability

A perturbation analysis of the nonlinear interaction of three-dimensional secondary modes with the basic flow and two-dimensional primary TS waves has been performed together with J. D Crouch under AFOSR Contract F46920-87-K-0005. This work has been continued in cooperation with J. D. Crouch who is now Postdoctoral Fellow at NRL. Our efforts aimed at identifying types of interactions and threshold conditions for the breakdown of the laminar flow. The effect of higher-order terms has been analyzed and documented. The study has been extended to lower frequencies where no experimental data can be obtained nor computer simulations can be performed. Our results show that transition at the more realistic lower frequencies is quite different from the known processes at high frequency and low Reynolds number studied in all previous work.

Some of our findings on threshold conditions were reported at the IUTAM Symposium "Laminar-Turbulent Transition" in Toulouse. The paper submitted for publication in the proceedings is contained in Appendix C. A more detailed description of the perturbation method, results for subharmonic and fundamental routes to transition, and comparison with experiments has been submitted for publication in Journal of Fluid Mechanics (Appendix D).

2.3. Perturbation Analysis of Nonlinear and Nonparallel Stability

To prepare for the analysis of streamwise variations on the evolution of secondary instabilities, we have clarified the effect of such variations on the stability of TS waves in (similar) boundary layers with or without pressure gradients. Various misconceptions and incorrect results in the literature have been revealed and a correct and consistent set of new results generated. These results largely confirm those of Gaster (1974). One of the main achievements is the rationality of our approach in the sense of perturbations methods. While previous work could account for either nonparallelism or nonlinearity, we can account for both simultaneously. High-order Landau series for the nonlinear stability of primary modes and third-order series for secondary modes have been successfully applied. In the work on secondary instability, we have applied an innovative iterative method for solving the large algebraic eigenvalue problem which will be very valuable for studies on compressible flows. Although we consider completing and publishing the results, our main attention has been given to the more promising approach described in the next section.

2.4. Parabolized Stability Equations

We have developed a new approach to the analysis of incompressible and compressible boundary-layer instability. This approach started from the observation (Herbert & Bertolotti 1987) that the streamwise development of a 2D disturbance of given frequency

ω and complex wavenumber α is governed by a locally valid parabolic differential equation. This equation is obtained from the Navier-Stokes equations by application of the boundary-layer approximation to mean flow and the slowly varying amplitude function $\phi(x,y)$ of the disturbance. The rapid variation of the disturbance that would violate the boundary-layer approximation is extracted by an exponential factor, in stream-function formulation

$$\psi(x,y,t) = \phi(x,y)\exp[\int_{x_0}^{x} i\alpha(\xi)d\xi - i\omega t] ,$$

where ω is the frequency and α the complex wavenumber. For given $\alpha(x_0)$ and initial amplitude distribution $\phi(x_0,y)$, the parabolic equation can be solved by suitable marching procedures. At the next step, however, the local wavenumber must be known to continue the procedure. Using a proper norm on $\phi(x,y)$, the small change in wavenumber can be obtained from the amplitude functions at the old and new position. The cyclic marching step - wavenumber update can be repeated in quite large steps in Reynolds number and is more efficient than the traditional step-by-step Orr-Sommerfeld solution and integration. What is needed is an initial condition and initial wavenumber. These data can be obtained from a local analysis at an initial position. The local equations are derived from the parabolic equation by use of Taylor expansions in x with higher derivatives neglected under the boundary-layer approximation. The local procedure requires simultaneously solving for the wavenumber (eigenvalue), the amplitude function, and its streamwise derivative.

Both local and marching procedure are mathematically pleasant since only the well-established boundary-layer approximation is applied. The approach to mean flow and disturbances is consistent. The local procedure is rational in the sense of perturbation methods while previous procedures were not. The parabolized stability equations (PSE) are valid in the complete boundary-layer region and are more general than unsteady boundary-layer equations and Orr-Sommerfeld equation which are special cases. Therefore, the PSE will be a valuable tool for receptivity studies without any asymptotic matching. Similar or nonsimilar boundary layers can be analyzed in the same uniform marching scheme. Perhaps the greatest advantage of the PSE is the ease of retaining nonlinear terms. Previously, no method was known to incorporate both nonparallelism and nonlinearity. The PSE is superior to the PNS approach since the convective terms for the oscillatory solutions are retained. The solution should, in fact, agree with the DNS solution if a sufficient number of harmonics is carried along. Recent results of P. Spalart obtained with a 2D DNS code in fact verify the accuracy of the nonlinear PSE solutions (see Appendix E, fig. 11, 12). A detailed description of our method, results, and comparison with previous work will be submitted shortly to Journal of Fluid Mechanics. A draft of this paper is contained in Appendix E.

2.5. Secondary Instability and Transition Simulation

The analysis of the secondary instability in periodically modulated flows requires simultaneous solution of the homogeneous equations for various Fourier modes constituting the secondary disturbance (Herbert 1988). This process is computationally very demanding, especially in compressible flows. We have developed an iterative scheme to solve the large eigenvalue problem. The increased efficiency of this scheme permits more extended studies in the multi-dimensional parameter space. This scheme is currently available for incompressible and compressible flows under the parallel-flow approximation.

For a more accurate description of the growth rate of secondary modes, we have developed the PSE approach of the previous section to incorporate the streamwise variation of both the mean flow and the primary disturbance into wave interactions in incompressible flow. Given the initial data for both a 2D and a 3D primary wave, the evolution of the primary wave and the parametric excitation and evolution of the secondary mode can be studied without resort to modeling by Floquet theory. The secondary instability arises as in DNS solutions from the nonlinear interaction of 2D and 3D wave components. Since nonlinearity is accounted for, the integration of the PSE also exhibits the feedback of the secondary modes on the primary 2D wave. In our previous work, Floquet theory provided only the parametric effects of the primary wave on the 3D modes, while the feedback had to be incorporated by an intricate perturbation approach (Crouch 1988, Herbert & Crouch 1989). A comparison of the growth rates obtained from Floquet theory and PSE solution is given in figure 1. Figure 2 shows the evolution of amplitudes for the 2D wave, 3D wave, and mean-flow distortion. The numerical (marching) approach has been extended to track the development up to the amplitude levels of the spike stage. Consistent with (usually temporal) DNS results, the evolution can be described with a modest number of modes in streamwise and spanwise direction. At this time, the only DNS results for comparison with our (spatial) results are those of Fasel et al. (1990). While the detailed comparison is difficult because of differences in generating the initial conditions and the 'moving down-stream boundary' in the DNS, the agreement in the gross features is evident (see figure 3). The spatial results are also similar to temporal simulations of the standard cases. A detailed comparison with experiments and DNS results (a matter of tedious post-processing) is on the way. The PSE results also confirm the results of the perturbation analysis of the nonlinear stage of secondary instability of Crouch & Herbert (Appendices C and D).

The PSE can be applied for the analysis of both temporal or spatial evolution in parallel or weakly nonparallel flows. Whenever the transition process is governed by convective instabilities and the 'upstream' influence appears negligible, solving the nonlinear PSE is an attractive alternative to DNS. The capability of efficiently tracking the spatial evolution makes the PSE a hot prospect for transition prediction in boundary layers. The present PSE code serves primarily to demonstrate the basic capabilities of the approach disregarding any sophistication of the numerics. Yet we integrate from the initial condition to breakdown in less than three minutes (Cray YMP8/864) while Fasel et al. (1990) require hundreds of hours on comparable machines (the exact figure is unknown to me).

With improvements in the numerical treatment we envision further improvements by a factor of five to ten. Besides the high efficiency, the PSE approach overcomes two other shortcomings of the DNS relevant at the lower frequencies where transition occurs in practice. DNS at low frequency would require larger domains and higher resolution because of the increased Reynolds number, and the computational cost would be inhibitive. Moreover (as discussed by Spalart in Appendix E), the large amplitude ratios (e^9) of disturbances in the upstream and downstream parts of the domain would increase the stiffness of the system and cause unsurmountable numerical problems. Runs of the PSE code (with modest increase in resolution) at low frequency are currently performed.

The local and marching procedures associated with the PSE concept have been ported to the compressible boundary layer. Computations have been performed up to $M = 4.5$, while reliable results have been obtained for $M \leq 3$. In the limit of $M \to 0$, we find perfect agreement with incompressible results. It is interesting to find that the strong nonparallel effects on oblique waves persist at lower Mach numbers (see figure 5) and, in fact, in the incompressible limit. This result escaped the attention of previous studies and indicates that Squire's theorem cannot be applied in nonparallel boundary layers.

3. Ongoing Work

The present capabilities to analyze nonlinear wave interactions with the PSE approach and the obvious prospects of further developing this approach have discouraged some of our efforts to apply perturbation methods, e.g. to study the nonlinear interactions between competing modes of secondary instability. We have performed theoretical studies on the secondary instability of oblique waves in boundary layers and developed the governing equations. However, we encountered a conceptual difficulty, a major discrepancy between the case of a single oblique wave and the case of a pair of oblique waves with opposite wave angles. The first case has no characteristic length scale along the direction of the wave crest, and therefore, exhibits stability characteristics qualitatively similar to those of the 2D problem. In the second case, however, the basic flow is doubly periodic and inaccessible to standard Floquet analysis. We continue the work on the theoretical basis (since this problem will reoccur in compressible flows with the dominant first modes being oblique) and prepare simulation of both cases with the PSE code.

The efforts to analyze the secondary instability of longitudinal vortices in parallel and nonparallel flows had been postponed to await (rather than duplicate) results of Liu & Yu (1989). This work was reactivated after learning about their approach and results. Liu & Yu consider the stability of velocity profiles parallel and normal to the wall and thus 'separate' the basic flow into profiles that depend on a single variable. While this approach is convenient, it is known to be neither justified nor conclusive (Davis 1976). Recent DNS results by Liu & Domaradzki (1989) for this problem show results different from those of Liu & Yu and those of Hall & Seddougui (1989) and Seddougui & Bassom (1990).

Owing to the strong nonlinearity of the vortices at the onset of secondary instability, the treatment of this stability problem (even under the parallel-flow assumption) must be based on partial differential equations for the eigenfunctions that depend on two spatial variables. We have successfully developed the basic elements of this approach and applied them to problems in finite domains. A report on this approach and potential applications has been given at the "International Conference on Spectral and High-Order Methods for Partial Differential Equations," ICOSAHOM '89 in Como, Italy, June 1989. Detailed results on the stability of Dean's flow in a coiled pipe have been presented at the APS-DFD Meeting in Palo Alto, November 1989. Current work aims at calculating the nonlinear basic flow in a semi-infinite strip and analyzing the spectrum of eigenmodes for secondary instability as a function of Görtler number, wave number, and amplitude. Results will be reported at the "First Symposium on Görtler Vortex Flows," Euromech 261, Nantes, France, June 1990. As a member of the Scientific Committee, I am involved in planning a IUTAM Symposium on "Stability of Strongly Nonparallel Flows" in 1992.

4. Personnel

The following personnel has participated in the work and partially has been supported under this contract:

Th. Herbert, principal investigator

Fabio P. Bertolotti, PhD student (now supported under NASA Training Grant NGT-50259)

Vasiliki Hartonas, MS student

Eun-Young Lee, PhD student

Charlotte Hawley, Research Assistant 2 Engineering

The graduate research assistantship of E.-Y. Lee has been terminated owing to his lacking performance. F. P. Bertolotti will receive his Ph.D. in Summer 1990. V. Hartonas will receive her M.S. at about the same time. Two new graduate students, M. Wang and R. Bayless, will cooperate in this program in 1990.

5. Publications

Herbert, Th. 1988 "Exploring Transition by Computer," submitted to J. Appl. Numer. Math. (Special Issue, SAE Meeting 1988).

Herbert, Th. & Bodonyi, R. J. 1989 "Studies of Transition in Boundary Layers," AIAA Paper No. 89-0034.

Herbert, Th. 1989 "Linear.x - A Code for Linear Stability Analysis," Proc. ICASE/NASA Workshop on Stability and Transition, May - June 1989, Hampton, Virginia. To be published by Springer Verlag.

Herbert, Th. 1989 "Theory of Stability and Transition," Position Paper, Proc. ICASE/NASA Workshop on Stability and Transition, May - June 1989, Hampton,

Virginia. To be published by Springer Verlag.

Herbert, Th. & Crouch, J. D. 1989 "Threshold Conditions for Breakdown of Laminar Boundary Layers," Proc. IUTAM Symposium "Laminar-Turbulent Transition," Toulouse, France, Sept. 1989. To be published by Springer Verlag.

Bertolotti, F. P. & Herbert, Th. 1989 "Linear stability of TS waves in compressible flow," Bull. Amer. Phys. Soc., Vol. 34, p. 2282.

Crouch, J. D. & Herbert, Th. 1990 "Nonlinear Evolution of Secondary Instabilities in Boundary-Layer Transition," submitted to J. Fluid Mech.

Bertolotti, F. P., Herbert, Th. & Spalart, P. R. 1989 "Linear and Nonlinear Stability of the Blasius Boundary Layer," to be submitted to J. Fluid Mech.

6. Technical Presentations

"Early Stages of Transition in Boundary Layers," by Th. Herbert, Department of Aerospace Engineering, Texas A&M Univ., College Station, TX (May 1988).

"Three-Dimensional Structure of Boundary Layer Transition", by Th. Herbert, AFOSR Meeting on Turbulence Research, Los Angeles, CA (June 1988).

"Analysis of Viscous Flows by Spectral Methods," by Th. Herbert, Seminars on Algorithms for Supercomputing, Ohio Supercomputer Center, Columbus, OH (September 1988).

"Exploring Transition by Computer," by Th. Herbert, Invited Lecture, SAE, Aerotech '88, Anaheim, CA (October 1988).

"Nonlinear Evolution of Secondary Instabilities in Boundary Layers," by J. D. Crouch and Th. Herbert, 41st Annual Meeting of the Division of Fluid Dynamics, American Physical Society, Buffalo, NY (November 1988).

"Studies of Transition in Boundary Layers," Invited Lecture, by Th. Herbert and R. J. Bodonyi, AIAA 27th Aerospace Sciences Meeting, Reno, NV (January 1989).

"Appearance of Transition in Boundary Layers," by Th. Herbert, NASA Ames Research Center, Moffet Field, California (January 1989).

"Theory of Stability and Transition," ICASE/NASA Workshop on Stability and Transition, Hampton, VA (May/June 1989).

"Appearance of Transition in Boundary Layers," by Th. Herbert, 1989 Newport Conference on Turbulence, Newport, RI (June 1989).

"Stability and Bifurcation of Fluid Motions Governed by Partial Differential Equations," by Th. Herbert, Int. Conf. on Spectral and High Order Methods for Partial Differential Equations, Como, Italy (June 1989).

"Threshold Conditions for Breakdown of Laminar Boundary Layers," by Th. Herbert and

J. D. Crouch, Third IUTAM Symposium on Laminar-Turbulent Transition, Toulouse, France (Sept. 1989).

"Stages of Transition in Boundary Layers," Department of Mechanical and Aerospace Engineering, University of Cincinnati (November 1989).

"Linear Stability of TS Waves in Compressible Flow," by F. P. Bertolotti and Th. Herbert, 42nd Annual Meeting of the Division of Fluid Dynamics of the American Physical Society, Palo Alto, CA (Nov. 1989).

"Flows in a Loosely Coiled Pipe and Their Stability," Th. Herbert and H. Y. Feng, 42nd Annual Meeting of the Division of Fluid Dynamics of the American Physical Society, Palo Alto, CA (Nov. 1989).

7. References

Crouch, J. D. 1988 "The nonlinear evolution of secondary instabilities in boundary layers," Ph.D. Thesis, Virginia Polytechnic Institute and State University, Blacksburg, Virginia.

Davis, S. H. 1976 "The stability of time-periodic flows," Ann. Rev. Fluid Mech., Vol. 8, pp. 57-74.

Gaster, M. 1974 "On the effects of boundary-layer growth on flow stability," J. Fluid Mech., Vol. 66, pp. 465-480

Fasel, H. F., Rist, U. & Konzelmann, U. 1990 "Numerical investigation of the three-dimensional development in boundary-layer transition," AIAA Journal, Vol. 28, pp. 29-37.

Hall, P. & Seddougui, S. O. 1989 "On the onset of three-dimensionality and time-dependence in Görtler vortices," J. Fluid Mech., Vol. 204, pp. 405-420.

Herbert, Th. 1988 "Secondary instability of boundary layers," Ann. Rev. Fluid Mech., Vol. 20, pp. 487-526.

Herbert, Th. & Bertolotti, F. P. 1987 "Stability Analysis of Nonparallel Boundary Layers," Bull. Amer. Phys. Soc., Vol. 32, p. 2079.

Herbert, Th. & Crouch, J. D. 1989 "Threshold Conditions for Breakdown of Laminar Boundary Layers," Proc. IUTAM Symposium "Laminar-Turbulent Transition," Toulouse, France, Sept. 1989. To be published by Springer Verlag.

Liu, J. T. C. & Yu, X. 1989 "Nonlinear instabilities of three-dimensional inflectional velocity profiles resulting from longitudinal vorticity elements in boundary layers," Proc. IUTAM Symposium "Laminar-Turbulent Transition," Toulouse, France. To be published by Springer Verlag.

Liu, W. & Domaradzki, J. A. 1989 "Transition to turbulence in the flow of two counter-rotating vortices," Bull. Amer. Phys. Soc., Vol. 34, p. 2290.

Malik, M. R. 1988 "Numerical methods for hypersonic boundary layer stability," HTC Report No. 88-8.

Seddougui, S. O. & Bassom, A. P. 1990 "On the instability of Görtler vortices to traveling waves," ICASE Report No. 90-1.

Figure 1. Spatial growth rates of primary 2D wave and subharmonic 3D wave according to Floquet theory for parallel flow (o) and PSE marching code (lines).
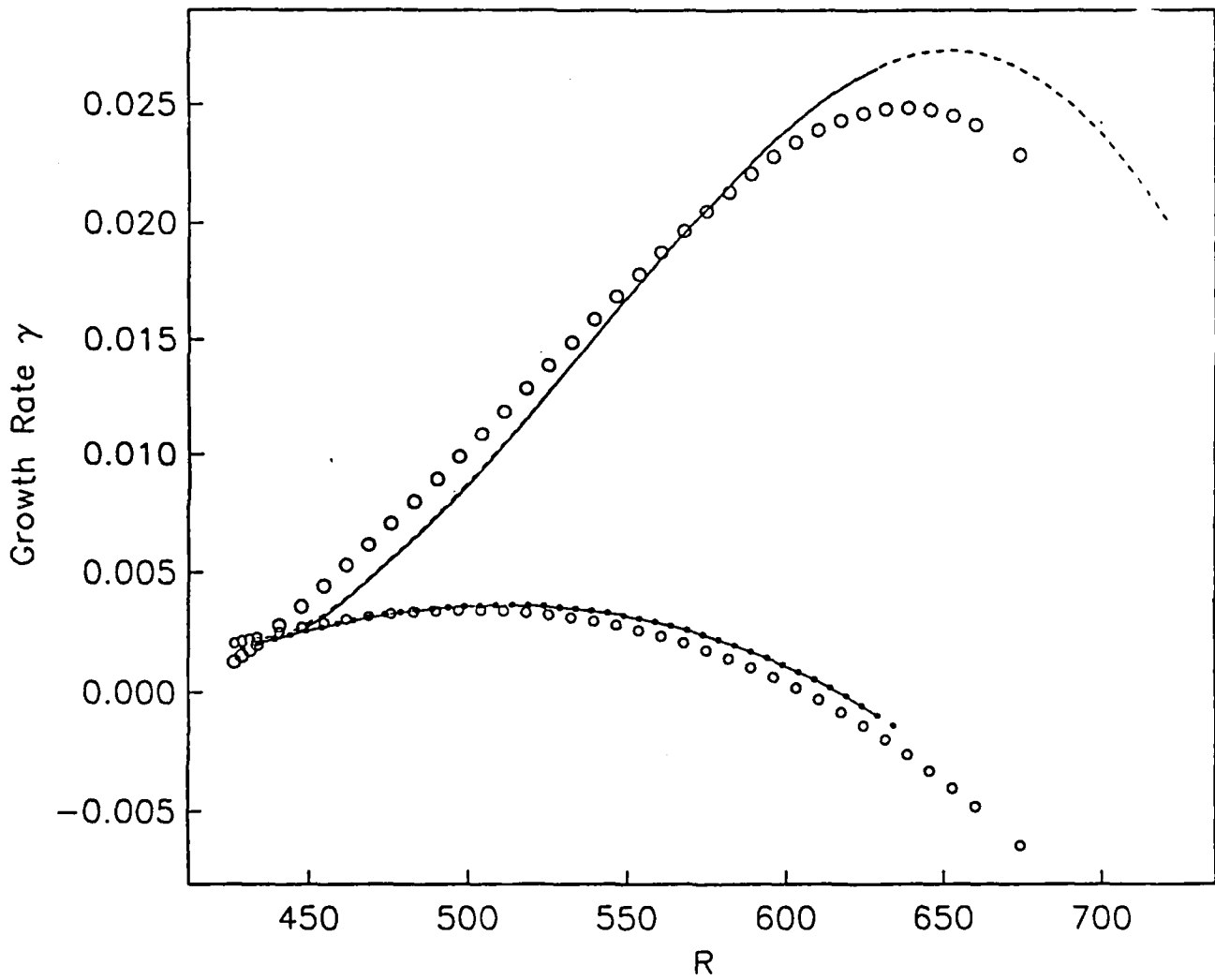
Figure 2. Streamwise development of primary 2D wave, subharmonic 3D wave, and mean flow distortion obtained with the PSE marching code.
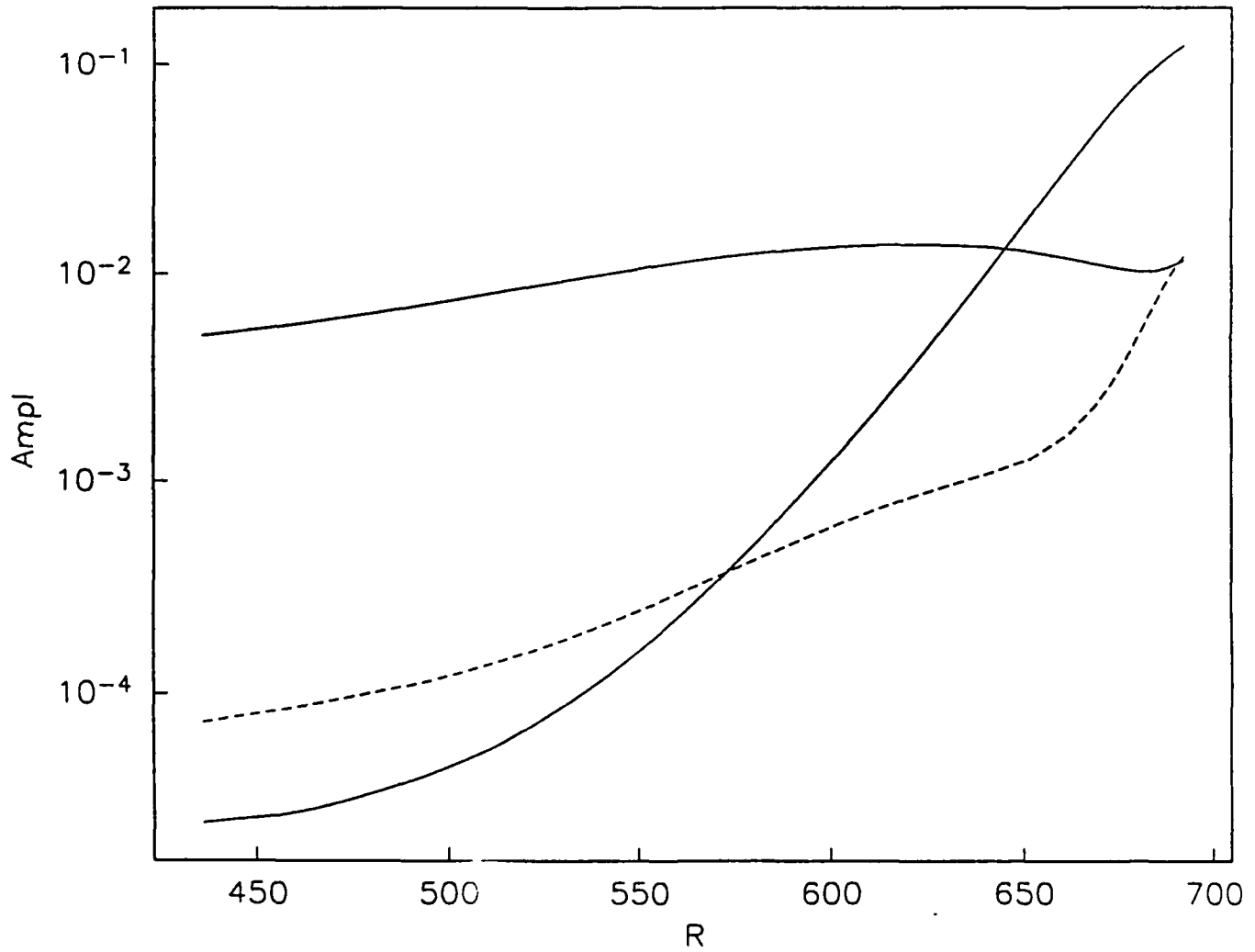
Figure 3. Spatial transition simulation of the Kachanov-Levchenko experiment at $F = 124$ with the PSE code. An integral measure of the amplitude is used.

NONLINEAR TS & SUBH.   25/1/90

TS   init ampl = 0.5% Umax rms

Sub init ampl = 0.00126% Umax rms

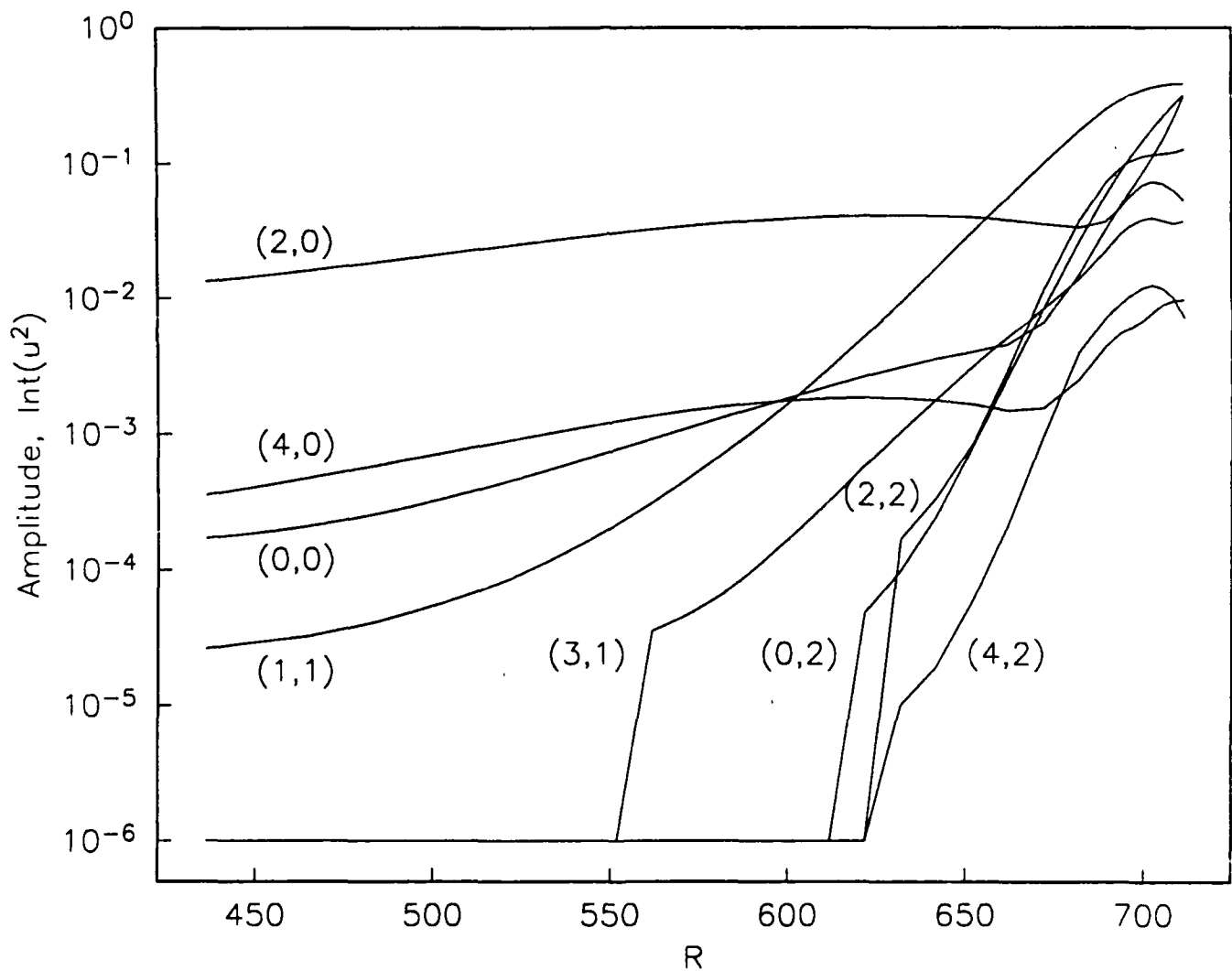Initial Step size 10 R,   JJ=28

Nw=4, Kw=2   (2.43 min YMP)

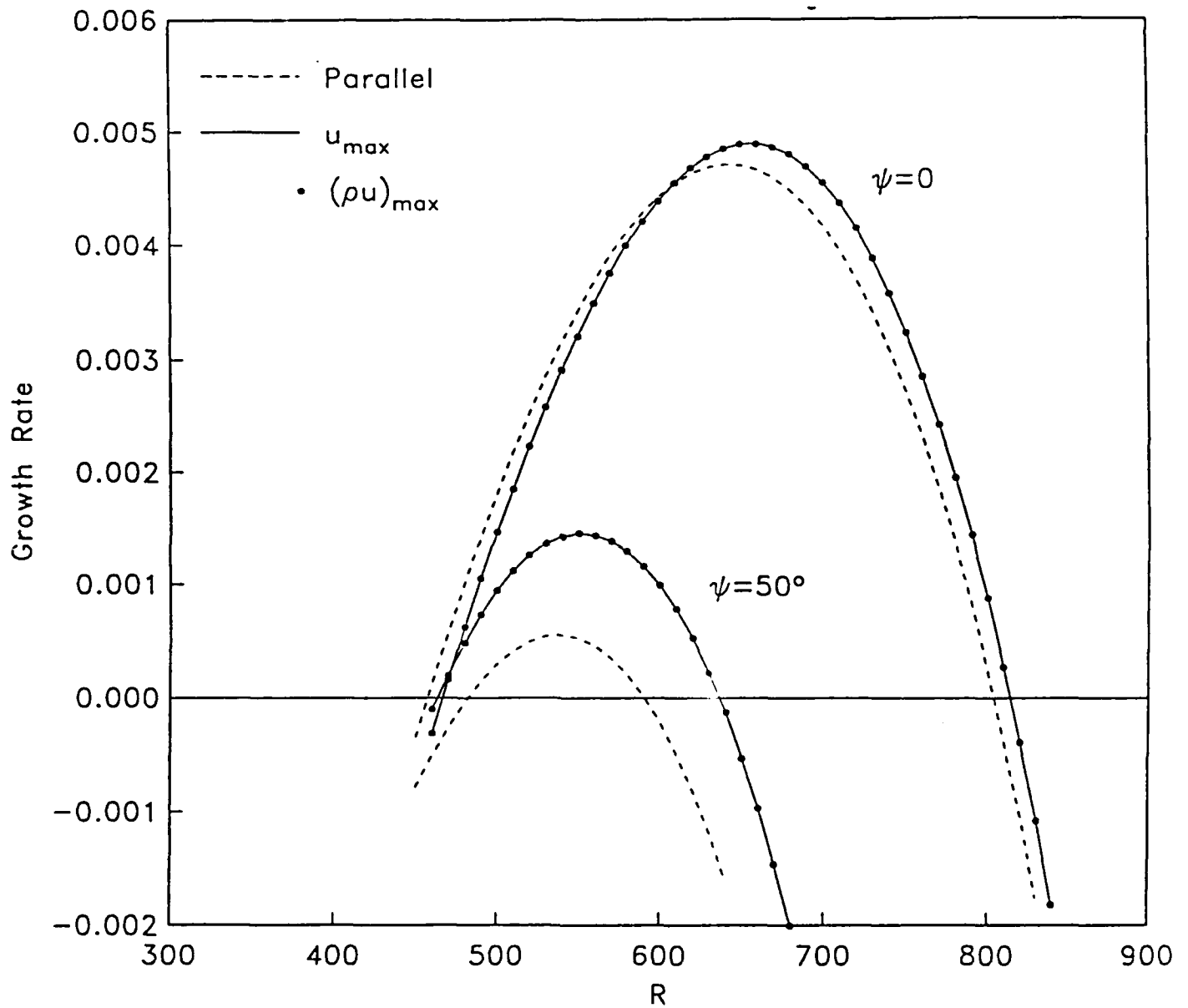Figure 4. Growth rates vs. Reynolds number for 2D waves and oblique waves ($\psi = 50^{\circ}$) at $M = 0.05$, $F = 86$, $T_e = 273$. Comparison of parallel and nonparallel results of the PSE marching code.

Appendix A

Appendix A

"Linear.x - A Code for Linear Stability Analysis"

by Th. Herbert

Proc. ICASE/NASA Workshop on Stability and Transition
May - June 1989, Hampton, Virginia.
To be published by Springer Verlag.

Linear.x
A Code for Linear Stability Analysis
Version 1.0

Thorwald Herbert

Department of Mechanical Engineering
Department of Aeronautical and Astronautical Engineering
The Ohio State University
Columbus, Ohio 43210, U. S. A.

Linear.x is a spectral code for the analysis of the linear stability of some basic state. The code is generic and void of any particular physical problem yet provides for various common tasks:

global — eigenvalue spectra,
local — single eigenvalues and eigenfunctions,
table — one- or more-dimensional tables of eigenvalues
curve — (neutral) curves in parameter space

and others. A specific physical problem can be defined in a set of usually very short files. Some of these files are included at compile time, while definitions, tasks, and parameters are read during run time. The code is written in Fortran 77. The standard version has been used in various Unix environments and under VAX-VMS. The code has been successfully used for a variety of classical stability problems and is currently utilized to analyze the stability of compressible flows.

1. Introduction

Over the past 25 years, I have written reams of stability codes implementing different mathematical or numerical methods, different fluid flows, different aspects of stability, and different computers. I have often regretted the waste of time - my own, my colleagues', or the students' time - spent on developing another or tailoring an existing program for a particular application, often to generate just a few stability results that are unavailable in the literature. On the other hand, I have realized that many of my programs are alike and differ essentially only in major categories: linear stability, weakly nonlinear stability or mode interaction, nonlinear equilibrium states, secondary instability, and so on. The code *linear.x* is the first step to consolidate ideas, techniques, and subroutines into as few as possible generic programs that can be used in a standardized way on most any computer. After initial use by the students of my Fall 1988 course on "Stability of Fluid Motions," the extended version has meanwhile been used for stability research in various areas and has not only performed well, but replaced previously used codes.

The positive experience with the current version suggests to make the code available to those interested in its application. This experience also motivates to further extend the present version for linear stability analysis and to incorporate higher levels of stability analysis into a family of codes with common elements. Version 1.0 is essentially a batch program. An obvious extension for use on workstations will be an interactive interface (or various interfaces to handle different

window systems). Another extension currently developed in cooperation with Dr. Gordon Erlebacher (NASA Langley Research Center) is the graphical output in real time, either locally or remotely. In the remote version, the stability code runs in some Cray while menus for interactive parameter changes and graphics are displayed on the workstation. The common graphics library CGL that enables this remote mode between Cray and SGI Iris workstations over Ethernet or Arpanet was developed and kindly provided by Diana Choi (NASA Ames Research Center).

Linear_x was not developed to compete with other codes in speed or otherwise. Except for challenging "big" problems like compressible stability, computer time is not a crucial issue any more. The code was developed to be able to obtain some additional results in a few minutes after the thought (if the specific insert files are available) and to obtain the first results for a new problem within a few hours (if the equations are available). Since the specifications of a new problem are usually short, the debugging effort is usually small. The code tries to check what the user does and prints error messages before termination but is not foolproof: garbage in — garbage out. The basic operation of the code will be explained in the following, and some understanding will help to get things right. In case of emergency, a look at the moderately commented source code may help. More recently, malfunction of the code was caused in every case by incorrect input or physical/mathematical intricacies, not by hidden bugs.

The code comes with the source of all subroutines. The user may choose the libraries of a specific computer, e.g. vectorized routines for the Cray, instead of the subroutines algr.f and algc.f (and Eispack RG and CG) that consume most of the CPU time. The goal to keep the code generic and to use Fortran 77 for its wide availability and use (in spite of its lacking features) required compromises. Especially the Fortran hierarchy of statements (which prohibits e.g. dimension after data statements) made the placement and structure of the "physics insert files" mandatory. The standard version is for the Unix environment, uses the C-preprocessor to include the physics and machine-specific lines, and has a Makefile to produce the executable code. Some examples are included. For non-Unix environments, the code can be produced "by hand" with the editor.

2. Basic Approach

A stability problem is defined by a *basic state* (or basic flow) and *stability equations*. We consider basic states that depend on a single independent variable $\hat{y}$, e.g. a stratified fluid with density $\rho(\hat{y})$, $\hat{y}$ pointing opposite to gravity, circular Couette flow with azimuthal velocity $V = C_1\hat{y} + C_2/\hat{y}$, plane Poiseuille flow with streamwise velocity $U = 1 - \hat{y}^2$, or a compressible boundary layer with streamwise velocity $U(\hat{y})$, temperature $T(\hat{y})$, density $\rho(\hat{y})$, and viscosity $\nu(\hat{y})$. The basic state may depend on *constants* such as C_1 and C_2 in the case of Couette flow or the ratio $C_1(=\gamma)$ of specific heats for the boundary layer. The basic state may also depend on *parameters* such as the Mach number P_1 of the boundary layer. (The distinction of constants and parameters will be justified below.) Note that the basic state may be defined in a finite domain, $a \le \hat{y} \le b$, in a semi-infinite domain, $0 \le \hat{y} < \infty$, or in an infinite domain, $-\infty < \hat{y} < \infty$. We may also wish to name the independent variable $\hat{y}$, or C_i and P_k in a different, more problem-oriented way.

The linear stability of basic states of above form is in general governed by a system of stability equations that are homogeneous, linear, ordinary differential equations (ODE's) for the *variables* $v_n(\hat{y})$ with homogeneous boundary conditions at the end points of the domain. In the simplest case, there is only one variable v_1, and the system of ODE's reduces to a single ODE of (at least)

second order. In other cases, we deal with more variables (five for the compressible boundary layer) and the same number of differential equations of different orders. The basic state and its derivatives appear in the coefficients of the differential equations together with various *parameters* P_k (e.g. Reynolds or Taylor number, wavenumber(s), growth rate) and *constants* C_i.

The goal of any stability analysis is to find solutions of the characteristic equation $F(P) = 0$ of the problem, where $P = (P_k)$ is the vector of *parameters*. Obviously, F depends also on the basic state. The interest can be in a single solution (eigenvalue) P^v, the associated variables $v(\hat{y}) = (v_n)$, or all solutions (eigenvalue spectrum) of the characteristic equation. How many eigenvalues and what types of spectra (discrete, continuous) result in a given problem is discussed in monographs and journal articles. Here, we try to find solutions to the characteristic equation of a discretized problem numerically. With this approach, we will certainly find only a finite number of eigenvalues including those of most physical relevance. How accurately we approximate higher discrete eigenvalues depends on how well we can resolve the associated eigenfunctions numerically. Continuous spectra are approximated by discrete spectra, with the eigenvalues lined up along curves. As the resolution changes, members of the discrete spectrum approximate a fixed value, while the members of the "continuous" spectrum keep moving along shifting curves.

The stability equations may be real or complex. If the equations are real, the eigenvalues may be real or complex. The distinction of real and complex quantities in programming languages (and the larger computational effort for the latter case) suggest two separate codes if one wants to exploit the higher efficiency of the real version. The complex version can handle all cases but needs more memory and CPU time. To enhance the versatility of the code, all parameters (and constants) are considered real. Hence, real and imaginary parts of complex quantities are treated as separate parameters with provisions to use them in combined form in complex arithmetic operations. When solving the characteristic equation, we can select in the real version any single parameter, in the complex version any two parameters as "eigenvalue." This approach permits searching directly for points on the neutral curve and a variety of other useful relations, e.g. the relation between temporal and spatial growth rates.

Some restrictions apply for eigenvalue spectra. The complex version requires a complex quantity as an eigenvalue. Real or complex, the eigenvalue must appear linearly in the stability equations. This requirement explicitly excludes spectra for cases where the eigenvalues affect the basic state. If the eigenvalue appears to some small power (usually, wavenumbers appear at least up to second power), the stability equations may be rewritten in an extended form that contains the eigenvalue linearly (see the example of the Orr-Sommerfeld equation below).

A spectral collocation method is used to convert the homogeneous boundary value problem for ODE's into an algebraic problem. The user does not need any expertise in spectral methods to apply the code. All that needs to be specified is the number of collocation points which affects the number of eigenvalues obtainable and the accuracy of the solutions, one of two choices of collocation points (Gauss or Gauss-Lobatto points, the "default"), the choice of boundary conditions for each of the variables, one of the built-in transformations of the physical interval to the standard interval $-1 \leq \hat{x} \leq 1$ for Chebyshev spectral methods, and the symmetry of the approximation for each dependent variable, if applicable. For those interested: linear combinations of Chebyshev polynomials are used for the spectral expansions. The linear combinations are chosen such that the expansion functions satisfy the boundary conditions. For a detailed account of spectral methods,

see Canuto et al. (1988).

In essence, the global procedure converts the stability problem into the algebraic eigenvalue problem $(A - \sigma B)a = 0$ with matrices A, B, and the eigenvalue σ. B is usually singular and Eispack (and many other) routines are not prepared for this case. However, many routines solve problems of the form $(C - \lambda I)w = 0$. Therefore, we use internally $C = A^{-1}B$ and $\lambda = -\sigma^{-1}$ to obtain the eigenvalue spectrum with Eispack (routines RG or CG). The singularity of B usually introduces some very large spurious eigenvalues that may be suppressed in the results. The local procedure, table, and curve use variations of Newton's method to solve the nonlinear algebraic form of the problem for the spectral expansion coefficients and the eigenvalue. The application of Newton's method requires that the user provides not only the stability equations but also the derivatives of these equations with respect to all those parameters he or she wishes to consider as eigenvalue candidates. Moreover, Newton's method requires an initial guess for the eigenvalue and converges only if this guess is sufficiently close to a root (maybe not the desired root) of the characteristic equation. An initial guess can be found without prior knowledge if the global procedure is applicable for at least one of the possible eigenvalues. Any eigenvalue of the spectrum can be continued using the *table* option on various routes through the parameter space. If desired, the local procedure also provides the values of the variables at the collocation points.

The production of tables is a relatively straightforward task that requires only sufficiently small steps (for Newton's method to converge) and avoiding conflicts between prescribed parameters and eigenvalues. Generating curves in some coordinate plane of the parameter space is less trivial. These curves may or may not be closed, may have rapid variations of curvature, and follow tortuous routes. The tracing of curves uses an arc-length continuation procedure in scaled variables with internal control of the step size. The iteration direction for Newton's method is (nearly) normal to the curve. The user specifications are similar to those necessary when preparing plots of data (choice of axes, scales, and a "window"). Both *table* and *curve* require that a starting point be given by the *local* procedure.

Constants and *Parameters* are distinguished by their role in the problem. Constants are necessary but remain essentially fixed during the stability analysis. Typical examples are the ratio of specific heats in a study of compressible boundary layers, or switches that determine which relation to use between temperature and viscosity or whether to solve the small-gap or the full equations for the Taylor-Couette problem. Constants are read and printed only once. *Parameters* are all quantities that may vary in tables and curves or as eigenvalues. They are read every time the global or local procedure is executed and printed for every eigenvalue found by any task. Parameters, therefore, require more input and cause more output than constants (that's all). If the user wants to study the eigenvalue as a function of the ratio of specific heats, he or she just needs to redefine the constant as a parameter (an effort of a few minutes, including recompilation of the code).

The principal output and error messages appear on standard output, typically on the terminal or window. The line length may exceed the standard 80 or so characters. A copy of the input is appended to an input-log file that can be rerun if necessary. A copy of the output is appended to an output-log file for later inspection. In addition, numerous smaller task-specific files are produced that contain the data in a form suitable for producing quick plots with packages like *igraph* or *plotxy*.

By the way, if you feel this code can be written in a different way, I completely agree. Change it if you so desire. Note that close to 100% of the CPU time is used in the linear-algebra subroutines (algr, algc, Eispack CG, and RG) and improvements in the main code will barely affect the overall efficiency. If you have a serious problem, or a really good idea, or a truly superior subroutine, or an elaborate set of insert files for a problem of broader interest, mail it to me, E-mail: tht@apollo.eng.ohio-state.edu. Include your authorship and contact address - it will stay there for others to know. In the same way, I expect you to acknowledge the use of this code whenever you use it in original or modified form to produce results for publication.

3. The Physics Files

From the foregoing, it is obvious that various data must be specified to adapt the generic code to a specific problem. We describe the specifications for the complex version of the code (comments on modifications for the real version are given in a separate section). It is often advantageous to follow the directions with a specific example in mind. I suggest to look at one of the examples while reading this section. The physical problem is specified in the following files:

common.ins	*Definitions*
bstate.ins	*Parameters*
complex.ins	
vector.ins	

The files with suffix *.ins* are included in the code during compile time. Which programs are affected by changing a certain .ins file is given in the section "Dependencies" of the Makefile. The data affecting the array sizes and specific storage areas for the basic state are defined in *common.ins*. The file *bstate.ins* provides the values of the basic state and its derivatives (with respect to $\hat{y}$ and parameters, if needed) at the collocation points by explicit calculation (in simple cases like plane Poiseuille flow), by reading these values from a file (e.g. for the Blasius profile that is independent of parameters), by calling a subroutine, or otherwise. The file *complex.ins* declares the complex quantities in the stability equations. The file *vector.ins* defines the stability equations by giving (the matrix of) the coefficients of each derivative in the stability equations at the collocation points and a similar set of data for the derivatives with respect to parameters (for Newton's method). Note that different stability equations can be applied to a given basic state. Vice versa, different basic states can be analyzed with the same stability equation (e.g. the Orr-Sommerfeld equation). For the "professional" user, it may be advisable to spend the time for developing systematically the complete insert files (see the example "Plane Poiseuille Flow").

The remaining files are read at run time. The file *Definitions* provides the data affecting the spectral method, the names of variables, names and values of constants (if any), and the names and characteristics of the parameters. The file *Parameters* is the file frequently changed after the initial setup has proved correct. This file defines various tasks to be performed in sequence until an error occurs or termination is requested. Every task requires input data to be specified after its invocation. These details are discussed below.

A shortcoming of the current version 1.0 is the internal reference to parameters and constants by number or input sequence, not by name. Alternatives using table lookup suffer from pitfalls, typing errors, and the need for fixed-format input (owing to unavailability of standardized internal read

statements in Fortran compilers). This shortcoming will be removed in a menu-driven version for workstations. In version 1.0, we can only recommend precision in writing the initial setup and leaving relevant comments in the input (especially the parameter) files as shown in the examples.

4. Preparing the Code

In the following, we discuss the details of the insert files. In the examples, the user-provided information is printed in capitals while lower-case code is of concern only for those who wish to study or modify the code.

4.1. common.ins

This file specifies the data affecting the array sizes and the storage areas for the basic state. The file also specifies the implicit type of the real variables as real*8 (the default on the Cray). The following data must be provided:

JX The highest index of the collocation points, $j = 0, \cdots JX$. The number $JX+1$ of points can reach from as few as 8, say, to as many as 200 or so. For even larger numbers, round-off errors in the basic data for the spectral method come into play. For the standard problems of classical stability theory, 10 collocation points are a reasonable choice except if critical layers or center modes are involved. Blasius flow or Poiseuille flow (using symmetry) require 20 - 25 points for reasonable accuracy, with an increasing number for increasing Reynolds number. With spectral methods, improvements in accuracy can be obtained by small increases in JX.

NEQU The number of equations (and variables, NVAR=NEQU) in the stability equations. This number should be as small as possible since $(JX+1)\cdot NEQU$ determines the dimension of the algebraic systems to be solved.

NX The highest order of differentiation in any single ODE of the system of stability equations. Usually, NX = 2 or NX = 4. NX is *not* the total order of the system.

NCON The number of constants or zero (if there are no constants).

NPAR The number of parameters. Note that complex parameters count as two real parameters.

In addition, the common block COMMON /MSTATE/ must be specified to accommodate the basic state and its derivatives, e.g.

  COMMON /MSTATE/ UM(0:JX,0:2),TM(0:JX,0:2)

to provide the mean flow $UM = U_{mean}$ (second index 0) and its first (second index 1) and second (second index 2) derivatives and the same for the mean temperature at the collocation points. While the mean temperature is of no interest when solving the Orr-Sommerfeld equation, the more general setup also allows for extended sets of stability equations including the energy equation. The common block MSTATE will be filled with values in the next file, bstate.ins.

4.2. bstate.ins

bstate.ins provides the values of the basic state (and derivatives) at the collocation points by explicit calculation, by reading these values from a file, by calling a subroutine, or otherwise.

When entering the file *bstate.ins*, the following information is available:

j	the index of the collocation point, $j = 0, \cdots JX$
chy(j)	the collocation point $\hat{y}_j$
par(k)	the array containing the parameters P_k, $k = 1, \cdots NPAR$
	and the data defined in *common.ins*, including the arrays for the basic state

The following additional names are internally used: chfy, itask, con, dpar, ipar, conname, parname, varname, problem, and the statement label 1.

4.3. complex.ins

The file *complex.ins* declares the complex quantities in the stability equation. The file consists of the single statement *complex*16 q1,q2, $\cdots$* (or *complex q1,q2, $\cdots$* for the Cray), where *q1,q2, $\cdots$* is the list of the complex quantities used in *vector.ins*.

4.4. vector.ins

The file *vector.ins* defines the stability equations by giving (the matrix of) the coefficients of each derivative in the stability equation(s) at the collocation points and a similar set of data for the derivatives with respect to parameters (for Newton's method). To properly derive the basis for this file, we first list the stability equations and variables in some convenient (or arbitrary) order and assign numbers to both equations and variables, starting with 1. The total numbers of equations and variables must be the same (NEQU in file *common.ins*). We obtain the stability equations in the general form

$$\sum_{l=1}^{NEQN} L_{il} (v_l) = 0 , \quad i = 1, \cdots NEQN \tag{1}$$

where L_{il} is a linear differential operator applied to the l-th variable v_l in the i-th equation. Second, we write every differential operator L_{il} in the form

$$L_{il} = \sum_{0}^{NX} p_{inl}(\hat{y}, \mathbf{P}) D^n , \quad D = \frac{d}{d\hat{y}} \tag{2}$$

where the p_{inl} are the coefficients of the n-th derivative of the l-th variable in the i-th equation. Many of these p_{inl} are zero, others depend only on the parameters, and a few depend also on $\hat{y}$ since they contain the basic state or its derivatives. Third, we make a list of all constants and parameters and assign numbers starting with 1 both for the first constant and for the first parameter, but counting real and imaginary part separately. Fourth, we could write down the derivatives of the p_{inl} with respect to the parameters we wish to consider as eigenvalues. However, this step is in fact easier to perform with the editor on the computer.

When entering the file *vector.ins*, the following information is available:

ideriv	to indicate whether the coefficients (ideriv=0) or their derivatives (ideriv=1) are needed
j	the index of the collocation point, j = 0, $\cdots$ JX
chy(j)	the collocation point $\hat{y}_j$
par(k)	the array containing the parameters P_k, k = 1, $\cdots$ NPAR
	the data defined in *common.ins* including the arrays for the basic state
	the real constants ZRO=0, ONE=1,
	and the complex constants ZERO=(0,0), UIMAG=(0,1)

The following additional names are internally used: chfy, rvec, itask, con, dpar, ipar, conname, parname, varname, problem, and the statement labels 1 - 4.

At the beginning of *vector.ins*, it is useful to store the parameters par(k) in variables with problem-oriented names, using the list made above. This step can be done for j=0 only, or for any j (since it consumes little time). Real and imaginary parts can be combined into complex quantities to simplify the arithmetic statements. (The complex quantities must be declared in *complex.ins*.) The file provides two branches for the coefficients (if ideriv=0) and their derivatives (if ideriv=1), respectively.

For given parameters, the coefficients p_{inl} depend only on $\hat{y}$, $p_{inl}(\hat{y})$. To produce the first part of *vector.ins*, the $p_{inl}(\hat{y}_j)$ have to be assigned to the array PVEC(j,i,n,l,0), using the available information. Zero elements can be skipped since the array PVEC is set to zero before entering *vector.ins*. While j is given, the user must provide the lines for i = 1, $\cdots$ NEQU, l = 1, $\cdots$ NEQU, n = 1, $\cdots$ NX of nonzero coefficients.

The second part of the file requires to assign to PVEC(j,i,n,l,k) the derivative of p_{inl} with respect to the parameter P_k at the j-th collocation point. One may easily verify that PVEC($\cdots$,k) is the derivative of PVEC($\cdots$,0) with respect to P_k. Here again, the elements have been reset to zero and only nonzero derivatives must be provided. While k can vary from 1 to NPAR, the derivatives are needed only with respect to those parameters P_k that will be considered eigenvalue candidates. Suppose there is a single complex eigenvalue $\sigma = \sigma_r + i\sigma_i$ which in this file is defined as SIGMA=CMPLX(PAR(4),PAR(5)), and we plan to generate tables of this eigenvalue as a function of the other parameters. In this case, the derivatives must be provided only for k = 4, 5. Note that $\partial p_{inl}/\partial \sigma_r = \partial p_{inl}/\partial \sigma$, while $\partial p_{inl}/\partial \sigma_i = i\,\partial p_{inl}/\partial \sigma$ and hence in our example we set PVEC($\cdots$,5) = UIMAG*PVEC($\cdots$,4).

The file *vector.ins* can be easily produced by symbolic manipulators like Macsyma or Mathematica.

After preparation of the above four files, the code is ready for compilation. Details on this step are given in the section "Installation."

5. Preparing the Input Files

5.1. Definitions

The *Definitions* consist of various small groups of data described in the following:

(1) A single line of text with ≤ 80 characters specifying the *problem*.

(2) One or more lines with NEQU integers idsy(n), n=1, $\cdots$ NEQU, specifying the symmetry of each dependent variable with respect to the transformed variable $\hat{x}$, where

        -1   indicates no symmetry in $\hat{x}$

         0   indicates symmetry in $\hat{x}$

         1   indicates antisymmetry in $\hat{x}$

If the mean flow is symmetric, exploiting symmetries can save one half of the collocation points and make calculations more efficient. With the proper (larger) number of collocation points, however, the same results can be obtained without using symmetry (-1 for all variables). In other problems, symmetry and the half-interval $0 \leq \hat{x} \leq 1$ may be used for different reasons, as in the example of boundary layers, where many points are needed near the wall.

(3) One or more lines with NEQU integers idbc(n), n=1, $\cdots$ NEQU, specifying the boundary conditions for each variable, where

         0   indicates no boundary condition on v_n

         1   indicates $v_n = 0$ at the boundaries

         2   indicates $Dv_n = 0$ at the boundaries

         3   indicates $v_n = Dv_n = 0$ at the boundaries

Additional types of boundary conditions can be implemented in the subroutine *chttoff*. Version 1.0 does not provide for different types of conditions at the two end points of the interval.

(4) One line with one integer idpts specifying the type of collocation points:

         0   Gauss points

         1   Gauss-Lobatto points

(see Canuto et al. 1988). Normally, I use idpts=1 which places collocation points at the end points (± 1). Only if these end points cause problems (e.g. in cylindrical problems on the axis), I use idpts=0.

(5) One line specifying the transformation $\hat{y} \rightarrow \hat{x}$ which consists of three data:

        idtrf   the type of transformation

        atrf   the first parameter of the transformation (or zero)

        btrf   the second parameter of the transformation (or zero)

The values of atrf and btrf must be specified even if they are not needed. The following transformations are available:

        idtrf=0 $\hat{x} = \hat{y}$. No transformation. atrf=btrf=0

idtrf=1 $\hat{x} = (2\hat{y} - a - b)/(b - a)$ with atrf=a, btrf=b. This linear transformation maps the interval $\hat{y} \in [a,b]$ into $\hat{x} \in [-1,1]$.

idtrf=2 $\hat{x} = a/(\hat{y} + a)$ with atrf=a, btrf=0, the algebraic mapping of $\hat{y} \in [0,\infty)$ into $\hat{x} \in [0,1]$ where $\hat{x} = 1$ for $\hat{y} = 0$. This mapping is used for boundary layers. For the Blasius profile, the parameter is typically atrf=4.5, which places half the collocation points inside the displacement thickness.

idtrf=3 $\hat{x} = \exp(-\hat{y}/a)$ with atrf=a, btrf=0, the exponential mapping of $\hat{y} \in [0,\infty)$ into $\hat{x} \in [0,1]$ where $\hat{x} = 1$ for $\hat{y} = 0$ and typically atrf=20 for the Blasius boundary layer.

idtrf=4   The algebraic mapping $\hat{x} = \hat{y}(\hat{y}^2 + a^2)^{-1/2}$ of $\hat{x} \in [-1,1]$ into $\hat{y} \in (-\infty,\infty)$ where $\hat{x} \to 1$ as $\hat{y} \to \infty$. Typically, atrf=2.

idtrf=5   The hyperbolic tangent mapping $\hat{x} = \tanh(\hat{y}/a)$ of $\hat{x} \in [-1,1]$ into $\hat{y} \in (-\infty,\infty)$ where $\hat{x} \to 1$ as $\hat{y} \to \infty$. Typically, atrf=2.

(6) NCON lines, each line giving the name and value of the constant in fixed FORMAT (A8,1X,E16.8)

     conname   the name of the constant, up to eight characters

     value   the value of the constant, right adjusted in columns 10-25

All constants are considered real. This section may be missing if NCON=0.

(7) NEQU=NVAR lines, each line giving the name of one dependent variable in fixed FORMAT (A8)

     varname   the name of the variable, up to eight characters

The name of the independent variable in printouts is always x (transformed) or y (physical).

(8) NPAR lines, each line giving the name and the two identifiers ipar1, ipar2 for one parameter in fixed FORMAT (A8,1X,I2,1X,I2)

     parname   the name of the parameter, up to eight characters

     ipar1   first identifier (see below)

     ipar2   second identifier (see below)

where the meaning of the identifiers is as follows:

     ipar1=0   the parameter appears linear in the equations

     ipar1=1   the parameter appears nonlinear in the equations

     ipar1=2   the parameter affects the basic state

If more than one of these characteristics are true, choose the highest value for ipar1.

     ipar2=0   the parameter is real

     ipar2=1   the parameter is the real part of a complex quantity

     ipar2=2   the parameter is the imaginary part of a complex quantity

Real and imaginary parts must immediately follow each other (for the global procedure to work).

Although tedius to describe, the *Definitions* are usually quick done. However, it is important to prepare this file carefully since the sequence of data must be correct.

6. Tasks and Parameters

The file *Parameters* contains a sequence of tasks for the code to perform. Each task requires certain input data. All data are read in free input format. It is advantageous, however, to describe (and use) certain data in groups and to separate tasks by blank lines. The code can perform the following tasks:

itask=0	*global* procedure to find eigenvalue spectra
itask=1	*local* procedure to find a single eigenvalue
itask=2	*local* procedure to find eigenvalue and eigenfunction
itask=3	*table* of eigenvalues in 1, 2, or 3 dimensions
itask=4	*curve* of solutions in the plane of two parameters
itask >4	terminate
itask=-1	*close and reopen* the file *Parameters* after pause
itask < -1	terminate

These tasks are described in the following sections.

6.1. Eigenvalue Spectra

Finding the eigenvalue spectrum is a computationally "expensive" task (in comparison with finding single eigenvalues) with "extensive" output. Therefore, tables of spectra are not implemented. To obtain the spectrum for a certain parameter combination, the file *Parameters* requires the following information:

itask=0	to indicate the desired task
iev1	the number of the parameter that gives the real part of the eigenvalue
par(k)	k=1, $\cdots$ NPAR, the list of all parameters (most convenient: one at a line), where the values of par(iev1) and par(iev1+1) are irrelevant (=0).

Note that the imaginary part of the eigenvalue must be par(iev1+1).

6.2. Single Eigenvalues

In contrast to the previous global procedure to find spectra, the local procedure searches for the values of two real parameters that solve the characteristic equation but are not necessarily real and imaginary part of a complex quantity. We denote these two parameters as the "first and second eigenvalue parameter." To obtain an eigenvalue with the local procedure (Newton's method), an initial guess must be specified. If such an estimate is not available, itask=0 can help to provide many eigenvalues (if the eigenvalue appears linearly in the stability equations). Otherwise, itask=3 (table) can help to analytically continue an eigenvalue known at different parameters to the desired

point. To obtain a single eigenvalue for a certain parameter combination, the file *Parameters* requires the following information:

itask=1	to indicate the desired task
iev1	the number of the first eigenvalue parameter
iev2	the number of the second eigenvalue parameter
par(k)	k=1, $\cdots$ NPAR, the list of all parameters, including the initial guess for par(iev1) and par(iev2).

6.3. Eigenvalue and Eigenfunction

This task is identical with itask=1 except the coefficients of the Chebyshev series and the values of the variables at the collocation points are evaluated. Except for itask, the specifications are the same as in the previous section:

itask=2	to indicate the task
iev1	the number of the first parameter to be found
iev2	the number of the second parameter to be found
par(k)	k=1, $\cdots$ NPAR, the list of all parameters, including the initial guess for par(iev1) and par(iev2).

6.4. Tables of Eigenvalues

This task enables calculation of one-, two-, or three-dimensional tables of eigenvalues. The local procedure (itask=1,2) must be performed at least once to provide a starting point for this task. The values of iev1 and iev2 that specify the eigenvalue are taken from the previous task. The required input is:

itask=3	to indicate the desired task
kdim	the dimension of the table

and kdim lines, each line containing:

kpar	the parameter to be varied
kstep	the number of steps
step	the step size

The first parameter specified is varied in the innermost loop.

6.5. Curves in Parameter Planes

This task enables the direct calculation of neutral curves (or curves of constant amplification) and other useful curves in the plane of two parameters with a third parameter completing the eigenvalue problem. The local procedure (itask=1,2) must be performed at least once to provide a starting point for this task. To describe the input, we imagine a three-dimensional coordinate system with the horizontal, vertical, and normal axes formed by the three parameters par(iv1), par(iv2), and par(iv3), respectively, and a curve in the plane spanned by par(iv1) and par(iv2). Beginning at some starting point provided by the local procedure, we want to proceed in one of the two possible

directions and find new points of the curve. All but the three parameters used as coordinates maintain the starting values along the curve. In particular, for a neutral curve, the growth rate in the starting point must be zero. Since the parameters involved may have quite different orders of magnitude, we have to choose proper scale values. For this step, we envision a plot of the curve on a sheet of paper and choose the scales such that the curve looks "nice" without squeezing it in either axis. In the scaled plot, the distance between points should be neither too large nor unnecessarily small. Also, the plot has a "window" defined by the minimum and maximum of the variables plotted. The input required is as follows:

> itask=4   to indicate the required task

and two lines, the first for the "horizontal" direction, the second for the "vertical" direction, each line containing:

> iv1,2   the associated parameter
>
> vgrid1,2   the scale value
>
> vmin1,2   the minimum value
>
> vmax1,2   the maximum value

The iteration for the eigensolution can neither use par(iv1) (if the curve's tangent is horizontal) nor par(iv2) (if the tangent is vertical) as the first eigenvalue parameter but internally iterates normal to the curve in the plane of par(iv1), par(iv2). The second eigenvalue parameter is par(iv3). The input continues with one line specifying this third dimension of the eigenvalue problem:

> iv3   the second eigenvalue parameter in the "normal" direction

The next line specifies

> angle   the initial direction in the plane of the curve as the positive or negative angle (in degrees) measured from the horizontal axis
>
> radius   the distance between points along the curve in scaled variables

and the final line specifies

> npoints   the number of points (or arc length in multiples of the radius) to be traced.

A safe recipe for the choice of the various data cannot be given here since it depends on the (assumed unknown) properties of the curve. A reasonable choice for the scale values would be the order of magnitude or the physical values of the parameters par(iv1), par(iv2) of some point at the curve. In the case of plane Poiseuille flow (see Examples), with par(iv1)=Re, par(iv2)=α,and par(iv3)=ω_r, the choice vgrid1=10000, vgrid2=1 would be almost the same as vgrid=20000, vgrid2=2 and be as good as vgrid1=5772, vgrid2=1. Note, however, that the radius is the distance in scaled variables. With a radius of 0.01, the maximum physical steps in the horizontal direction would be 100, 200, or 57.72 in the three cases, while the maximum vertical steps would be 0.01, 0.02, or 0.01. These steps should be small enough to obtain a nice plot (and rapid convergence) and because problems may arise if the distance between multiple branches of the curve is smaller than the radius. If the steps are too large for convergence, or if the specified radius exceeds π/8th of the curve's radius of curvature, the radius will be automatically divided by increasing powers of 2, hence you may obtain 2, 4, or more points per step. The procedure tries to double the reduced internal step size after every point until it proceeds with the original radius. Hence, the

continuation procedure will slow down in regions of strong curvature.

Ideally, the angle (in degrees) would be the positive or negative angle between the horizontal and the curve's tangent in the starting point. The two signs correspond to the two directions in which the procedure can proceed. The choice of the angle is not critical as long as the radius is sufficiently small and the initial direction is not normal to the curve. Trial and error with npoints=4 and a small radius will help (the angle and radius for the last point are printed). Note that the angle changes with the ratio vgrid1/vgrid2.

The procedure terminates if the number of (full) steps exceeds npoints, if the distance between any point (after the third) and starting point is less than the radius (to prevent unnecessary loops through closed curves), and if the curve crosses the window given by the minimum/maximum values. It is often desirable to specify extreme values for npoints or the window size.

6.6. Close and Reopen the Input File

This task enables to suspend the program execution, edit or replace the *Parameters*, and resume execution either on a multi-window workstation or on a terminal under Unix. The input is as follows:

> itask=-1   to indicate the required task

The program will close the file *Parameters* and pause until continuation is requested. During this time, the file can be changed. After continuation, the new *Parameters* will be read starting at the top.

7. The Real Version

The real version of *linear_x* performs the same functions as the complex version yet permits some simplifications and higher efficiency. The physics files *common.ins* and *bstate.ins* are unchanged. There is no *complex.ins*, and *vector.ins* neither provides nor accepts complex data. In the *Definitions*, all parameters are real (ipar2 is not read). In the *Parameters* for itask=0, iev1 characterizes the eigenvalue. Note that the spectrum may contain complex eigenvalues. Only real eigenvalues can be handled by the other tasks. For the local procedures, itask=1, 2, only iev1 is read. The input for table, itask=3, is unchanged. For curves, itask=4, the parameter iev3 for the normal direction is absent. Source files with the same name in the real and complex version may be different.

8. Installation

The installation procedure is easy for Unix systems. To conform with the original, make and use a new directory

> *mkdir w.linear*
> *cd w.linear*
> *tar xvf /dev/tape*

to read the tape (cartridge) where */dev/tape* stands for the proper device. There will be three new directories: w.doc with this and other text (to be printed with eqn linear.txt | ptroff -ms on a Postscript printer), w.real with the real version and examples, and w.complex with the complex

version and examples. Edit the Makefiles in w.real and w.complex (especially the FFFLAGS for f77, CPFLAGS for cpp, and LDFLAGS for ld to reflect your system if necessary. The C preprocessor cpp is used since include statements and conditional compilation are not standardized and sometimes missing in Fortran. Note the setting of CASE to the specific directory (here w.example) that contains the physical files, Definitions, and Parameters. Run

make

There may be some warnings (e.g. for loops that are not executed if NEQU=1). If no errors occur, you will find the executable code in the proper subdirectory (here w.example). The output of the C preprocessor (complete set of Fortran files) will be in w.code. The command

make clean

removes w.code, the object programs, and prompts whether you want to delete the executable code. Execute

cd w.example
linear.x

If the code runs to completion, you should find all the files given in the subdirectory w.results, with identical content.

I recommend to prepare new applications in directories on the same level as w.examples and to set CASE in the Makefile properly. The work on a specific problem would then be performed in a single directory under either w.real or w.complex.

If you work on a non-Unix system, you may replace the cpp directives (with the # sign in column 1) by other directives such as the INCLUDE statement (e.g. VAX-VMS Fortran). Directives for conditional compilation such as #ifdef CRAY can be replaced or commented by hand.

9. Examples

Two examples are included to illustrate the use of the real and the complex version. These examples show a variety of applications of the code that will not be discussed in detail. You may consider keeping the examples for later reference.

For the real version, the example is the small-gap approximation to the Taylor-Couette problem for axisymmetric disturbances in the form

$$(D^2 - \alpha^2 - \sigma)(D^2 - \alpha^2)u + Ta\,\alpha^2 g(y)v = 0 \qquad (3)$$

$$-u + (D^2 - \alpha^2 - \sigma)v = 0 \qquad (4)$$

where $g(y) = 1 + (\omega - 1)y$ with $\omega = 0$ for a fixed outer cylinder, and Ta, α, and σ are the Taylor number, wavenumber, and growth rate, respectively. The boundary conditions are

$$u = Du = v = 0 \quad \text{at} \quad y = 0, 1 \qquad (5)$$

The example for the complex version is the Orr-Sommerfeld equation for three-dimensional disturbances

$$[(D^2 - \gamma - iRe\{\alpha U - \omega\})(D^2 - \gamma) + i\alpha Re(D^2 U)]v = 0 \qquad (6)$$

with the boundary conditions

$$v = Dv = 0 \quad \text{at the boundaries} \tag{7}$$

where $\gamma = \alpha^2 + \beta^2$, α and β are streamwise and spanwise wavenumbers, respectively, Re is the Reynolds number, and ω the frequency. The basic flow is set to plane Poiseuille flow, $U(y) = 1 - y^2$, between boundaries at $y = \pm 1$. For the assignments to PVEC ($\cdots$, 0), it is useful to rewrite eq. (6) in the form

$$D^4v + [-2\gamma - iRe\{\alpha U - \omega\}]D^2v + [\gamma(\gamma + iRe\{\alpha U - \omega\}) + iRe\,\alpha(D^2U)]v = 0 \tag{8}$$

The equation is written in terms of the complex frequency ω but can be changed easily to the complex phase velocity $c = \omega/\alpha$. We consider β as real while α is in general complex. Hence, we can use the local procedure for both temporal and spatial growth. However, we can use the global procedure only to obtain the spectrum of temporal eigenvalues ω.

The wavenumber α appears nonlinearly in eq. (8), more precisely, up to the fourth power, α^4. To obtain a spectrum of spatial eigenvalues α, eq. (8) must be rewritten in form of four equations that are linear in α, e.g.

$$D^4v_1 + (-2\beta^2 + iRe\,\omega)D^2v_1 + \beta^4v_1 + (-iReUD^2v_2 + iRe\,(D^2U)v_2 \tag{9a}$$

$$- 2D^2v_3 + (2\beta^2 - iRe\,\omega)v_3 + iReUv_4 + \alpha v_4 = 0$$

$$\alpha v_1 - v_2 = 0 \,, \quad \alpha v_2 - v_3 = 0 \,, \quad \alpha v_3 - v_4 = 0 \,, \tag{9b,c,d}$$

where $v_1 = v$. This form is not unique since α-independent terms in v_n, $n > 1$, can be converted into α-dependent terms in v_{n-1} by using eqs. (9b, c, d). The system has now NEQN=4 and four variables v_n with identical boundary conditions (and symmetries). Obviously, solving this larger system (9) is more costly than solving the equivalent equation (8).

10. Availability

The complete code of about one half mega-byte is available as tarfile via ftp, on cartridge tape (Apollo, Sun, HP, SGI-150MB), or 5 1/4 inch floppy (Apollo). A second version with straight ASCII files for non-Unix systems is in preparation. To obtain a copy of the code, contact me by mail or E-mail: tht@apollo.eng.ohio-state.edu.

11. Acknowledgment

Appendix B

Appendix B

"Theory of Instability and Transition"

- Position Paper -
by Th. Herbert

Proc. ICASE/NASA Workshop on Stability and Transition
May - June 1989, Hampton, Virginia.
To be published by Springer Verlag.

THEORY OF INSTABILITY AND TRANSITION

Thorwald Herbert

Department of Mechanical Engineering
Department of Aeronautical and Astronautical Engineering
The Ohio State University
Columbus, Ohio 43210, U. S. A.

1. Introduction

The theory of instability and transition has seen remarkable progress over the past decade. For certain classes of flows such as the Bénard and Taylor problem, the progress is largely due to the application of new analytical techniques and the ability to describe the dynamics by relatively simple amplitude equations. This analytical work is supported by current experimental and computational studies.

The attempt to model, simplify, and analyze the dynamics of through-flow systems, especially boundary and mixing layers, with similar techniques has not yet succeeded. Some of the reasons are the lack of a true Reynolds number (as in boundary and mixing layers), the unavailability of nonlinear equilibrium motions (in boundary and mixing layers, pipe flow, plane Couette flow), and the nonlinear subcritical instability and consequent "snap-through" transition in the few remaining prototype flows (e.g. plane Poiseuille flow). Once the flow becomes unstable, it develops through some stages of distinguished character into a turbulent flow without settling into any regular motion or stable equilibrium. Nevertheless, equilibrium states, bifurcation points, and symmetry breaking have been revealed for plane Poiseuille flow and these results have strongly influenced the theoretical developments for other flows, in particular for boundary layers. Owing to the complexity of the dynamical equations, the theoretical work on through-flow systems has strong computational aspects and is in many cases closely related to spectral simulations of nonlinear instability and transition.

New results have been obtained and methods of analysis have been developed for various classes of flows that permit mathematical rigor:

- Parallel flows with velocity vector $\mathbf{V} = (U(y), 0, W(y))$ or $\mathbf{V} = (U(y), 0, 0)$, such as plane Poiseuille flow. Here, U is in the streamwise x direction.

- 3D flows with $\mathbf{V} = (U, V, W)$ and $\mathbf{V} = \mathbf{V}(y, z)$, as in rectangular ducts, or $\mathbf{V} = \mathbf{V}(r, \phi)$, as in curved or elliptic pipes.

- Periodic flows with periodicity in different variables.

The class of periodic flows has found broad interest owing to their frequent occurrence in practical applications and as a source of parametric secondary instabilities. The main groups studied are:

- Time periodic with $\mathbf{V} = (U(y, t), 0, 0)$ and $U(y, t) = U(y, t + \lambda_t)$ (Davis 1976),

- Periodic in the cross-stream direction with $\mathbf{V} = (U(y), 0, 0)$ and $U(y) = U(y + \lambda_y)$ (Gotoh & Yamada 1986),

- Periodic in the streamwise direction with $\mathbf{V} = (U(x, y), V(x, y), 0)$ and $\mathbf{V}(x, y) = \mathbf{V}(x + \lambda_x, y)$.

The last group incorporates 2D equilibrium states in parallel flows as they develop in the nonlinear stage of primary instability (Orszag & Patera 1980, Herbert 1981, 1983, Nagata & Busse 1983,

Pierrehumbert & Widnall 1982). Even the states associated with traveling waves are steady in a Galilean frame that moves with the phase velocity of the waves.

With appropriate approximations, new analytical and numerical tools have also been developed for the technologically important class of weakly nonparallel flows where the basic flow involves the boundary layer approximation (Hall 1983, Herbert & Bertolotti 1987). The local approach (leading to ordinary differential equations) is complemented or replaced by solving parabolic partial differential equations for given initial conditions. Besides nonparallelism, the nonlinear evolution of the disturbance field can be studied. The need for initial conditions, however, poses a new challenge to clarify the receptivity issue.

Many of the tools developed and established for incompressible flows are currently ported to tackle the stability of compressible flows. In this area, stability theory has barely progressed beyond the classical linear analysis, and the physical mechanisms of instability still await clarification and deeper understanding.

2. Weakly and Strongly Nonlinear Theories

The charge to this panel is to place emphasis on the strongly nonlinear area of theory. Considered that the phenomena under consideration are governed by the Navier-Stokes equations in more or less complex form, one has to compromise. Direct numerical simulation is feasible but more a replacement for laboratory experiments, not theory. Asymptotic theories for large Reynolds (or other) numbers lead to simplified equations that allow closed-form solutions (in exceptional cases) or ease numerical solutions to nonlinear problems (see panel discussion, F. T. Smith). These theories based on early asymptotic studies (Lin 1955) enlist impressive results for linear problems and local (e.g. receptivity) phenomena that can be captured within a single asymptotic structure. However, the structures are different for solutions near branch I (triple deck) and branch II (five decks) of the neutral curve. Therefore, studies of physically relevant nonlinear mode interactions (as those causing secondary instability) or the streamwise evolution of the disturbance field seem outside any single structure of the asymptotic theory. Moreover, various phenomena in the transition process critically depend on the combination of physical parameters and may not be accessible to asymptotic methods for high Reynolds numbers.

Linear and "weakly" nonlinear (i.e. perturbation) theories are not as ineffectual as the notation suggests. "It is not the process of linearization that limits insight. It is the nature of the state we choose to linearize about." (E. T. Eady). Moreover, perturbation methods can solve strongly nonlinear problems provided they are rational in the sense of Van Dyke (1975), consider higher-order terms, and are combined with the arsenal of tools for analyzing, improving, and extending the convergence of perturbation series (Van Dyke 1984). The weaknesses of the weakly nonlinear theory are essentially the inappropriate formulation in earlier work (Herbert 1983) and the lack of guidance for the choice of the lowest-order basis. When properly applied, there should be in fact no difference between a weakly nonlinear or perturbation theory, a nonlinear theory, and a truly nonlinear theory. Perturbation methods can be very relevant to obtain insight into the nonlinear transition process.

In the following, we discuss three areas of theoretical/numerical development that contribute to understanding the transition mechanisms, and moreover, provide new means for quantitatively analyzing and predicting transition. The incompressible flow over a flat plate with zero-pressure gradient is chosen as an example while applications range to other shear flows, including three-dimensional and compressible boundary layers.

3. Nonlinear Stability of Nonparallel Flows

Boundary layers, mixing layers, jets, and wakes are interesting subjects to stability studies, but are solutions to the Navier-Stokes equations only within the boundary-layer approximation. Usually, the stability analysis at a fixed streamwise position (and Reynolds number) neglects the streamwise variation and small transverse velocity, and assumes a locally parallel flow. While this assumption can be tolerated for disturbance waves with sufficiently large streamwise wavenumbers α (Herbert & Morkovin 1980), it is incorrect for small wavenumbers, especially for $\alpha = 0$. The most affected disturbances with $\alpha = 0$ are longitudinal vortices, including Görtler vortices, and nonlinear distortions of the mean flow.

For Görtler vortices, the effect of the transverse velocity is of first order, not of order $O(Re^{-1})$ (Herbert 1976). It is necessary, therefore, to pose the stability problem as an initial-boundary-value problem for parabolic partial differential equations (Hall 1983), in essence the 3D boundary-layer equations for a spanwise periodic flow. For initial conditions in the form of traditional normal modes, some features of earlier parallel-flow and weakly-nonparallel-flow results are qualitatively reproduced (Day, Herbert, & Saric 1988), however, the local growth rates and integrated N factors are quite different and depend on the initial conditions. The concept of a branch I of the neutral curve, the traditional go-sign for instability and the integration of N factors, does not carry over to the new approach. Considered that N factors are a cornerstone of transition prediction in engineering practice, theory should not only push forward into virgin territory but also scrutinize all those convenient assumptions that were made along the way.

TS waves with $\alpha > 0$ cannot be described by the boundary-layer equations, but the effect of nonparallelism on the linear stability can be captured by perturbation methods. Earlier work suffers criticism since the perturbation approach is not rational in Van Dyke's sense. Moreover, the approach cannot incorporate nonlinear effects of finite TS amplitude. To overcome these deficiencies, Herbert & Bertolotti (1987) introduce a multiplicative decomposition of the waves in a nonparallel flow into a strictly periodic wave function and an amplitude function. Within the boundary-layer approximation, the amplitude function is governed by a parabolic differential equation that can be solved by a marching scheme for given initial wavenumber and initial amplitude distribution. The streamwise change of the complex wavenumber can be extracted from the amplitude function. A method to obtain the local solution to the stability problem similar to earlier work has been derived without further approximation. This method requires simultaneously solving for the local wavenumber, amplitude function, and streamwise amplitude variation, thus solving for all terms of order $O(Re^{-1})$ at once.

The parabolized stability equations (PSE) permit accurate and very efficient calculation of spatial growth rates and N factors, but moreover, they offer various capabilities not previously available. The equations contain both the unsteady boundary-layer equations and the Orr-Sommerfeld equation as special cases, and therefore govern the link between their solutions (Goldstein 1983) without using matched asymptotic expansions. This link is key to the receptivity for sound. The PSE can maintain nonlinear terms and describe the evolution of harmonics and mean flow distortion. The PSE can also be utilized to analyze mode interactions and the linear and nonlinear stages of secondary instability without the need for a downstream boundary condition.

The results of both local and marching solution of the PSE for linear TS waves agree and largely confirm Gaster's (1974) results. In contrast to the findings of Saric & Nayfeh (1977) and Smith (1979), the incorporation of nonparallel effects does not improve the agreement of the neutral curve with the experimental data. The neutral curve shown by Saric & Nayfeh is based on a different measure for growth than that used in the experiments. We conclude that the disagreement between

theoretical and experimental results is caused by experimental inaccuracies combined with the sensitivity of the problem (see panel discussion, W. S. Saric). The results of the marching scheme for the nonlinear development of TS waves are consistent with the weakly nonlinear parallel-flow results of Herbert (1974) and Itoh (1974), and in perfect agreement with numerical solutions to the Navier-Stokes equations (Bertolotti, Herbert, & Spalart 1989).

4. Linear Secondary Instability

Significant progress in the analysis of the transition process has been achieved by the theory of linear secondary instability of shear flows (Bayly, Orszag, & Herbert 1988, Herbert 1988). The concept of a three-dimensional secondary instability parametrically excited by the primary TS waves in a boundary layer was first used in a largely unnoticed paper by Maseev (1968) and revived by Herbert & Morkovin (1980).

In a coordinate system moving with the wave speed, a parallel flow with a superposed wave of fixed amplitude is strictly periodic and its linear stability is governed by a Floquet system of differential equations with periodic coefficients. General form, properties, and classification of disturbances can be derived with mathematical rigor. For cases like the 2D periodic equilibrium motions in a plane channel that are associated with nonlinear TS instability, the "primary instability," parametric resonance can lead to "secondary instability" with respect to a variety of 2D or 3D, subharmonic, fundamental (peak-valley splitting), or combination modes. The physical mechanism of this instability rests on tilting and stretching of vortices periodically arranged by the primary wave and is essentially of inviscid nature (Bayly, Orszag, & Herbert 1988). Accordingly, the growth of secondary modes on a convective scale can be much stronger than the slow, viscous growth of TS amplitudes.

Physical mechanism and classes of secondary modes are common to a wide variety of unstable flows. Unstable boundary layers exhibit the same types of secondary instabilities (Herbert 1988). For boundary layers, applicability of the Floquet analysis requires some approximations: the parallel-flow assumption and the neglect of the TS-amplitude growth. Both these approximations are well justified in regions of strong secondary disturbance growth. (These approximations need scrutiny, however, for other primary disturbances such as Görtler vortices or cross-flow vortices.) With the new concepts for incorporating streamwise changes discussed above, the assumptions of earlier work can be relaxed.

The Floquet theory of secondary instability provides convincing explanations for numerous puzzling observations and establishes a framework for quantitatively studying the later stages of transition. Formal and numerical results are in encouraging agreement with detailed experimental data for subharmonic modes (Kachanov & Levchenko 1984) and fundamental modes (Klebanoff, Tidstrom, & Sargent 1962, Cornelius 1985) in the Blasius flow. The predicted characteristics of combination modes are consistent with the scarce set of observations.

Combined with numerical results, the theory also permits asymptotic studies that provide guidance for properly modeling the primary-wave interaction in weakly nonlinear theories. Craik's (1971) resonant triad appears as a special case of subharmonic resonance as the TS amplitude tends to zero. Other weakly nonlinear theories have not been found relevant to the explanation or quantitative analysis of the secondary instability. Smith & Stewart (1987) have developed an asymptotic theory of the subharmonic resonant-triad interaction based on a triple-deck structure. Their results for the experimental conditions of Kachanov & Levchenko disagree with those provided by the Floquet theory (and the experiment) in various aspects such as the wave angle, growth rate, and streamwise variation of the growth rate. The discrepancies cannot be removed by incorporating the

nonlinear interaction between TS wave and 3D subharmonic mode. A possible explanation may be the difference in the physical mechanisms. In the experiments and in the Floquet theory, the subharmonic secondary instability originates from the interaction of an upper-branch TS wave with a lower-branch subharmonic wave, while the triple-deck structure is appropriate only for lower-branch waves.

Both temporal and spatial growth concepts have been pursued with the Floquet theory. Other than in Gaster's transformation for primary disturbances, the leading term of the temporal-to-spatial transformation of growth rates for secondary disturbances is the phase speed of the primary wave and higher terms are small. Hence, transformed temporal and directly calculated spatial growth rates are very similar. This result explains some of the striking similarities between temporal Navier-Stokes simulations and spatial experiments. The results of the Floquet theory have not only stimulated numerous transition simulations but agree with their results and permit their interpretation up to the stage where nonlinear coupling between TS wave and 3D secondary modes comes into play. The theory yet bears the advantage of not being bound to a pre-selected computational domain that restricts the wavenumbers of the 3D disturbance field. The work of Spalart & Yang (1987) with a large spanwise domain is a notable exception.

5. Nonlinear Wave Interaction

In the absence of a nonlinear interaction of the 3D secondary modes with the primary TS wave, the secondary modes decay as their parametric excitation fades away. Analysis of the energy balance between mean flow, 2D wave, and 3D waves shows, however, that the 3D wave may feed energy into the 2D field (Herbert 1988). This contribution to the 2D field increases quadratically with the amplitude of the 3D mode and may halt the decay of the primary wave, thus leading to a feedback loop for self-sustained growth of both 2D and 3D disturbance field. A more detailed analysis of the processes involved (Crouch & Herbert 1989) is based on a perturbation method expanding simultaneously in the amplitudes of primary and secondary modes to maintain the mechanism of parametric excitation. Subharmonic and peak-valley-splitting route to transition turn out to be quite distinct in their sequence of events. In both cases, however, the nonlinear interaction can lead to either an ultimate decay of the disturbance field or to a simultaneous growth of 2D and 3D components. The threshold conditions for such simultaneous growth can be exploited to predict breakdown and transition in a given disturbance environment (Herbert & Crouch 1989).

The results for fundamental modes are in close agreement with the experimental data of Cornelius (1985) up to the stage where an increasing number of spikes heralds the breakdown of the laminar flow. Peak-valley splitting can lead to breakdown only if the 3D disturbance reaches a threshold amplitude upstream of branch II. In contrast, subharmonic modes can cause self-sustained growth even downstream of branch II as observed by Kachanov & Levchenko (1984) and Corke & Mangano (1987). The strong growth of the 2D component is owing to a purely forced 3D-3D interaction while the TS amplitude reaches an almost constant level. The two main contributions to the 2D component can be clearly identified in the velocity profiles at different streamwise positions measured by Kachanov, Kozlov, & Levchenko (1977). The theoretical results are in good agreement with direct simulations of transition, although the number of Fourier modes in the streamwise and spanwise direction is relatively small. The ability to represent the essence of the transition process with crude Fourier approximations was also noted by Rozhdestvensky & Simakin (1984) and Kleiser & Gilbert (1989).

6. Future Directions

Building on the encouraging results of the theoretical concepts, present work aims at their integration into an efficient and reliable tool to analyze a broader variety of flows and wave interactions, especially those affected by nonparallelism. To further develop understanding and predictive capabilities for transition, emphasis will be on

- Receptivity, in particular leading-edge receptivity, to provide the relation between environment and the initial and boundary conditions for the transition analysis.

- Breakdown and evolution of small scales, to provide the link between transitional and turbulent flows.

- Compressible flows, to gain insight, predictive capabilities, and support for numerical simulations.

In view of the difficulties of gathering detailed experimental data at high Mach numbers under realistic conditions, the development of reliable theoretical and computational methods for studies on transition in compressible flows has high priority.

7. References

Bayly, B. J., Orszag, S. A., and Herbert, Th. (1988) "Instability mechanisms in shear flow transition," *Ann. Rev. Fluid Mech.,* Vol. 20, pp. 359-391.

Bertolotti, F. P., Herbert, th., and Spalart, P. R. (1989) "On the Stability of the Blasius Boundary Layer.," *J. Fluid Mech.* In preparation.

Corke, T. C. and Mangano R. A. (1987) "Transition of a boundary layer: controlled fundamental-subharmonic interactions," in Proc. IUTAM Symposium on Turbulence Management and Relaminarization, Ed. H. W. Liepmann and R. Narasimha, Springer-Verlag.

Cornelius, K. C. (1985) "Three dimensional wave development during boundary layer transition," Lockheed Georgia Research Report LG85RR0004.

Craik, A. D. D. (1971) "Nonlinear resonant instability in boundary layers," *J. Fluid Mech.,* Vol. 50, pp. 393-413.

Crouch, J. D. and Herbert, Th. (1989) "Nonlinear evolution of secondary instabilities in boundary layers," *J. Fluid Mech.* In preparation.

Davis, S. H. (1976) "The stability of time-periodic flows," *Ann. Rev. Fluid Mech.,* Vol. 8, pp. 57-74.

Day, H. P., Herbert, Th., and Saric, W. S. (1988) "Comparing local and marching analysis of Görtler instability," *AIAA J.* Submitted for publication.

Gaster, M. (1974) "On the effects of boundary-layer growth on flow stability," *J. Fluid Mech.,* Vol. 66, pp. 465-480.

Goldstein, M. E. (1983) "The evolution of Tollmien-Schlichting waves near a leading edge," *J. Fluid Mech.,* Vol. 127, pp. 59-81.

Gotoh, K. and Yamada, M. (1986) "Stability of spatially periodic flows," in Encyclopedia of Fluid Mechanics, pp. 589-610, Gulf Publ. Co., Houston.

Hall, P. (1983) "The linear development of Görtler vortices in growing boundary layers," *J. Fluid Mech.,* Vol. 130, pp. 41-58.

Herbert, Th. and Morkovin, M. V. "Dialogue on bridging some gaps in stability and transition research," in Laminar-Turbulent Transition, Ed. R. Eppler and H. Fasel, pp. 47-72, Springer-Verlag.

Herbert, Th. (1974) "Über endliche Amplituden periodischer Störungen der Grenzschicht an der ebenen Platte," Deutsche Luft- und Raumfahrt, DLR FB 74-53. (Engl. Translat.: European

Space Agency ESA TT-169, 1975)

Herbert, Th. (1976) "On the stability of the boundary layer along a concave wall," *Arch. of Mech.*, Vol. 28, p. 1039.

Herbert, Th. (1981) "A secondary instability mechanism in plane Poiseuille flow," *Bull. Am. Phys. Soc.*, Vol. 26, p. 1257.

Herbert, Th. (1983) "Secondary instability of plane channel flow to subharmonic three-dimensional disturbances," *Phys. Fluids*, Vol. 26, pp. 871-874.

Herbert, Th. (1988) "Secondary instability of boundary layers," *Ann. Rev. Fluid Mech.*, vol. 20, pp. 487-526.

Herbert, Th. and Bertolotti, F. P. (1987) "Stability analysis of nonparallel boundary layers," *Bull. Am. Phys. Soc.*, Vol. 32, p. 2079.

Herbert, Th. and Crouch, J. D. (1989) "Threshold conditions for breakdown of laminar boundary layers," in Proc. IUTAM Symposium on Laminar-Turbulent Transition, Ed. R. Michel and D. Arnal, Toulouse, France.

Itoh, N. (1974) "Spatial growth of finite wave disturbances in parallel and nearly parallel flows, Part 2.," *Trans. Japan Soc. Aeron. Space Sci.*, Vol. 17, pp. 175-186.

Kachanov, Yu. S. and Levchenko, V. Ya. (1984) "The resonant interaction of disturbances at laminar-turbulent transition in a boundary layer," *J. Fluid Mech.*, Vol. 138, pp. 209-247.

Kachanov, Yu. S., Kozlov, V. V. and Levchenko, V. Ya. (1977) "Nonlinear development of a wave in a boundary layer," *Izv. AN USSR, Mekh. Zhidk. i Gaza*, Vol. 3, pp. 49-53. (In Russian)

Klebanoff, P. S., Tidstrom, K. D., and Sargent, L. M. (1962) "The threedimensional nature of boundary-layer instability," *J. Fluid Mech.*, Vol. 12, pp. 1-34.

Kleiser, L. and Gilbert, N. (1989) "Simulation of transition to turbulence," in Proc. 1989 Newport Conference on Turbulence, Newport, RI. To be published.

Lin, C. C. (1955) *The Theory of Hydrodynamic Stability*, Cambridge University Press.

Maseev, L. M. (1968) "Occurrence of three-dimensional perturbations in a boundary layer," *Fluid Dyn.*, Vol. 3, pp. 23-24.

Nagata, M. and Busse, F. M. (1983) "Three-dimensional tertiary motions in a plane shear layer," *J. Fluid Mech.*, Vol. 135, pp. 1-28.

Orszag, S. A. and Patera, A. T. (1980) "Subcritical transition to turbulence in plane channel flows," *Phys. Rev. Lett.*, Vol. 45, pp. 989-993.

Pierrehumbert, R. T. and Widnall, S. E. (1982) "The two- and three-dimensional instabilities of a spatially periodic shear layer," *J. Fluid Mech.*, Vol. 114, pp. 59-82.

Rozhdestvensky, B. L. and Simakin, I. N. (1984) "Secondary flows in a plane channel: their relationship and comparison with turbulent flows," *J. Fluid Mech.*, Vol. 147, pp. 261-289.

Saric, W. S. and Nayfeh, A. H. (1977) "Nonparallel stability of boundary layers with pressure gradients and suction," in Laminar-Turbulent Transition, pp. 6/1-21, AGARD CP-224.

Smith, F. T. (1979) "Nonlinear stability of boundary layers for disturbances of various sizes," *Proc. Roy. Soc. Lond. A*, Vol. 368, pp. 573-589. (And corrections 1980, A371, p. 439).

Smith, F. T. and Stewart, P. A. (1987) "The resonant-triad nonlinear interaction in boundary-layer transition," *J. Fluid Mech.*, Vol. 179, pp. 227-252.

Spalart, P. R. and Yang, K.-S. (1987) "Numerical study of ribbon-induced transition in Blasius flow," *J. Fluid Mech.*, Vol. 178, pp. 345-365.

Van Dyke, M. (1975) *Perturbation Methods in Fluid Mechanics*, Parabolic Press, Stanford, CA.

Van Dyke, M. (1984) "Computer-extended series," *Ann. Rev. Fluid Mech.*, Vol. 16, pp. 287-309.

Appendix C

Appendix C

"Threshold Conditions for Breakdown of Laminar Boundary Layers,"

by Th. Herbert and J. D. Crouch

Threshold Conditions for Breakdown of Laminar Boundary Layers

Thorwald Herbert

Department of Mechanical Engineering
Department of Aeronautical and Astronautical Engineering
The Ohio State University
Columbus, Ohio 43210, U. S. A.

Jeffrey D. Crouch

Laboratory for Computational Physics and Fluid Dynamics
Naval Research Laboratory, Code 4420
Washington, DC 20375, U. S. A.

Summary

A perturbation method based on a simultaneous expansion for primary and secondary modes of instability is used to study the flow field in the later stages of transition. Results of the analysis are in good agreement with experimental data for amplitudes in excess of 5% that cause immediate breakdown. Threshold conditions for sustained growth of subharmonic modes past branch II are calculated. These conditions are presented both in terms of branch II amplitudes and initial amplitudes.

1. Introduction

Boundary-layer experiments show that TS waves of sufficiently small amplitude harmlessly grow and decay. At larger amplitudes, the TS waves cause 3D structures in the form of peak-valley splitting (Klebanoff, Tidstrom, & Sargent 1962), subharmonic modes (Kachanov & Levchenko 1984), or combination modes. The occurrence of these 3D structures is a necessary prerequisite but no assurance for breakdown of the laminar flow. Experimental and computational results (Kachanov & Levchenko 1984, Spalart & Yang 1987) suggest the existence of threshold conditions above which disturbance growth ultimately leads to breakdown.

Onset and evolution of the 3D structures can be modeled as a parametric resonance with the TS wave and are well described by the Floquet theory of linear secondary instability (Herbert 1988). In this linear framework, however, 3D modes ultimately decay since the TS wave fades away downstream of branch II. Therefore, breakdown must originate from a nonlinear interaction between 3D modes and TS waves at certain levels of their amplitudes. This interaction will change both the 2D and 3D disturbance field and dictate either the decay of the modes or their continued growth toward the breakdown of the laminar flow.

To analyze the nonlinear 2D-3D interaction, it is necessary to permit changes to the mean flow and the 2D mode while maintaining the parametric secondary instability. This latter requirement precludes application of the conventional weakly nonlinear models which

were not yet successful in describing the secondary instability. We have developed an elaborate perturbation scheme based on a simultaneous expansion in primary and secondary modes of instability (Crouch & Herbert 1986, Crouch 1988). The decomposed flow field reveals intricate details of the interaction process unaccessible to experiments and computer simulations. We outline the perturbation approach and present some of the basic results with emphasis on the threshold phenomena.

2. Perturbation Analysis

We consider the stability of the Blasius boundary layer under the parallel flow assumption. All quantities are nondimensionalized using the outer velocity, U_∞, and the reference length $\delta_r = (\nu x/U_\infty)^{1/2}$ which results in the Reynolds number $R = U_\infty \delta_r/\nu = (R_x)^{1/2}$. The flow is governed by the Navier-Stokes equations which we write in the form of a generalized nonlinear Squire's equation

$$(\frac{1}{R}\nabla^2)\frac{\partial\eta}{\partial z} - \frac{\partial}{\partial t}\frac{\partial\eta}{\partial z} - \frac{\partial}{\partial z}(v\cdot\nabla)\,\eta + \frac{\partial}{\partial z}(\omega\cdot\nabla)\,v = 0 \ , \tag{1}$$

and Orr-Sommerfeld equation

$$(\frac{1}{R}\nabla^2)\,\nabla^2\,v - \frac{\partial}{\partial t}\,\nabla^2\,v - \frac{\partial}{\partial x}(v\cdot\nabla)\,\zeta$$

$$+ \frac{\partial}{\partial x}(\omega\cdot\nabla)\,w + \frac{\partial}{\partial z}(v\cdot\nabla)\,\xi - \frac{\partial}{\partial z}(\omega\cdot\nabla)\,u = 0 \ , \tag{2}$$

with the boundary conditions

$$u = v = w = 0 \quad at \quad y = 0 \ , \tag{3}$$

$$u \to 1 \ , \ w \to 0 \quad as \quad y \to \infty \ , \tag{4}$$

where $\omega = \nabla \times v = (\xi,\eta,\zeta)$ and $v = (u,v,w)$.

To examine the evolution of disturbances within the boundary layer, the velocity is decomposed into

$$v(x,y,z,t) = v_0(y) + v_1(x,y,t) + v_3(x,y,z,t) \ . \tag{5}$$

The function v_0 is the Blasius profile, v_1 is the two-dimensional TS wave, and v_3 contains the 3D secondary mode and 2D as well as 3D interaction components. Following the linear parametric approach, the function v_1 is considered a primary TS instability, i.e. $v_1 \gg v_3$ initially. The self-interaction of the TS wave is neglected since its effects are small compared to the 2D-3D interaction (Crouch 1988). Thus, the solution to the primary instability problem is

$$v_1(x,y,t) = A(t)v_A(x,y) \ . \tag{6}$$

In the absence of any secondary mode, $A(t)$ would grow according to the TS growth rate. To accommodate the feedback from a 3D secondary mode, the TS amplitude is decomposed as $A = A^* + \hat{A}$ where $A^* \gg \hat{A}$. The component A^* is temporarily assumed constant when calculating the secondary and interaction modes v_3. This component provides the parametric forcing for the secondary instability. To capture the effects of the secondary

mode on A, the component $\hat{A}$ evolves according to the third-order Landau equation

$$\frac{d\hat{A}}{dt} = a_A \hat{A} + a_{B^2} B^2 + a_{AB^2} \hat{A} B^2 \; . \tag{7}$$

The first term describes pure TS growth while the second term gives the modification owing to resonance with a 3D self-interaction term of amplitude B^2. The third term describes the effect of this 2D field at the next order.

Substituting eqs. (6) and (7) for v_1 into eqs. (1) - (4) provides the governing equations for v_3. The third order expansion for v_3 is

$$
\begin{aligned}
v_3(x,y,z,t) = &[B \; v_B(x,y) + \hat{A}B \; v_{AB}(x,y) + B^3 \; v_{B^3_1}(x,y)] \; 2\cos\beta z \\
&+ [B^2 \; v_{B^2_0}(x,y) + \hat{A}B^2 \; v_{AB^2_0}(x,y)] \\
&+ [B^2 \; v_{B^2_2}(x,y) + \hat{A}B^2 \; v_{A^3^2_2}(x,y)] \; 2\cos 2\beta z \\
&+ [B^3 \; v_{B^3_3}(x,y)] \; 2\cos 3\beta z
\end{aligned}
\tag{8}
$$

where $\hat{A}$ and B are functions of t. The first-order term $B v_B 2\cos\beta z$ is the 3D secondary mode resulting from the parametric forcing with $A^* v_A$. At second order, v_{AB} modifies v_B due to $\hat{A} v_A$ and $v_{B^2_0}$ modifies v_A due to $B v_B$. In addition, a second harmonic in β is generated, given by $v_{B^2_2}$. At third order, $v_{B^3_1}$ modifies the 3D mode as a result of the 3D self-interaction, while $v_{AB^2_0}$ modifies the 2D component. Also at third order, $v_{AB^2_2}$ appears owing to interaction of the 2D wave with the 3D second harmonic and $v_{B^3_3}$ is the 3D third harmonic. The amplitude growth of the secondary mode is given by

$$\frac{dB}{dt} = b_B \; B + b_{AB} \; \hat{A}B + b_{B^3} B^3 \; . \tag{9}$$

Here b_B is the linear growth rate at the primary amplitude A^*, and b_{AB} describes the modification owing to $\hat{A}$. The total second-order growth rate of B is $b_B + \hat{A} b_{AB}$ which is directly related to the first-order growth rate resulting from a parametric forcing with amplitude $A^* + \hat{A}$.

Introducing the velocity expansion (8) and the Landau equation (9) into the equations for v_3, we obtain sets of equations governing the functions of x,y at each order. The Floquet theory provides each of these functions in the form

$$f(x,y) = \sum_{n=-\infty}^{n=\infty} f_n(y) e^{in\hat{\alpha}x} \quad , \quad \hat{\alpha} = \frac{\alpha}{2} = \frac{\pi}{\lambda_x} \quad , \tag{10}$$

where f_{-n} is the complex conjugate of f_n. The modes with n even and n odd decouple into two distinct classes of modes designated as fundamental and subharmonic modes, respectively (Herbert 1988). Using spectral collocation methods, the equations and boundary conditions governing the functions f_n are converted into an algebraic system. For numerically solving this system, the series (10) is truncated at $|n| \leq 4$ and 20 collocation points are used.

3. Results

The evolution of disturbances for any set of parameters $F = 10^6 \cdot \omega \nu / U_\infty^2$, $b = 10^3 \cdot \beta / R$, and initial values A_0, B_0 of the amplitudes at R_0 is controlled by Landau constants and the corresponding velocity functions. Using the Landau constants at a sequence of locations for $R > R_0$, amplitude curves for A^*, $\hat{A}$, and B can be calculated. In conjunction with the velocity functions, these data provide the physically observable velocity distributions and rms amplitudes (defined as the maximum of the streamwise component). Here we present only a limited set of results in the large parameter space.

3.1 Amplitude Evolution

The early evolution of the 2D mode is described by the linear theory of TS waves. For sufficiently large 2D amplitudes, 3D modes are excited, characterized by $b_B > 0$. Provided the 3D amplitudes remain small, these modes initially grow but decay as the TS wave vanishes. For larger 3D amplitudes of the order $O(B) \approx O(A)$, a nonlinear 2D-3D interaction takes place. The effects of this interaction depend on the 3D mode type (subharmonic or fundamental), the initial amplitudes, and the parameters F, b, and R.

3.1.1 Subharmonic Modes

For subharmonic modes, the Landau constant a_{B^2} is positive, $a_{B^2} > 0$, in some region of F, b, R, and A. Interactions in this region lead to a continued slow growth of A. The third-order constant a_{AB^2} is positive in a similar region, thus reinforcing the second order effects. For higher frequencies (above $F \approx 45$) the region where $a_{B^2} > 0$ extends to Reynolds numbers R downstream of branch II. Sufficiently large 3D amplitudes lead to sustained growth of the 2D wave, characterized by $dA/dt > 0$ past branch II.

Figure 1 shows the evolution of the components A^*, $\hat{A}$, B, and the associated physical amplitudes of the 2D and subharmonic components. These results are for a second-order analysis at $F = 124$, $b = 0.33$. The Reynolds number at which sustained growth initiates is designated R_s. The dramatic increase in the 2D amplitude which was also observed in simulations (Spalart & Yang 1987) results from the B^2 component. During the decay of A, the 3D amplitude experiences a decrease in growth rate. Figure 2 shows a comparison of the amplitude curves with the experiment of Corke & Mangano (1987). The theory correctly predicts the change in the subharmonic growth rate. The results are in good agreement until breakdown occurs.

The principal effects at third order occur at larger amplitudes (above $B \approx 5\%$). At this order, the magnitude of A during the period of continued slow growth is larger than at second order, while the difference between A and the total 2D amplitude is smaller. As a result of $b_{B^3} < 0$, the 3D mode ultimately saturates. However, the value of R_s does not significantly change between second- and third-order results.

3.1.2 Peak-Valley Splitting

For fundamental modes, the constant a_{B2} is negative, $a_{B2} < 0$ (for all conditions F, b, R we considered). However, the third-order constant a_{AB2} is positive over a significant region of F, b, R which extends past branch II. With a_{B2} large and negative, interactions at small amplitudes lead to decay of both modes downstream of branch II. Only the larger growth rates a_A at lower frequencies permit continued growth of the modes after onset of the interaction. For larger amplitudes, the growth continues past branch II and at higher frequencies since $a_{AB2} > 0$.

The differences between second-order and third-order results are more significant than for subharmonic modes. At second order, the amplitude curves at the peak and valley positions are very similar to the first-order results. The third-order results, however, are quite different, especially for larger amplitudes as shown in figure 3. At first (and second) order, the amplitudes at peak and valley grow concurrently to very large values, while they saturate at different levels when third-order terms are considered. Figure 4 compares the third-order results with experimental data of Cornelius (1985) for $F = 64.4$, $b = 0.44$. The theory is in good agreement up to the single-spike stage. The difference in saturation levels between the theory and experiment may be a result of the limited number of modes included in the theory.

3.2 Threshold Conditions

Although the breakdown process is highly nonlinear and probably involves some tertiary mechanisms for the generation of small scales, its initiation is clearly linked to the nonlinear evolution of secondary instabilities. The growth of TS waves occurs on a slow viscous time scale over a relatively large streamwise distance. Secondary instabilities, on the other hand, grow on a fast convective time scale. Starting at amplitudes much smaller than the TS wave, secondary modes can reach the same order of magnitude within a fraction of the region of TS growth. The occurrence of the nonlinear 2D-3D mode interaction then produces radical changes over a yet smaller streamwise distance. When the interaction favors continued growth, breakdown follows immediately. Therefore, predicting the conditions for this interaction is "awfully close to predicting breakdown and transition" (M. V. Morkovin).

For fixed values of F and β, breakdown can be initiated at different R locations depending on the initial disturbance amplitudes. As the initial amplitudes decrease, the breakdown location moves downstream, until for sufficiently small values the disturbances harmlessly fade away. The threshold conditions are specified in terms of the smallest disturbance amplitudes that will ultimately result in breakdown. For small 2D amplitudes, subharmonic modes have larger growth rates than fundamental modes and thus are the preferred route to breakdown (Herbert 1988). Subharmonic interactions at small amplitudes are well described at second-order. If 3D amplitudes are also small, the 2D-3D interaction occurs downstream of branch II. Thus the threshold conditions represent a demarcation between amplitudes leading to sustained growth, and those leading to decay past branch II.

At lower frequencies (below $F \approx 45$), the region of interaction leading to continued growth is upstream of, or near, branch II. For these frequencies, small amplitudes can lead to breakdown just downstream of branch II without (or before) satisfying $dA/dt > 0$. This development results from the weak 2D decay yet strong 3D growth which enables the 3D wave to reach a high amplitude sufficient for initiating breakdown. Threshold conditions at these frequencies must account for the actual magnitude of the 3D amplitude, not only the conditions for sustained growth.

Higher frequencies have a region of interaction favorable to sustained growth which extends well beyond branch II. Low amplitude interactions lead to decay, while larger amplitudes cause $dA/dt > 0$ past branch II. Figure 5 shows the Reynolds number for sustained growth, R_s, plotted against the subharmonic amplitude at branch II for different 2D amplitudes at branch II. This figure is for $F = 124$, $b = 0.33$. For large subharmonic amplitudes, R_s becomes increasingly independent of the amplitude values. Associated with each 2D amplitude is a minimum (or threshold) subharmonic amplitude, below which sustained growth does not occur. A plot of these branch II threshold amplitudes is given in figure 6 along with values calculated for $F = 64.4$, $b = 0.17$. Amplitudes to the right of the curves lead to sustained growth while amplitudes to the left ultimately decay. The effect of frequency is only to shift the curve slightly. Using the appropriate N-factors, these curves are projected to the initial amplitudes that are given in figure 7. This presentation shows the critical link between breakdown and the background disturbance field. The difference in frequency results in a shift by an order of magnitude of the initial amplitudes necessary for breakdown.

4. Conclusions

By revealing the details of the 2D-3D mode interaction, the analysis contributes toward clarifying the picture of transition. For peak-valley splitting at low amplitudes, the 3D mode has a damping effect on the 2D mode. Continued growth of the disturbance modes owing to nonlinear interaction occurs only upstream of branch II and only for lower frequencies. For larger amplitudes, the 3D mode can lead to a continued slow growth of the 2D wave, thus allowing continued growth past branch II and at higher frequencies.

Subharmonic modes at higher frequencies can cause sustained growth of both the 2D and 3D mode past branch II. Evaluating the initial amplitudes necessary for sustained growth provides a threshold condition for breakdown. Calculated thresholds change very little for different frequencies when expressed in terms of branch II amplitudes. In terms of initial amplitudes, the threshold values change by an order of magnitude between $F = 124$ and $F = 64.4$. For lower frequencies, the subharmonic mode becomes large enough to initiate breakdown without the condition of sustained growth being satisfied. The second order theory provides no clear demarcation for breakdown under these conditions.

T. C. Corke and R. A. Mangano (1987) "Transition of a boundary layer: controlled fundamental-subharmonic interactions," Fluid Dynamics Center Rep. No. 87-1, Illinois Institute of Technology, Chicago, Illinois..

K. C. Cornelius (1985) "Three dimensional wave development during boundary layer transition," Lockheed Georgia Res. Rep. LG85RR0004, Marietta, Georgia..

J. D. Crouch (1988) "The nonlinear evolution of secondary instabilities in boundary layers," VPI & SU, Ph.D. thesis..

J. D. Crouch and Th. Herbert (1986) "Perturbation analysis of nonlinear secondary instabilities in boundary layers," *Bull. Am. Phys. Soc.*, Vol. 31, pp. 1718.

Th. Herbert (1988) "Secondary instability of boundary layers," *Ann. Rev. Fluid Mech.*, Vol. 20, pp. 487-526.

Yu. S. Kachanov, V. V. Kozlov, and V. Ya. Levchenko (1977) "Nonlinear development of a wave in a boundary layer," *Izv. AN USSR, Mekh. Zhidk. i Gaza*, Vol. 3, pp. 49-53. (In Russian)

Yu. S. Kachanov and V. Ya. Levchenko (1984) "The resonant interaction of disturbances at laminar-turbulent transition in a boundary layer," *J. Fluid Mech.*, Vol. 138, pp. 209-247.

P. S. Klebanoff, K. D. Tidstrom, and L. M. Sargent (1962) "The three-dimensional nature of boundary-layer instability," *J. Fluid Mech.*, Vol. 12, pp. 1-34.

P. R. Spalart, and K.-S. Yang (1987) "Numerical study of ribbon-induced transition in Blasius Flow," *J. Fluid Mech.*, Vol. 178, pp. 345-365.

- 8 -
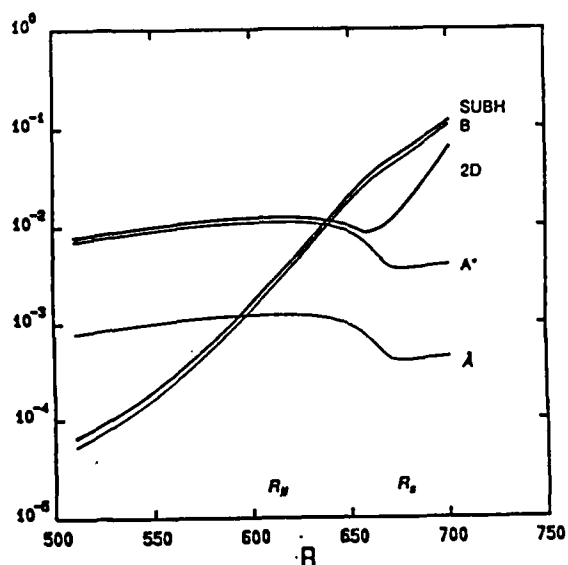
Figure 1. Amplitude growth curves for principal components of subharmonic breakdown ($F = 124$, $b = 0.33$).
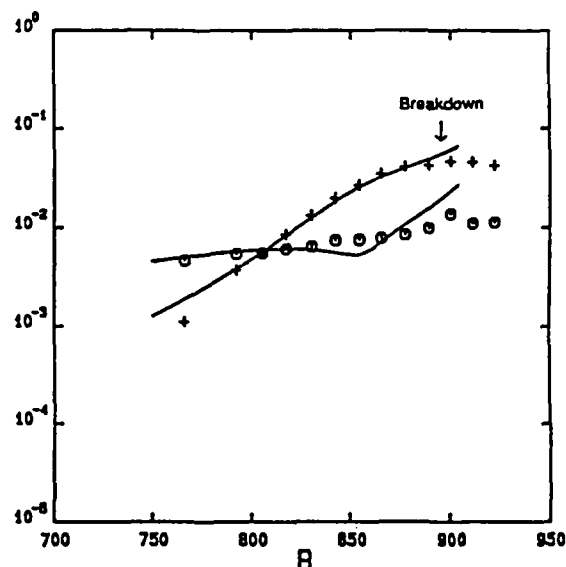
Figure 2. Amplitude growth curves for $F = 82.7$, $b = 0.129$. Comparison between (———) second-order theory and experiment (Corke & Mangano 1987) for (o) 2D and (+) subharmonic modes.
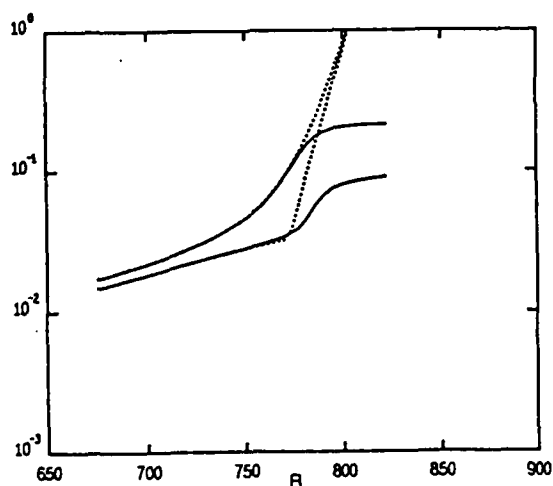
Figure 3. Amplitude growth curves for peak-valley splitting ($F = 64.4$, $b = 0.44$). Comparison between (----) first-order and (———) third-order results.
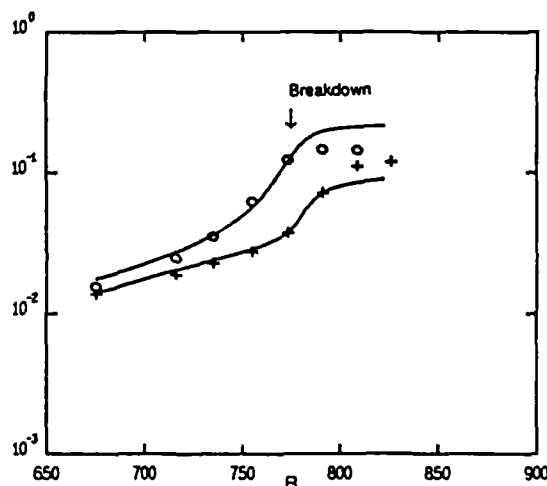
Figure 4. Amplitude growth curves for $F = 64.4$, $b = 0.44$. Comparison between (———) third-order theory and experiment (Cornelius 1985) for (o) peak and (+) valley.

- 9 -
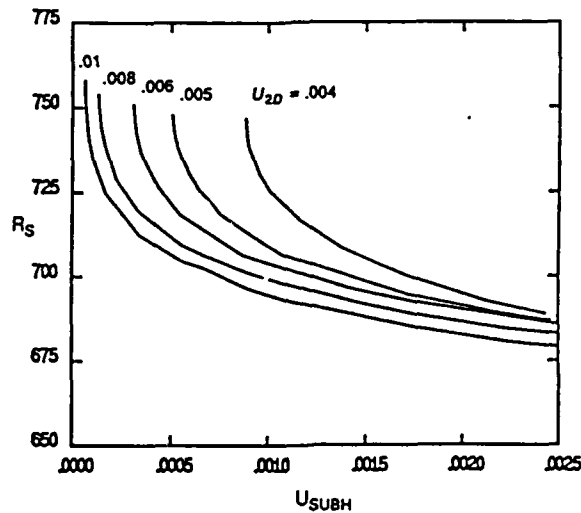
Figure 5. Reynolds number for sustained
growth, R_s, for different branch II amplitudes
($F = 124$, $b = 0.33$).
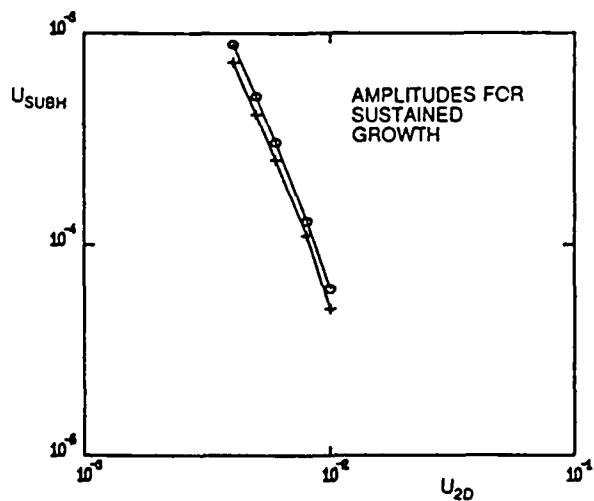
Figure 6. Threshold amplitudes for sustained growth in terms of branch II values at (o) $F = 124$, $b = 0.33$ and (+) $F = 64.4$, $b = 0.17$.
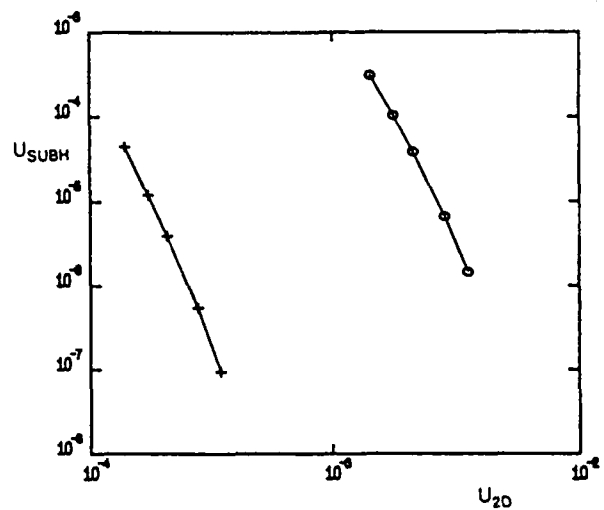
Figure 7. Threshold amplitudes for sustained growth in terms of initial values at (o) $F = 124$, $b = 0.33$ and (+) $F = 64.4$, $b = 0.17$.

Appendix D

Appendix D

"Nonlinear Evolution of Secondary Instabilities in
Boundary-Layer Transition,"

by J. D. Crouch and Th. Herbert

submitted to J. Fluid Mech.

ABSTRACT

Methods of the nonlinear stability theory are applied to analyze the disturbance evolution in the three-dimensional stage immediately preceding the breakdown of the laminar boundary-layer. A perturbation scheme is used to solve the nonlinear equations and to develop a dynamical model for the interaction of primary and secondary instabilities. The first step solves for the two-dimensional primary wave in the absence of secondary disturbances. Once this finite-amplitude wave is calculated, it is decomposed into a basic-flow component and an interaction component. The basic-flow component acts as a parametric excitation for the three-dimensional secondary wave, while the interaction component captures the resonance between the secondary and primary wave. Results are presented in two principal forms: amplitude growth curves and velocity profiles. Our results agree with experimental data and results of transition simulations and, moreover, reveal the origin of the observed phenomena. The method described establishes the basis for physical transition criteria in a given disturbance environment.

1. Introduction

In the process of boundary-layer transition, an unstable ordered state undergoes qualitative changes toward a disordered and chaotic state. Energy extracted from the mean flow is transferred into disturbance waves that consequently grow, interact, and change each other and the mean flow. Although certain qualitative changes necessarily occur, the details of the transition process are not unique.

Studies of boundary-layer transition have revolved around the induction and subsequent growth of disturbances within the boundary layer. Controlled experiments in low-noise environments have shown distinct stages in the development of these disturbances. The first stage is characterized by the onset of instability to two-dimensional TS waves. The dominant mode (most unstable or of highest initial amplitude) then grows within a virtually two-dimensional framework without significant spanwise variations. At some point, however, these TS waves 'give over' to a three-dimensional wave field. Once initiated, spanwise variations grow rapidly and in general lead to the ultimate breakdown of the laminar flow.

The early work of Schubauer & Skramstad (1948) demonstrates the actual presence of TS waves within the laminar boundary layer. For sufficiently small amplitudes, these waves harmlessly grow and decay as the Reynolds number varies downstream. However, if the amplitudes grow to larger values, peak-valley splitting occurs and causes spanwise periodic variations of the flow (Klebanoff et al. 1962). This disturbance field is characterized by a streamwise wavelength equal to that of the TS wave and a spanwise wavelength of the same order. Unlike the TS wave, these three-dimensional disturbances grow rapidly and lead to breakdown within a few TS wavelengths.

Other experiments exhibit a second type of three-dimensional development where the streamwise wavelength is twice that of the TS wave (Knapp & Roache 1968; Kachanov & Levchenko 1982). This subharmonic behavior is observed for intermediate amplitudes of the TS wave. In addition to demonstrating the occurrence of three dimensionality for lower disturbance amplitudes, these experiments reveal the non-uniqueness of the transition process. The experimental results have stimulated intense efforts to find the mechanisms associated with the onset and evolution of the three-dimensional waves.

Most of the theoretical approaches belong to one of two categories, mutually resonant interaction models (Nayfeh 1987) or parametric interaction models (Herbert 1988a). This distinction characterizes how the three-dimensional wave interacts with the two-dimensional wave. The mutually resonant interaction models consist of one or more two-dimensional waves and a pair of three-

dimensional waves that interact through resonance (Nayfeh 1985). The wave amplitudes are considered to be of the same order so that an interaction occurs without any bias given to the two-dimensional wave. At first order, these waves are solutions to the two- or three-dimensional Orr-Sommerfeld equation or Squire's equation. At second order, the two-dimensional/three-dimensional resonance occurs, consisting of interactions between the different Squire and Orr-Sommerfeld modes. The most successful of these models is Craik's resonant triad (Craik 1971). Even though this model requires a priori a particular spanwise wave number for resonance, it yields good results for low-amplitude two-dimensional waves. In addition, Craik's model establishes analytically a subharmonic path to transition. The mutual interaction models seem justified for small two-dimensional amplitudes but fail at larger amplitudes.

The parametric interaction model is based on the preeminence of the two-dimensional wave at the onset of three-dimensionality. This model consists of a two-dimensional primary wave of amplitude A and a three-dimensional secondary wave of amplitude B (Herbert 1984a). Although both amplitudes are small with respect to the mean flow, the secondary wave amplitude B is also considered small with respect to A. This assumption results in a linear Floquet system governing the secondary wave. This system admits a wide variety of solutions that vary in prominence depending on the value of A. For large values of A, primary resonance produces the fundamental mode associated with peak-valley splitting. At smaller amplitudes A, the principle parametric resonance dominates and yields subharmonic modes. In the limit $A \to 0$, the spanwise wave number for maximum growth is consistent with Craik's mechanism. The resulting disturbance profiles and amplitude growth curves (Herbert 1984a; 1985) are in good agreement with the experiments of Klebanoff et al. (1962) and Kachanov & Levchenko (1982)

The results of the parametric approach together with experimental data provide a consistent and operational model for the early stages of transition (Herbert 1988b). The first stage originates from primary instability, the onset and evolution of the TS wave. In the second stage, the TS wave reaches sufficiently large amplitudes A to cause the onset and growth of a secondary instability. Once the secondary amplitude B becomes comparable with A, the waves interact and produce changes in the primary wave, the secondary wave, and the mean flow. This interaction initiates the third stage of transition that is characterized by the breakdown of the laminar flow. The effects of B on A, however, are not accessible within the linear approach to the parametric interaction.

Based on formulation and results of the parametric approach, Croswell (1985) analyzed the energy exchange between mean flow, two-dimensional waves, and three-dimensional waves for plane Poiseuille flow. This work establishes a possible feedback loop that could cause the self-sustained growth of the three-dimensional wave. Under conditions of primary instability, the energy transfer initially occurs from the mean flow into the two-dimensional wave. This wave in turn acts as a catalyst (Orszag & Patera 1983) for the stronger transfer of energy from the mean flow into the three-dimensional wave. A part of the energy received by the three-dimensional wave is dissipated, but the major part causes an increase in amplitude or is transferred to the two-dimensional wave. As illustrated in figure 1, this chain of energy transfers suggests a feedback loop provided the modified two-dimensional wave continues to act as a strengthened catalyst. In this case, the three-dimensional wave undergoes self-sustained growth. The final proof for the action of this positive feedback loop, however, is outside the scope of the energy analysis.

The present study focuses on the mechanisms associated with the nonlinear stages of the transition process. The details of these mechanisms are hidden in the intricate interactions of finite amplitude waves. Therefore, we aim at revealing the conditions under which these waves interact to produce a disturbance field that in turn will stimulate their own growth. Establishing such positive feedback is equivalent with a criterion for the onset of breakdown.

Our model of the transition stages is formulated for the geometrically simple case of Blasius flow under the parallel-flow assumption. Recognizing the initial prominence of the TS wave, this model extends the linear parametric model to account for the mutual interaction between the primary and secondary waves. This procedure requires a complicated decomposition of the velocity field since the two-dimensional wave is both part of the basic flow and result of the interaction. In addition to the mean flow and the TS wave (which constitute the basic flow) and the three-dimensional disturbance, we introduce a new two-dimensional disturbance that interacts with the secondary wave through mutual resonance and captures the nonlinear effect of the secondary wave. The total two-dimensional field contains both the TS component and the nonlinear modifications.

To account for the rapid streamwise evolution in the three-dimensional stage of the transition process and to maintain the parametric interaction, we apply a step-by-step pseudo-marching scheme. As a first step, the finite-amplitude two-dimensional primary wave is calculated in the absence of any three-dimensional disturbances. This primary wave is then split into a basic-flow component and

an interaction component. The basic-flow component provides the parametric forcing that causes the three-dimensional secondary wave. The interaction component captures the resonance effects between the primary and secondary waves. Thus, while maintaining a parametric secondary wave, modifications to the primary wave are permitted. The only restriction on the arbitrary splitting of the primary wave is that the interaction component be 'small' compared to the basic-flow component. By continually splitting and recombining the primary wave, the resonance effects are distributed over the entire wave through the pseudo-marching scheme.

This paper presents the key features of the interaction model, some results, and their implications. Chapters 2 to 4 discuss the overall problem formulation and the detailed approach to primary waves, secondary waves, and nonlinear components. Chapter 5 describes the solution technique. Results are presented in Chapter 6. These results have been selected to enable comparison with other work and to demonstrate new findings. The final Chapter 7 gives an appraisal of the model and discusses our perception of the processes leading to breakdown.

2. Governing Equations

The equations governing the motion of an incompressible fluid of kinematic viscosity v are the continuity equation

$$\nabla \cdot \mathbf{v} = 0 \qquad (2.1)$$

and the Navier-Stokes equations

$$\frac{\partial \mathbf{v}}{\partial t} + (\mathbf{v} \cdot \nabla) \, \mathbf{v} = -\nabla p + \frac{1}{R} \nabla^2 \mathbf{v} \ . \qquad (2.2)$$

Cartesian coordinates (x',y,z) are used and the velocity vector $\mathbf{v}$ has the respective components (u,v,w). The streamwise direction is x', the spanwise direction z, and the surface normal direction y. The boundary conditions governing the flow are

$$u = v = w = 0 \quad \text{at} \quad y = 0 \ , \qquad (2.3)$$

$$u \rightarrow 1 \ , \quad v \rightarrow 0 \ , \quad w \rightarrow 0 \quad \text{as} \quad y \rightarrow \infty \ . \qquad (2.4)$$

Taking the curl of the momentum equation and using continuity removes the explicit dependence on the pressure p and provides the vorticity transport equation

$$\frac{1}{R}\nabla^2\omega - \frac{\partial\omega}{\partial t} - (v\cdot\nabla)\omega + (\omega\cdot\nabla)v = 0 \ . \tag{2.5}$$

These are three scalar equations for the vorticity components that are related to the velocity vector through

$$\nabla \times v = \omega = (\ \xi, \eta, \zeta\ )\ . \tag{2.6}$$

The reference quantities for nondimensionalization are $\delta_r = (vx'/U_\infty)^{1/2}$ and U_∞. The Reynolds number is defined as $R = U_\infty\delta_r/v$. Taking the derivative $\partial/\partial z$ of the η-vorticity equation leads to the generalized Squire's equation

$$L^s(v) - \frac{\partial}{\partial t}M^s(v) + N^s(v,v) = 0 \ , \tag{2.7}$$

where

$$L^s(v) = (\frac{1}{R}\nabla^2)\ \frac{\partial\eta}{\partial z}\ , \tag{2.7a}$$

$$M^s(v) = \frac{\partial\eta}{\partial z}\ , \tag{2.7b}$$

$$N^s(v,v) = -\frac{\partial}{\partial z}(v\cdot\nabla)\ \eta + \frac{\partial}{\partial z}(\omega\cdot\nabla)\ v\ . \tag{2.7c}$$

Taking $\partial/\partial x$ of the ζ-vorticity equation and subtracting $\partial/\partial z$ of the ξ-vorticity equation leads to the generalized Orr-Sommerfeld equation

$$L^o(v) - \frac{\partial}{\partial t}M^o(v) + N^o(v,v) = 0 \ , \tag{2.8}$$

where

$$L^o(v) = (\frac{1}{R}\nabla^2)\ \nabla^2 v\ , \tag{2.8a}$$

$$M^o(v) = \nabla^2 v\ , \tag{2.8b}$$

$$N^o(v,v) = -\frac{\partial}{\partial x}(v\cdot\nabla)\ \zeta + \frac{\partial}{\partial x}(\omega\cdot\nabla)\ w + \frac{\partial}{\partial z}(v\cdot\nabla)\ \xi - \frac{\partial}{\partial z}(\omega\cdot\nabla)\ u\ . \tag{2.8c}$$

To examine the evolution of disturbances within the boundary layer, the velocity is decomposed into a one-dimensional mean flow, a two-dimensional primary wave, and a general three-dimensional disturbance,

$$v(x',y,z,t) = v_0(y) + v_1(x',y,t) + v_3(x',y,z,t)\ . \tag{2.9}$$

The velocity v_0 is the mean flow, consisting of the Blasius profile subject to the parallel flow assumption. The velocity v_1 represents a TS wave calculated as an instability of the Blasius flow. The velocity v_3 consists of the three-dimensional

secondary wave as well as higher-order terms (both two- and three-dimensional) produced by resonant wave interaction. Substituting (2.9) into (2.7), (2.8), (2.3), and (2.4) and subtracting the equations for the mean flow yields

$$L_0^s(v_1) - \frac{\partial}{\partial t} M^s(v_1) + N^s(v_1, v_1) + L_0^s(v_3)$$

$$- \frac{\partial}{\partial t} M^s(v_3) + N^s(v_1, v_3) + N^s(v_3, v_3) = 0 \quad , \tag{2.10}$$

$$L_0^o(v_1) - \frac{\partial}{\partial t} M^o(v_1) + N^o(v_1, v_1) + L_0^o(v_3)$$

$$- \frac{\partial}{\partial t} M^o(v_3) + N^o(v_1, v_3) + N^o(v_3, v_3) = 0 \quad , \tag{2.11}$$

$$v_1 = v_3 = 0 \quad \text{at} \quad y = 0 \quad , \tag{2.12}$$

$$v_1 \rightarrow 0 \quad , \quad v_3 \rightarrow 0 \quad \text{as} \quad y \rightarrow \infty \quad . \tag{2.13}$$

For the stability analysis, v_0 is considered known. Therefore, we introduce new linear operators $L_0^s(v) = L^s(v) + N^s(v_0, v)$ for Squire's equation and $L_0^o(v) = L^o(v) + N^o(v_0, v)$ for the Orr-Sommerfeld equation.

3. Primary Wave

The first step in analyzing equations (2.10) and (2.11) is to consider the two-dimensional mode v_1 as a primary wave that independently satisfies

$$L_0^s(v_1) - \frac{\partial}{\partial t} M^s(v_1) + N^s(v_1, v_1) = 0 \quad , \tag{3.1}$$

$$L_0^o(v_1) - \frac{\partial}{\partial t} M^o(v_1) + N^o(v_1, v_1) = 0 \quad . \tag{3.2}$$

These equations contain the nonlinear self-interaction which governs the formation of a finite-amplitude two-dimensional wave in the Blasius mean flow. These equations are solved using a perturbation expansion about the linear solution at fixed R and α. Following Herbert (1983), the temporal growth concept is used to obtain a Landau equation for the representative amplitude. This equation needs extension, however, if the nonlinear interaction with the secondary wave is considered.

3.1 Fourier Expansion

Because the coefficients in (3.1) and (3.2) are independent of x', i.e. $\mathbf{v}_0 = (u_0(y),0,0)$, the velocity $\mathbf{v}_1$ can be expanded in a Fourier series in x'. Starting from the linear solution and accounting for higher harmonics, the mean-flow distortion, and the distortion of the linear wave itself yields

$$\mathbf{v}_1(x',y,t) = \sum_{k=-\infty}^{\infty} \tilde{\mathbf{v}}_{1_k}(y,t)e^{ik\theta} \ , \quad \theta = \alpha x' - \gamma(t) \ , \tag{3.3}$$

where $\tilde{\mathbf{v}}_{1_{-k}}$ is equal to the complex conjugate of $\tilde{\mathbf{v}}_{1_k}$. In this form, the solution can account for changes in both the frequency and growth rate at finite amplitude. The function $\gamma(t)$ describes the temporal oscillation while the growth is contained in $\tilde{\mathbf{v}}_{1_k}(y,t)$. Substituting the expression (3.3) into eqs. (3.1) and (3.2) produces a set of coupled nonlinear partial differential equations in y and t.

3.2 Amplitude Expansion

Using perturbation methods, the set of partial differential equations generated from eqs. (3.1) and (3.2) is further reduced to a set of ordinary differential equations. Since the harmonics of the linear primary wave $\tilde{\mathbf{v}}_{1_1}(y,t)$ are of higher order, we write the Fourier coefficients in the form

$$\tilde{\mathbf{v}}_{1_k}(y,t) = A^k \mathbf{v}_{1_k}(y,t) \ , \tag{3.4}$$

where A is the amplitude of the linear wave.

This form leads to a decoupling of the nonlinear equations since $\mathbf{v}_{1_k}$ contains no terms smaller than $O(A^k)$. The time derivatives in eqs. (3.1) and (3.2) together with (3.3) and (3.4) produce coefficients that contain the growth rate a and the frequency ω (or wave speed c_r),

$$a = \frac{dA}{Adt} \ , \quad c_r = \frac{\omega}{\alpha} = \frac{d\gamma}{\alpha dt} \ . \tag{3.5}$$

Following the method of strained parameters, both the functions $\mathbf{v}_{1_k}(y,t)$ and the coefficient $\lambda = a - i\alpha c_r$ are expanded in terms of the amplitude A. It can be shown (Herbert 1983) that these expansion series progress in even powers of A, resulting in

$$\mathbf{v}_{1_k}(y,t) = \sum_{p=0}^{\infty} \mathbf{v}_{1_{kp}}(y)A^{2p} \ , \tag{3.6}$$

$$\lambda = \sum_{p=0}^{\infty} \lambda_p A^{2p} \ , \quad \lambda_p = a_p - i\alpha c_{r_p} \ . \tag{3.7}$$

Finally, substituting and collecting terms in like powers of A results in two

- 8 -

coupled ordinary differential equations for each harmonic at every other successive order of A. The order of a function depends on both k and p. Similar expressions and procedures are used when considering the secondary mode and its interaction with the primary wave.

As a result of this procedure, the expansion for the primary wave up to third order is

$$v_1(x',y,t) = \frac{1}{2}[A^2v_{1_{01}}(y)] + [Av_{1_{10}}(y) + A^3v_{1_{11}}(y)]e^{i\theta}$$

$$+ [A^2v_{1_{20}}(y)]e^{i2\theta} + [A^3v_{1_{30}}(y)]e^{i3\theta} + c.c. \qquad (3.8)$$

In addition to the fundamental wave, v_1 now contains a mean-flow correction and a second harmonic. The growth rate and wave speed take the form

$$\frac{dA}{Adt} = a_0 + A^2a_1 \;, \qquad (3.9)$$

$$c_r = c_{r_0} + A^2c_{r_1} \;. \qquad (3.10)$$

Given an initial amplitude, eq. (3.9) describes the amplitude growth in time while eq. (3.10) provides the corresponding wave speed. The third-order solution consists of the velocity functions $v_{1_{10}}$, $v_{1_{01}}$, $v_{1_{20}}$, $v_{1_{11}}$ and the constants a_0, a_1, c_{r_0}, c_{r_1} that are independent of the value of A. The actual velocity functions in eq. (3.3), the growth rate, and the wave speed, however, depend on the value of A.

In section 4, the effect of the secondary wave on the amplitude A will be incorporated. According to eqs. (3.8) and (3.10), this effect will immediately influence velocity functions and wave speed. However, to fully capture the interaction effects, additional functions and constants must be included in the expansions.

3.3 Two-Dimensional Basic Flow

Given a fixed amplitude A^* and the third-order solution for the primary wave, v_1 can be substituted into eqs. (2.10) and (2.11). Linearization in v_3 provides the formal basis for the analysis of parametric secondary instabilities. At the same time, this linearization removes the terms crucial for the modification of the primary wave in the presence of a finite-amplitude secondary mode. Therefore, to study the two-dimensional/three-dimensional wave interaction, the nonlinear terms in v_3 must be retained. Since the secondary mode is permitted to grow or decay, the two-dimensional wave and its amplitude A will vary in time while A^* must be held fixed for the Floquet analysis to be valid.

To overcome this dilemma, we decompose the primary wave amplitude into a fixed component A^* and a variable component $\hat{A}$, $A = A^* + \hat{A}$, where $\hat{A} \ll A^*$. The actual choice of A^* and $\hat{A}$ is arbitrary provided that A satisfies equation (3.9) in the absence of any secondary wave. With this decomposition, the two-dimensional wave can be split into a basic flow component that contains only A^*, and a perturbation that contains also the variable $\hat{A}$. The basic flow interacts parametrically with the secondary wave (one-way interaction), while the perturbation interacts through resonance (two-way interaction). Since A^* will be predefined, only $\hat{A}$ needs to be determined to obtain A and to fully define the primary wave.

Substituting for A in eq. (3.8) and collecting coefficients in like powers of $\hat{A}$ yields

$$v_1 = v_1^* + \hat{v}_1 \ , \tag{3.11}$$

where v_1^* contains all terms independent of $\hat{A}$ and constitutes the known basic flow. The second term $\hat{v}_1$ can be written as

$$\hat{v}_1 = \hat{A}\, v_A + \hat{A}^2\, v_{A^2} + \hat{A}^3\, v_{A^3} + O(A^{*4}) \ ,$$

i.e. as a perturbation expansion of $\hat{v}_1$ in terms of the amplitude $\hat{A}$. Substitution for A into eq. (3.10) gives the expanded form of the wave speed .

$$c_r = c_r^* + \hat{c}_r \ . \tag{3.12}$$

Finally, eq. (3.9) takes the form

$$\frac{dA^*}{dt} + \frac{d\hat{A}}{dt} = (A^* a_0 + A^{*3} a_1) + \hat{A}(a_0 + 3A^{*2} a_1)$$

$$+ \hat{A}^2 (3A^* a_1) + \hat{A}^3 (a_1) + O(A^{*5}) \ . \tag{3.13}$$

Isolating the terms depending only on the amplitude A^* provides

$$\frac{dA^*}{dt} = A^* a_0 + A^{*3} a_1 \ , \tag{3.14}$$

while the growth of $\hat{A}$ owing to self-interaction of the primary wave is governed by the equation

$$\frac{d\hat{A}}{dt} = \hat{A}(a_0 + 3A^{*2} a_1) + \hat{A}^2 (3A^* a_1) + \hat{A}^3 (a_1) + O(A^{*5}) \ ,$$

or, in other form,

$$\frac{d\hat{A}}{dt} = \hat{A} a_A + \hat{A}^2 a_{A^2} + \hat{A}^3 a_{A^3} + O(A^{*5}) \ . \tag{3.15}$$

Thus far, we have not considered the feedback of the secondary wave on the primary wave. In the absence of this feedback, the primary wave v_1 satisfies eqs. (3.1) and (3.2).

4. Secondary Wave and Interaction Modes

The interaction of the primary and secondary wave causes two effects. First, the interaction modifies the primary amplitude, $\hat{A}$, owing to higher-order resonances with the secondary wave. In this case, eq. (3.15) acquires additional terms that cause residuals $R^s(\hat{v}_1)$ and $R^o(\hat{v}_1)$ in eqs. (3.1) and (3.2), respectively. The exact form of these residuals is yet to be determined. Second, the interaction modifies the disturbance velocity functions. To account for this effect, two-dimensional functions are included in v_3.

Subtracting eqs. (3.1) and (3.2) from eqs. (2.10) and (2.11), respectively, yields the governing equations for the secondary and interaction modes

$$L_0{}^s(v_3) - R^s(\hat{v}_1) - \frac{\partial}{\partial t}M^s(v_3) + N^s(v_1,v_3) + N^s(v_3,v_3) = 0 \ , \qquad (4.1)$$

$$L_0{}^o(v_3) - R^o(\hat{v}_1) - \frac{\partial}{\partial t}M^o(v_3) + N^o(v_1,v_3) + N^o(v_3,v_3) = 0 \ . \qquad (4.2)$$

Substituting $v_1 = v_1{}^* + \hat{v}_1$ provides

$$L_0{}^s(v_3) + L_1{}^s(v_3) - R^s(\hat{v}_1) - \frac{\partial}{\partial t}M^s(v_3)$$
$$+ N^s(\hat{v}_1,v_3) + N^s(v_3,v_3) = 0 \ , \qquad (4.3)$$

$$L_0{}^o(v_3) + L_1{}^o(v_3) - R^o(\hat{v}_1) - \frac{\partial}{\partial t}M^o(v_3)$$
$$+ N^o(\hat{v}_1,v_3) + N^o(v_3,v_3) = 0 \ . \qquad (4.4)$$

Since $v_1{}^*$ is considered known, new linear operators $L_1{}^s(v_3) = N^s(v_1{}^*,v_3)$ and $L_1{}^o(v_3) = N^o(v_1{}^*,v_3)$ have been introduced. Equations (4.3) and (4.4) contain the linear parametric forcing of v_3, the nonlinear cross-interactions between v_3 and $\hat{v}_1$, and the self-interaction of v_3.

The self-interaction of the two-dimensional wave contributes only to the mean flow and the two-dimensional field without affecting the three-dimensional wave. The self-interaction of the three-dimensional wave, however, produces both two- and three-dimensional higher-order terms. Therefore, $N(\hat{v}_1,v_3)$ and

$N(v_3,v_3)$ together provide the primary/secondary interaction.

For the application of Floquet theory to obtain the secondary wave and the associated interaction terms, the amplitude A^* is assumed constant. This assumption is in conflict with eq. (3.14) for the temporal evolution of A^*. However, the relative variation of A^* is small for small increments in time (or, for an observer moving with the phase speed c_r, in space).

For constant A^*, the variable coefficients associated with L_1^s and L_1^o can be simplified since the basic-flow component v_1^* is periodic in both x' and t. In a Galilean frame moving with the two-dimensional wave, $x = x' - \gamma(t)/\alpha$, v_1^* satisfies

$$v_1^*(x',y,t) = v_1^*(x,y) = v_1^*(x + \lambda_x,y) \ , \tag{4.5}$$

where $\lambda_x = 2\pi/\alpha$ is the wavelength. The time dependence of v_1^* is removed. Expressing the periodic component of the basic flow in terms of the stream function $\psi_1^*(x,y)$ yields the standard form of the linear operators L_1^s and L_1^o that govern the secondary instability (Herbert 1984b).

4.1 Fourier Expansion

Since the coefficients in eqs. (4.3) and (4.4) are independent of z, the velocity v_3 can be expanded in a Fourier series in z

$$v_3(x,y,z,t) = \sum_{m = -\infty}^{\infty} v_{3_m}(x,y,t) \, e^{im\beta z} \ . \tag{4.6}$$

Including a time modulation $e^{-im\delta(t)}$ (similar to the primary mode) would have no effect. The function $\delta(t)$ appears in the equations as the imaginary part of the Landau constants for $d\delta/dt$ but the system is real since the equations depend only on β^2. For real velocities the Landau constants are necessarily real.

Substituting the series (4.6) into eqs. (4.3) and (4.4) removes their dependence on z. The nonlinear terms in $N^s(v_3,v_3)$ and $N^o(v_3,v_3)$ contain products of Fourier series. Balancing the harmonics, the nonlinear operators can be rewritten as $N^s(v_{3_\mu},v_{3_\nu})$ and $N^o(v_{3_\mu},v_{3_\nu})$, respectively. The indices μ and ν assume the role of m in the series (4.6). Only terms with $\mu + \nu = m$ contribute to the mth harmonic equation. Substituting (4.6) into the continuity equation and dividing by the index m for $m \neq 0$, yields for w_{3_m}

$$i\beta w_{3_m} = -\frac{1}{m}(\frac{\partial u_{3_m}}{\partial x} + \frac{\partial v_{3_m}}{\partial y}) \ , \quad m \neq 0 \ . \tag{4.7}$$

Using this expression, w can be removed from eqs. (4.3) and (4.4). The case

$m = 0$ is irrelevant since it describes two-dimensional resonance terms with the spanwise velocity component identically zero.

4.2 Amplitude Expansion

The application of the perturbation method to the secondary and interaction modes follows conceptually the same steps as for the primary wave. The presence of two interacting amplitudes, however, requires a more general approach for the construction of the velocity functions and amplitude equations. The amplitude equations can be developed up to arbitrary order by examining the interactions and identifying those in resonance with the primary or secondary wave. A similar approach was successfully used by Li (1986) to analyze the evolution of the first and second harmonics for the Taylor problem.

Higher-order terms are generated by the nonlinear interaction of the linear secondary wave $B\mathbf{v}_B(x,y)e^{i\beta z}$ and the first-order primary interaction term $\hat{A}\mathbf{v}_A(x,y)$. Of particular interest are the terms associated with $m = 0$ and $m = 1$. The terms with $m = 1$ are in resonance with the secondary wave. Constructing $\mathbf{v}_{3_1}$ to third order and noting $\hat{A} = \hat{A}(t)$ and $B = B(t)$ provides

$$\mathbf{v}_{3_1}(x,y,t) = B\ \mathbf{v}_B(x,y) + \hat{A}B\ \mathbf{v}_{AB}(x,y)$$
$$+ \hat{A}^2 B\ \mathbf{v}_{A^2B}(x,y) + B^3\ \mathbf{v}_{B^3}(x,y)\ . \tag{4.8}$$

The interaction terms with $m = 0$ are in resonance with the primary wave. To third order, $\mathbf{v}_{3_0}$ becomes

$$\mathbf{v}_{3_0}(x,y,t) = B^2\ \mathbf{v}_{B^2}(x,y) + \hat{A}B^2\ \mathbf{v}_{AB^2}(x,y)\ . \tag{4.9}$$

In addition to the functions in eqs. (4.8) and (4.9), the higher-order resonance terms also generate Landau constants that describe the effect on the amplitude associated with the particular resonance as part of the amplitude-growth equations. Recognizing the resonances for $m = 1$, the amplitude-growth equation for the secondary wave becomes

$$\frac{dB}{dt} = B\ b_B + \hat{A}B\ b_{AB} + \hat{A}^2 B\ b_{A^2B} + B^3\ b_{B^3}\ . \tag{4.10}$$

Similar consideration of the resonances for $m = 0$ provides the total growth equation for $\hat{A}$

$$\frac{d\hat{A}}{dt} = \hat{A}\ a_A + \hat{A}^2\ a_{A^2} + \hat{A}^3\ a_{A^3} + B^2\ a_{B^2} + \hat{A}B^2\ a_{AB^2}\ . \tag{4.11}$$

The first three terms describe the primary self-interaction (3.15). The last two

- 13 -

terms account for the secondary self-interaction and primary/secondary interaction, respectively. These additional terms produce the residuals in eqs. (4.3) and (4.4).

The result of the combined Fourier expansion and amplitude expansion is to convert of eqs. (4.3) and (4.4) into a system of linear equations. To develop these new equations, the expansions (4.6), (4.8), and (4.9) are substituted into eqs. (4.3) and (4.4). Differentiation with respect to time produces coefficients $d\hat{A}/dt$ and $d\hat{B}/dt$ multiplying the operators M. These derivatives are replaced by the Landau series (4.10) and (4.11). Collecting coefficients of $Be^{i\beta z}$ yields the linear secondary equations,

$$L_0{}^s(\mathbf{v}_B) + L_1{}^s(\mathbf{v}_B) - b_B \, M^s(\mathbf{v}_B) = 0 \ , \tag{4.12}$$

$$L_0{}^o(\mathbf{v}_B) + L_1{}^o(\mathbf{v}_B) - b_B \, M^o(\mathbf{v}_B) = 0 \ . \tag{4.13}$$

Solving this eigenvalue problem provides the linear growth rate b_B and the corresponding velocity function $\mathbf{v}_B(x,y)$.

At second order, there are equations for both two- and three-dimensional terms. The coefficients of $\hat{A}Be^{i\beta z}$ generate the equations for the secondary-wave modification while the coefficients of B^2e^{i0z} give the equations for the primary-wave modification. Higher-order equations are generated in a similar way.

4.3 Floquet Analysis

The formal result of the perturbation analysis is a pair of equations for each of the functions in eqs. (4.8) and (4.9). Since the coefficients in these equations depend on x and y, Fourier (or normal-mode) analysis cannot be used to derive ordinary differential equations. With the 'localized' assumption of a fixed amplitude A^*, however, the coefficients are periodic in x. This property allows the use of Floquet theory to reveal the dependence on x.

Earlier work of Herbert (1984a; 1984b; 1985) for parallel shear flows provides a guideline to the present application of this theory. The general form of the functions is $e^{\rho x} f(x,y)$ where f is x-periodic with wavelength λ_x. For the case of temporal stability, the characteristic exponent ρ is set to zero. Thus the functions of x,y can be written as a Fourier series with y-dependent coefficients similar to the application of Fourier analysis. Owing to the coupling through the x-periodic terms, however, we must solve for all functions of y in this series simultaneously.

To develop systems of ordinary differential equations, each of the functions in eqs. (4.8) and (4.9) is expanded as

$$f(x,y) = \sum_{n=-\infty}^{\infty} f_n(y)e^{in\hat{\alpha}x} \quad , \quad \hat{\alpha} = \frac{\alpha}{2} = \frac{\pi}{\lambda_x} \quad , \tag{4.14}$$

where f_{-n} is equal to the complex conjugate of f_n. When this expansion is substituted into the governing equations, a decoupling occurs between the modes with n even and n odd. The modes with even n have wavelength λ_x and are called fundamental modes. These fundamental modes originate from primary resonance in the x-periodic flow. The modes with odd n have wavelength $2\lambda_x$ and are designated subharmonic modes. These modes result from principal parametric resonance (Nayfeh & Mook 1979).

5. Method of Solution

5.1 Definition of Amplitudes

Calculating the secondary and interaction modes contained in v_3 has been reduced to solving sets of coupled ordinary differential equations. Associated with the decomposition of the velocity field, however, is an ambiguity in the definition of the amplitudes. In particular, the physical amplitudes can reside in both the velocity functions and the defined amplitudes. To establish meaningful evolution equations for $\hat{A}$ and B, a proper norm, or uniqueness condition, is applied that ensures that the Landau constants contain the growth information (Herbert 1983).

The solution of the first-order problem (4.12) and (4.13) results in an eigenvalue b_B and an eigenfunction v_B. The phase of this function is fixed by imposing a local norm condition at a fixed point y_0 in the profile. This point corresponds to the maximum of the primary-wave function at some initial Reynolds number. The principal reason for using a local norm instead of an integrated norm is the simplicity of implementation, especially at higher order.

In the second- and higher-order problems, the equations are inhomogeneous yet the associated homogeneous problem may possess a solution. For a nontrivial solution of the inhomogeneous problem to exist in such cases, a solvability condition must be satisfied. This solvability condition determines the Landau constants. Our definition of the amplitude requires the real part of the resonant higher-order velocity functions to vanish at y_0. This additional equation permits considering Landau constant as an additional unknown in the solution,

no matter whether or not the associated homogeneous problem possesses a solution. Without explicit use of the solvability condition, we obtain unique solutions for both functions and constants while the procedure ensures that $\hat{A}$ and B are meaningful, though dependent on the chosen norm. Unambiguous physical results for the velocity field are obtained by combining $\hat{A}$ and B with the velocity functions.

To determine physical two- and three-dimensional amplitudes e.g. for comparison with experiments, we consider the total composite functions for the streamwise component u and calculate the maximum rms fluctuation of appropriate Fourier components as the physical amplitudes. The selection of these Fourier components follows the experimental approach. The total two-dimensional velocity function is the sum of the expressions (3.8) and (4.9). Determining the amplitude of the disturbance component with frequency ω (e.g. Kachanov & Levchenko 1982) requires filtering out $k = \pm 1$ from the velocity (3.8) as defined in the series (3.3) and $n = \pm 2$ from (4.9) as defined in (4.14). Thus, the total two-dimensional function becomes

$$u_{2D}\ (x,y,t) = u_1\ (x,y,t)\ |_{k\,=\,1} + u_{3_0}\ (x,y,t)\ |_{n\,=\,2}\ . \tag{5.1}$$

The total three-dimensional function of wave number β is given by eq. (4.8) where $m = 1$. This function is characterized by one of two frequencies, depending on the mode of secondary instability. The subharmonic mode at frequency $\omega/2$ is obtained for $n = \pm 1$ as defined in eq. (4.14),

$$u_S\ (x,y,t) = u_{3_1}\ (x,y,t)\ |_{n\,=\,1}\ . \tag{5.2}$$

The fundamental mode at frequency ω is obtained for $n = 2$,

$$u_F\ (x,y,t) = u_{3_1}\ (x,y,t)\ |_{n\,=\,2}\ . \tag{5.3}$$

Both of these functions are multiplied by $e^{i\beta z}$ and thus have a net spanwise variation in the physical velocities.

Since both the fundamental and two-dimensional functions have the same frequency, it is useful to define a new three-dimensional function which contains the total velocity field at frequency ω (e.g. Klebanoff et al. 1962). Since u_F is real, combining the velocity components (4.6) with $m = \pm 1$ provides the real velocity

$$u_\omega\ (x,y,z,t) = u_{2D}\ (x,y,t) + 2\cos\beta z\ u_F\ (x,y,t)$$

$$+\ 2\cos 2\beta z\ u_{3_2}\ (x,y,t)\ |_{n\,=\,2} + 2\cos 3\beta z\ u_{3_3}\ (x,y,t)\ |_{n\,=\,2}\ . \tag{5.4}$$

This function is of particular interest at two spanwise locations, the 'peak' $z = 0$

- 16 -

and the 'valley' $z = \lambda_z/2$. At $z = 0$, u_{2D} and u_F combine in phase to produce the characteristic peak-velocity function

$$u_P (x,y,t) = u_{2D} (x,y,t) + 2 u_F (x,y,t)$$

$$+ 2 u_{3_2} (x,y,t)|_{n=2} + 2 u_{3_3} (x,y,t)|_{n=2} . \qquad (5.5)$$

At $z = \lambda_z/2$, u_{2D} and u_F combine out of phase to produce the valley-velocity function

$$u_V (x,y,t) = u_{2D} (x,y,t) - 2 u_F (x,y,t)$$

$$+ 2 u_{3_2} (x,y,t)|_{n=2} - 2 u_{3_3} (x,y,t)|_{n=2} . \qquad (5.6)$$

We further introduce the rms velocity functions in the usual way, e.g. for the subharmonic component

$$u_S' = \left[2\mathrm{Re}^2(u_S) + 2\mathrm{Im}^2(u_S) \right]^{1/2} . \qquad (5.7)$$

The physical rms amplitude is then defined as the maximum of the rms velocity functions, e.g. $u_S'_{max}$. Similar rms functions and amplitudes are calculated for other components.

5.2 Numerical Method

The systems of ordinary differential equations created by the perturbation analysis are solved by a spectral collocation method. The unbounded domain $y = [0, \infty)$ is mapped into the bounded domain $\eta = [1, 0]$ using the algebraic mapping $\eta = \bar{y}/(y + \bar{y})$. The parameter $\bar{y}$ controls the distribution of collocation points within the boundary layer.

The velocity functions are expanded in finite spectral series of odd Chebyshev polynomials. Because of the mapping applied, these polynomials implicitly satisfy the boundary conditions at infinity. The error introduced by using a finite series approximation is forced to zero at certain collocation points y_j (Gauss-Lobatto points) across the η domain.

The sizable equations derived during the problem formulation have been verified by MACSYMA, a computer program for symbolic algebra. Starting with the Navier-Stokes equations, we first developed the general form of the nonlinear Orr-Sommerfeld and Squire equations for the three-dimensional flow. Based on these equations we performed two different checks. First, we Fourier expanded the velocity in x and z in terms of $(n\alpha, m\beta)$. This provides a general expression for comparison with the numerical code. Second, we carried out each step in the problem formulation in succession. This procedure begins with the Fourier

expansion followed by the amplitude and Floquet expansions. For each single mode of wave numbers (α, β) the velocities are finally expanded in terms of odd Chebyshev polynomials. The resulting symbolic algebraic system is transformed into Fortran code and solved numerically by computer. The results provide a benchmark for comparison with the more efficient hand-coded numerical algorithm.

5.3 Pseudo-Marching scheme

The perturbation analysis and the numerical solution of the resulting equations yield the Landau constants and the velocity functions at any given Reynolds number. The goal of the pseudo-marching scheme is to convert this 'local' information into a continuous temporal or spatial evolution of the disturbance field. Given initial amplitudes and integration of the amplitude-growth equations are the building blocks for this conversion.

For ease of comparison with experiments, the temporal stability information is recast in terms of a spatial evolution. Gaster's transformation (Gaster 1962) allows rewriting the amplitude-growth equation (3.14) in terms of the independent variable R. The governing equation for the basic-flow component of the primary wave A^* becomes

$$\frac{dA^*}{dR} = \frac{2}{c_g} \left(A^* a_0 + A^{*3} a_1 \right) , \tag{5.8}$$

where c_g is the group velocity, defined as $c_g = c_r + \alpha(dc_r/d\alpha)$. The primary interaction amplitude $\hat{A}$ and the secondary amplitude B vary according to

$$\frac{d\hat{A}}{dR} = \frac{2}{c_r} \left(\hat{A} \, a_A + \hat{A}^2 \, a_{A^2} + \hat{A}^3 \, a_{A^3} + B^2 \, a_{B^2} + \hat{A}B^2 \, a_{AB^2} \right) \tag{5.9}$$

and

$$\frac{dB}{dR} = \frac{2}{c_r} \left(B \, b_B + \hat{A}B \, b_{AB} + \hat{A}^2 B \, b_{A^2 B} + B^3 \, b_{B^3} \right) , \tag{5.10}$$

respectively. These equations are consistent with the transformations derived by Bertolotti (1985) between linear growth rates of the secondary wave. He found the phase velocity to be the leading term in the temporal-spatial transformation for parametric secondary instabilities.

The simplest scheme for calculating the amplitude growths as a function of R is based on a two-phase approach. This scheme begins with given initial amplitudes A^*, $\hat{A}$, and B, at some Reynolds number R. The first phase consists of calculating primary Landau constants and functions at successive R locations.

Then, starting with the initial A^*, the basic flow component of the amplitude is extrapolated from one R location to the next using eq. (5.8). In the second phase, the secondary and interaction constants and functions are calculated at each R using the A^* values. With initial values for $\hat{A}$ and B, these amplitudes are then extrapolated to the next R location using eqs. (5.9) and (5.10) respectively.

In this approach, the basic-flow component of the primary wave is unaffected by the presence of the secondary wave. If the effects of the secondary wave on the primary wave are small, any changes to the basic-flow component A^* can be neglected. If these effects are not small, however, their neglect would be a major shortcoming of the analysis. To avoid this problem, we use the pseudo-marching scheme that permits accounting for the effect of the secondary mode on the total primary wave.

The pseudo-marching scheme aims at distributing the various resonance effects over both A and B. In the early stage of the amplitude evolution, the primary/secondary interaction is dominated by the (one-way) parametric resonance. However, as the secondary amplitude grows, mutual resonance becomes increasingly significant. To accommodate the changeover from the region of linear-parametric resonance to the region of significant mutual resonance, the primary amplitude A is repeatedly split into A^* and $\hat{A}$ and recombined.

Given the initial values of the primary amplitude A and the secondary amplitude B at some initial R, we specify the splitting parameter $\varepsilon = \hat{A}/A$ and calculate $\hat{A} = \varepsilon A$ and $A^* = A - \hat{A}$. Solving eqs. (3.1) and (3.2) with the perturbation scheme yields the constants and functions for the primary wave. With the current value of A^*, we first calculate the basic flow and interaction functions v_1^* and ϑ_1 and then determine the secondary and interaction functions and constants. Based on the set of Landau constants, the amplitude growth equations (5.8), (5.9), and (5.10) are integrated to obtain A^*, $\hat{A}$, and B at the next R location. At this new location, the total primary amplitude is evaluated as $A = A^* + \hat{A}$ which completes one step. For the next step, the amplitude is again decomposed using $\hat{A} = \varepsilon A$ and $A^* = A - \hat{A}$, and the calculation procedure is repeated.

This scheme provides an avenue for incorporating the changing basic-flow amplitude A^* and the appropriate modifications of the secondary and interaction terms. The repeated redistribution of A between A^* and $\hat{A}$ takes advantage of the arbitrariness in this split. As long as $\hat{A}$ is small relative to A^*, the evolution of B is independent of ε. Since $\hat{A}$ must be small, however, the maximum step

size in R is restricted such that $\hat{A}$ does not change 'too radically' relative to A^*. In regions of strong interaction the step size in R is automatically reduced if $\hat{A} < 10^{-5}$, and the integration is repeated. Controlling the splitting parameter ε and the step size in R is an indirect way to control the rate of exchange between $\hat{A}$ and A^*, and thus between mutual and parametric resonance. All the results on the amplitude evolution given below are obtained with the pseudo-marching scheme.

6. Results

6.1 Landau Constants

To numerically solve the equations, all summations must be truncated at some finite value. We have chosen the minimum values for which a 'reasonable' solution can be obtained (Crouch 1988). The Floquet system associated with the streamwise variation is truncated at $N = 3$. The number of collocation points is taken to be $J = 20$, which is sufficient for this analysis. The third truncation concerns the order of the primary wave. Since the primary self-interaction produces only a small change of 1%, say, in the Landau constants, this interaction is neglected. A further reason for neglecting the self-interaction is the inability to calculate the mean-flow distortion in the stable region at Reynolds numbers past R_{II} (Herbert 1983). The remaining truncations concern the order of the perturbation series for the primary/secondary interaction and the related spanwise Fourier series. Most of the calculations are carried out to second order, requiring only two Fourier modes. Third-order calculations with three spanwise modes are used to investigate peak-valley splitting, which occurs at larger amplitudes.

Using this perturbation approach allows us to examine the interactions of particular 'pieces' of the flow field. The Landau constants provide both the strength and the creative or destructive nature of specific interactions. Up to third order, the perturbation expansion (4.11), (5.9) involves five Landau constants governing the evolution of the interaction component of the primary wave, $\hat{A}$. The first-order constant $a_A = a_0 + 3A^{*2}a_1$ is essentially the linear growth rate. A small correction accounts for the finite amplitude A^*, even though $\hat{A}$ could be considered infinitesimal. The constants $a_{A^2} = 3A^*a_1$ and $a_{A^3} = a_1$ describe the third-order self-interaction of the primary wave. These constants contain both the mean-flow distortion and the second harmonic. Ignoring the self-interaction reduces a_A to the linear growth rate a_0 and both a_{A^2} and a_{A^3} to zero. The second-order constant a_{B^2} describes the effect of the secondary mode

- 20 -

on the primary wave. Associated with this constant is the velocity function v_{B^2}. The constant a_{B^2} incorporates the $O(B^2)$ effects on the amplitude $\hat{A}$, while the function represents the effect on the total two-dimensional velocity field. This $O(B^2)$ interaction is of key importance since it captures the distinct qualitative changes in the two-dimensional velocity field caused by the three-dimensional disturbance. Analysis of the energy balance for plane Poiseuille flow (Croswell 1985 ; Herbert 1986) has established a significant feedback from the three-dimensional field into the two-dimensional field. This result suggests that either $a_{B^2} > 0$ or, otherwise, $B^2 v_{B^2}$ must be of the order of the primary wave. At third order, the constant a_{AB^2} contains the combined effects of the velocity fields v_A and v_{B^2}.

The third-order expansion (4.10), (5.10) yields four Landau constants governing the evolution of the secondary amplitude, B. The constant b_B is the linear growth rate of the secondary wave owing to the parametric excitation by a TS wave of amplitude A^*. In the calculation of the first-order constant b_B, the primary wave amplitude is considered to be A^*. Actually, however, the amplitude is $A = A^* + \hat{A}$. The second-order constant b_{AB} accounts for the interaction component of the primary wave, $\hat{A}$. This constant merely gives the quantitative change in the linear secondary growth rate and offers nothing qualitatively new. The third-order constant b_{B^3} accounts for the self-interaction of the secondary wave. In particular, b_{B^3} describes how the two-dimensional velocity field that is produced by the secondary wave affects the growth of the three-dimensional wave. The final constant to be considered is the third-order constant b_{A^2B}. This constant is generated by the interaction of the secondary wave with the mean-flow distortion and harmonic of the primary wave. Similar to the second-order constant b_{AB}, b_{A^2B} contributes quantitatively but presents nothing qualitatively new. Detailed results for the Landau constants are given by Crouch (1988). Here, we focus the attention on the physical results in the form of amplitude-growth curves and disturbance-velocity profiles.

6.2 Subharmonic Amplitude-Growth Curves

Allowing the resonant interaction to influence the total TS wave through the continuous amalgamation and splitting of A^* and $\hat{A}$ causes dramatic variations in the wave amplitude. A strong interaction occurs in the amplitude evolution of the subharmonic mode when A and B are approximately of the same magnitude. This interaction initially results in a rapid decay of A, with A reaching a low level over a small Reynolds number range of 30–40 units. The reason for this decay is the large negative value of the Landau constant a_{B^2}. Before the amplitude A

tends to zero, however, the sign of a_{B^2} changes. As a result of this sign change, the decay is halted and the amplitude assumes a quasi-equilibrium value.

The key to understanding the progression of the physical amplitudes lies in the interrelationship of the various amplitude components. Figure 2 shows how these components evolve with the Reynolds number for a second-order interaction at $F = 124$, $b = 0.33$. When $B \approx A$, the secondary amplitude B forces through resonance the primary amplitude $A = A^* + \hat{A}$ to an equilibrium value. Simultaneous with the decay of A the secondary growth rate b_B is reduced. This reduced growth causes a change in the slope of B versus R. Once A settles to the slowly varying equilibrium value, the slope of the curve B versus R becomes almost constant. The composite amplitude $u_{2D}'_{max}$ is initially equivalent to $A = A^* + \hat{A}$. As B exceeds A and continues to grow, the component $B^2 u_{B^2}$ becomes increasingly dominant. The net effect of the primary/secondary interaction on $u_{2D}'_{max}$ is thus an initial reduction owing to the decay of A and a subsequent rapid 'lift-off' from the close-to-linear behavior owing to the presence and growth of the B^2 function. The development of $u_S'_{max}$ follows closely that of B. Note that B does not represent the maximum in the u_B profile, but rather the magnitude of u_B at fixed y_0.

Figure 3 shows the comparison of the first-, second-, and third-order amplitude evolutions for the conditions $F = 124$ and $b = 0.33$. The principal effect of the nonlinear interaction is to cause $u_{2D}'_{max}$ to 'dip' and then 'lift-off', and to reduce the growth of $u_S'_{max}$. For these amplitudes, third-order effects are qualitatively insignificant.

In the formulation of the method, the primary amplitude A is arbitrarily split into A^* and $\hat{A}$ to capture the nonlinear primary/secondary interaction through the pseudo-marching scheme. The relative size of the components is defined by the parameter $\varepsilon = \hat{A}/A$. Ideally, the results should be independent of ε or should converge to a fixed solution as $\varepsilon \to 0$. Figure 4 shows the development of $u_{2D}'_{max}$ and $u_S'_{max}$ for different values of ε. The changes are indeed small and decrease in size as ε becomes smaller.

With the general interaction characteristics assessed, we are now ready to compare these characteristics with the sparse data base of experimental results. The first case considered is for the conditions $F = 137$ and $b = 0.40$ and the experimental data of Kachanov & Levchenko (1984). Unfortunately, the spanwise wave number b was not recorded for their results at $F = 137$. As an estimate, we use the values recorded at the frequencies $F = 109$ and $F = 124$ to extrapolate a possible value at $F = 137$. The principal effect of using a different

wave number is the change in the linear secondary growth rate b_B. To isolate the interaction region for comparison, the experimental points are shifted in R. This fixed shift is introduced to reduce deviations owing to unknown and unpredictable effects such as nonparallelism, pressure gradients, and the virtual leading edge. Based on the match-up of theory and experiment for an isolated TS wave, the shift is chosen as $\delta R = -10$. The results in figure 5(a) show the comparison for a TS wave with small initial amplitude.

Increasing the initial TS amplitude results in the development of a secondary wave as shown in figure 5(b). The amplitude of the secondary wave never becomes large enough to allow a strong primary/secondary interaction. Therefore, both waves harmlessly decay in both theory and experiment. A yet larger initial TS amplitude produces significant growth of the secondary wave as seen in figure 5(c). For these conditions a strong interaction occurs as conferred by both second-order theory and experiment. The quantitative agreement is reasonably good although the theory shows a stronger 'lift-off' of the two-dimensional wave. The last comparison for this case is given in figure 5(d) where a high initial TS amplitude produces strong secondary growth and nonlinear interaction. The experimental data for the two-dimensional wave amplitude show a larger 'dip' before the 'lift-off'. The deviations for the subharmonic wave amplitude may be the result of a mismatch in the spanwise wave number which would produce a different linear growth rate.

The second comparison is for the case $F = 82.7$ and $b = 0.129$, the conditions of Corke & Mangano (1987). Figure 6 shows theoretical curves and experimental data points. The initial amplitudes were chosen to provide good agreement in the linear region before onset of the interaction. During these calculations, a singularity occurred owing to the similarity in shape of v_B and v_{AB}, and the AB constant and function are not included in this solution. There is no loss of information however, since the similarity implies that the total secondary wave is characterized by v_B. The agreement for the two-dimensional wave is fair and the experimental data do not clearly show the 'dip' or 'lift-off' as predicted by the theory. The agreement for the subharmonic wave amplitude is good until breakdown occurs in the experiments. The nonlinear reduction in the growth rate of $u_S'_{max}$ is consistent between theoretical and experimental data.

In addition to the experimental cases, we have evaluated the results for conditions similar to the numerical simulations of Spalart & Yang (1987). Their simulations involved a two-dimensional wave and the simultaneous growth of subharmonic and fundamental modes. The qualitative agreement is good but the theory predicts the two-dimensional 'lift-off' at an earlier point in the evolutions.

- 23 -

This difference may be caused by the different mean-flows in theory and computation or may result from considering only single modes in the perturbation analysis. The presence of a full spectrum allows for a broader transfer of energy that tends to weaken the growth of individual modes. The low-amplitude simulation run of Spalart & Yang (1987, figure 7) supports our finding of a possible quasi-equilibrium evolution without any rapid growth toward breakdown.

6.3 Subharmonic Velocity Functions

In conjunction with the amplitude curves, the velocity functions provide a detailed picture of the disturbance field produced by the wave interactions. In the early stages of strong interaction, the major changes in the composite velocity field result from amplitude changes. Since the amplitudes play the role of 'weighting parameters', a rapid change in amplitude produces a restructuring of the velocity field. As the strong interaction progresses, however, not only the amplitudes but also the velocity functions are affected, primarily via A^*.

Using the independent velocity functions and the amplitude-growth curves, we construct the total composite functions for comparison with measured data. Figure 7 shows a sequence of functions u_{2D} for the total two-dimensional velocity field. Initially, at $R = 630$, the velocity distribution closely resembles the TS-wave profile. As the strong interaction takes place (see figure 2), the function is transformed into the characteristic 'bell shape' observed by Kachanov et al. (1977). The qualitative features of the u_{2D} functions are consistent with the experimental data given in figure 8. The net effect is a shift of the largest amplitude fluctuations from $y \approx 0.6$ to $y \approx 1.5$ and the dramatic growth of the maximum, while the peak associated with the deformed TS wave looses significance. Over this same region of interaction, $R = 630$–680, the shape of the subharmonic velocity function u_S remains virtually unchanged, as substantiated by figure 9.

6.4 Fundamental Amplitude Growth Curves

Like the subharmonic mode, the fundamental modes experience a strong primary/secondary interaction when the values of A and B are sufficiently large and of the same order. However, the behavior of the primary wave is significantly different and depends on the values of the wave amplitudes when the interaction occurs. If the interaction occurs at small amplitudes, the Landau constant a_{3^2} is negative and thus reduces the primary growth. The constant a_{B^2} remains negative as A^* decreases. If a_A is small or negative as it is past R_{II}, the primary wave amplitude tends rapidly to zero, more rapidly than in absence

of the fundamental wave. Consequently, B levels off and ultimately decreases owing to the lack of parametric forcing. The decay of the primary wave can only be prevented by a large positive growth rate a_A. These results suggest that for relatively small TS amplitudes fundamental type (K-type) breakdown must be initiated upstream of R_{II}. TS waves of lower frequencies are associated with larger growth rates a_A and hence are more susceptible to K-type breakdown. According to our analysis, it is not coincidental that the subharmonic route to transition was discovered at high frequencies with feeble growth rates. At much larger amplitudes, third-order effects become significant and halt the decay of the primary mode. Therefore, if the primary amplitude is large, fundamental breakdown can occur past R_{II}.

Figure 10 shows the third-order evolution of the different amplitude components for the conditions $F = 64.4$, $b = 0.44$ (Cornelius 1985). The amplitude A is driven to an equilibrium value by the strong interaction beginning at $R \approx 765$. The reduction in A results in a decrease in the secondary growth rate b_B. The two-dimensional physical amplitude $u_{2D}'_{max}$ experiences a 'lift-off' from A owing to the component $B^2 u_{B^2}$. The large corresponding function u_{B^2} explains why $u_{2D}'_{max}$ is larger than $A + B^2$. The three-dimensional amplitude $u_F'_{max}$ initially coincides with B. This agreement is mandatory since B is a measure of u_B at y_0, which initially is the position of the maximum of u_F'. During the interaction, $u_F'_{max}$ separates from B as a result of the increasing component $B^3 u_{B^3}$ The principal effects of the nonlinear interaction are to change the linear growth rate of B and to produce a saturation of B caused by terms of order B^3.

Peak- and valley-amplitude curves for the conditions of figure 10 are given in figure 11. This figure also shows the comparison of first- and third-order results. The third-order curves level off owing to the saturation of B. Contributions from higher spanwise wave numbers prevent the peak and valley curves from being as close together as the curves for the first-order case. Finally, figure 12 gives a comparison with the experimental results of Cornelius (1985). The agreement is good for both peak and valley up to $R \approx 776$. At this Reynolds number, the occurrence of high-frequency spikes was observed for the conditions $F = 64.4$, $b = 0.21$. The lack of agreement in and beyond the single-spike stage is caused by physical processes not accounted for in our theoretical model.

6.5 Fundamental Velocity Functions

The composite functions for the fundamental mode are presented as u_P and u_V, the rms velocity fluctuations at the peak and valley position, respectively. Figure 13 shows a sequence of peak profiles at different R locations. Initially the shape is similar to a TS-wave profile. Moving downstream, the maximum shifts outward and the profile develops a narrow maximum. Figure 14 shows the sequence of the corresponding profiles in the valley. The first distribution at $R = 700$ is a mildly distorted TS-wave profile. This profile changes over to a broader distribution on which new maxima arise.

Finally, we compare the composite functions u_P and u_V with the experimental data of Cornelius (1985). The calculated functions correspond to the amplitudes given in figure 12. Figure 15 compares the three velocity profiles at the peak for the Reynolds numbers $R = 716$, 735, and 755. The agreement is good for $R = 716$ and $R = 735$. At $R = 755$ the experiment shows larger values on the outer portion of the profile which may be related to the occurrence of spikes. The profiles at the valley for the same R locations are given in figure 16. These profiles show good agreement between theory and experiment. Overall, the experimental data offer strong support for our theoretical treatment of this problem.

7. Conclusions

7.1 Appraisal of the Approach

The principal aim of this work is to provide some understanding and explanation of the primary/secondary mode interaction in boundary layers. The convincing agreement between theory, experiment, and computer simulation has established the parametric origin of the secondary instability. Under the conditions prevailing in the experiments, the assumptions of the parametric approach are well justified (Herbert 1984a). However, when the amplitude of the secondary mode grows to a significant level, a mutual interaction must be permitted. Modeling this process as a pure mutual interaction of multiple primary waves was not yet successful in maintaining the crucial parametric resonance. The alternative approach developed here provides the secondary mode through parametric resonance yet permits the mutual interaction of this mode with the primary wave.

The pseudo-marching scheme in conjunction with the perturbation method provides a continuous transition from the purely parametric to the increasingly mutual interaction. Judging the agreement with experimental data and results of

computer simulations, the method appears to capture the physics of the problem. Surprisingly, the comparison with experimental data shows good agreement up to breakdown stage where the amplitudes are in excess of 6% for the subharmonic (Corke & Mangano 1987) and 10% for the fundamental (Cornelius 1985) type of transition. The assumptions of the theory, though expressed in the weak terms of perturbation analysis like "sufficiently large" appear to be justified and not overly restrictive. Our results also suggest that the essence of the transition process up to the breakdown stage is contained in the interaction of relatively few Fourier modes. This conclusion is supported by the numerical simulations of transition in plane Poiseuille flow by Gilbert & Kleiser (1987) and Zores (1989).

Perhaps the greatest value of this approach comes from the ability to decompose the flow field into components of well-defined order. This decomposition provides new insights unobtainable from experiments and transition simulations. These qualitative insights and the quantitative analytical capabilities of the method developed here provide for the first time the physical basis for a transition criterion.

7.2 Conditions for Breakdown

The results of this study provide new scenarios for the early stages of 'ribbon induced' transition. The theoretical results suggest a set of parameters that could be monitored to detect the onset of sustained growth and ultimate breakdown.

Under idealized conditions, the transition process begins with the onset of the two-dimensional wave. This wave then evolves within a virtually two-dimensional framework. Given the frequency and an initial amplitude, the wave development can be described by weakly nonlinear methods. For sufficiently large amplitudes, the two-dimensional wave parametrically excites a three-dimensional secondary wave. This phenomenon is characterized by the first occurrence of a positive growth rate b_B at some initial conditions (R_1, A_1). From this point on, the two- and three-dimensional wave undergo simultaneous evolution, initially without any significant effect of the secondary on the primary wave. If the two-dimensional wave decays in this initial phase, the secondary mode grows with diminishing rate and ultimately decays. However, once the secondary wave amplitude reaches a substantial level, a resonant interaction between the primary and secondary waves occurs. In a quiet environment with low initial amplitudes of primary and secondary modes, the interaction typically starts when both amplitudes reach approximately 1%. For subharmonic modes, this interaction is always favorable to sustained growth and therefore leads to breakdown.

For fundamental modes at low amplitudes, the nonlinear interaction reduces the growth and ultimately causes a rapid decay of the primary wave. Therefore, a significant primary growth rate is necessary to initiate K-breakdown. For large amplitudes, the primary/secondary interaction is always favorable to sustained growth.

The feedback loop suggested by the energy analysis of Croswell (1985) exists but is not as strong as previously anticipated. Once the conditions for self-sustained growth are established, the primary amplitude remains virtually constant and provides a diminished parametric forcing for the continued growth of the secondary wave. The observed and theoretically predicted energy increase in the two-dimensional field is caused by a rapidly increasing component of order B^2. This component is generated by nonlinear self-interaction of the secondary wave and does not support the catalytic action of the two-dimensional field. However, the strong self-sustained growth of both two- and three-dimensional disturbances on a convective time scale is the precursor of immediate breakdown. The tertiary instabilities associated with this process are outside the scope of the present theory.

Acknowledgment

Bertolotti, F. P. (1985) "Temporal and spatial growth of subharmonic disturbances in Falkner-Skan flows," M. S. Thesis, VPI&SU.

Corke, T. C. and Mangano, R. A. (1987) "Transition of a boundary layer: controlled fundamental-subharmonic interactions," Fluid Dynamics Center Rep. No. 87-1, Illinois Institute of Technology, Chicago, Illinois.

Cornelius, K. C. (1985) "Three dimensional wave development during boundary layer transition," Lockheed Georgia Res. Rep. LG85RR0004, Marietta, Georgia.

Craik, A. D. D. (1971) "Nonlinear resonant instability in boundary layers," *J. Fluid Mech.*, Vol. 50, pp. 393-413.

Croswell, J. W. (1985) "On the energetics of primary and secondary instabilities in plane Poiseuille flow," M. S. Thesis, VPI&SU.

Crouch, J. D. (1988) "The nonlinear evolution of secondary instabilities in boundary layers," Ph. D. Thesis, VPI&SU.

Gaster, M. (1962) "A note on the relation between temporally-increasing and spatially-increasing disturbances in hydrodynamic stability," *J. Fluid Mech.*, Vol. 14, pp. 222-224.

Gilbert, N. and Kleiser, L. (1987) "Low-resolution simulations of transitional and turbulent channel flow," in *Proc. Int. Conf. Fluid Mech.*, pp. 67-72, Peking University Press.

Herbert, Th. (1983) "On perturbation methods in nonlinear stability theory," *J. Fluid Mech.*, Vol. 126, pp. 167-186.

Herbert, Th. (1984a) "Analysis of the subharmonic route to transition in boundary layers," AIAA Paper No. 84-0009.

Herbert, Th. (1984b) "Secondary Instability of Shear Flows," in *Special Course on Stability and Transition of Laminar Flow*, AGARD Report No. 709.

Herbert, Th. (1985) "Three-dimensional phenomena in the transitional flat-plate boundary layer," AIAA Paper No. 85-0489.

Herbert, Th. (1986) "Vortical mechanisms in shear flow transition," in *Direct and Large Eddy Simulation of Turbulence*, ed. U. Schumann and R. Friedrich, pp. 19-36, Vieweg-Verlag.

Herbert, Th. (1988a) "Secondary instability of boundary layers," *Ann. Rev. Fluid Mech.*, Vol. 20, pp. 487-526.

Herbert, Th. (1988b) "Onset of Transition in Boundary Layers," *Int. J. Num. Meth. Fluids.* In press

Kachanov, Yu. S., Kozlov, V. V., and Levchenko, V. Ya. (1977) "Nonlinear development of a wave in a boundary layer," *Izv. AN USSR, Mekh. Zhidk. i Gaza,* Vol. 3, pp. 49-53. (In Russian)

Kachanov, Yu. S. and Levchenko, V. Ya. (1982) "Resonant interactions of disturbances in transition to turbulence in a boundary layer," Preprint No. 10-82, I.T.A.M., USSR Acad. Sci., Novosibirsk. (In Russian)

Kachanov, Yu. S. and Levchenko, V. Ya. (1984) "The resonant interaction of disturbances at laminar-turbulent transition in a boundary layer," *J. Fluid Mech.,* Vol. 138, pp. 209-247.

Klebanoff, P. S., Tidstrom, K. D., and Sargent, L. M. (1962) "The three-dimensional nature of boundary-layer instability," *J. Fluid Mech.,* Vol. 12, pp. 1-34.

Knapp, C. F. and Roache, P. J. (1968) "A combined visual and hot-wire anemometer investigation of boundary-layer transition," *AIAA J.,* Vol. 6, pp. 29-36.

Li, R. (1986) "Analysis for Taylor-Vortex Flow," Ph. D. Thesis, VPI&SU.

Nayfeh, A. H. (1985) "Three-dimensional spatial secondary instability in boundary-layer flows," AIAA Paper No. 85-1697.

Nayfeh, A. H. (1987) "Nonlinear stability of boundary layers," AIAA Paper No. 87-0044.

Orszag, S. A. and Patera, A. T. (1983) "Secondary instability of wall-bounded shear flows," *J. Fluid Mech.,* Vol. 128, pp. 347-385.

Nayfeh, A. H. and Mook, D. T. (1979) *Nonlinear Oscillations,* Wiley.

Schubauer, G. B. and Skramstad, H. K. (1948) "Laminar boundary-layer oscillations and transition on a flat plate," N.A.C.A. Rep. No. 909.

Spalart, P. R. and Yang, K.-S. (1987) "Numerical study of ribbon-induced transition in Blasius flow," *J. Fluid Mech.,* Vol. 178, pp. 345-365.

Zores, R. (1989) "Numerische Untersuchungen mit einem grobauflösenden Simulationsmodell für die turbulente Kanalströmung," DFVLR Report IB 221-89 A 24.

Figure Captions

Figure 1.   Schematic of energy transfer between the mean flow and the two-
and three-dimensional waves. The dashed line signifies the 'cata-
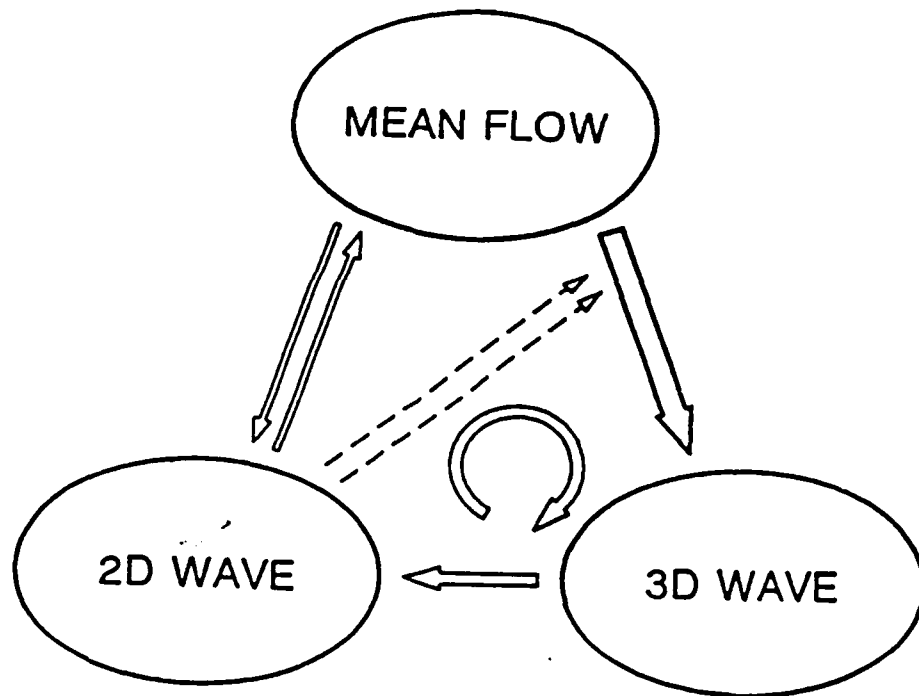lytic' parametric excitation (Herbert 1988a).

Figure 2.   Evolution of the different amplitude components A^*, $\hat{A}$, B, $u_{2D}'_{max}$,
and $u_S'_{max}$. Second-order results for the subharmonic mode at
$F= 124$, $b= 0.33$, and $\varepsilon= 0.1$. Initial values are $A= 7.82 \cdot 10^{-3}$ and
$B= 5.3 \cdot 10^{-5}$ at $R= 510$.

Figure 3.   Comparison of the first-, second-, and third-order evolutions of
$u_{2D}'_{max}$ and $u_S'_{max}$. Results for the subharmonic mode at $F= 124$,
$b= 0.33$, and $\varepsilon= 0.005$. Initial values are $A= 5 \cdot 10^{-3}$ and $B= 10^{-4}$ at
$R= 510$.

Figure 4.   Effect of the value of ε on the amplitude evolution of $u_{2D}'_{max}$ and
$u_S'_{max}$ for a second-order interaction. Results for the subharmonic
mode at $F= 124$, $b= 0.33$, and $\varepsilon= 0.05, 0.1, 0.15$. Initial values are
$A= 7.82 \cdot 10^{-3}$ and $B= 5.3 \cdot 10^{-5}$ at $R= 510$.

Figure 5.   Comparison of the evolution of $u_{2D}'_{max}$ and $u_S'_{max}$ with the experi-
ments of Kachanov & Levchenko (1984, figure 2). Second-order
results for the subharmonic mode at $F= 137$, $b= 0.40$, and $\varepsilon= 0.05$.
(a) The TS wave with initial values $A= 5.2 \cdot 10^{-4}$ at $R= 500$ in the
absence of the secondary mode. Initial values at $R= 510$ are (b)
$A= 0.4 \cdot 10^{-2}$ and $B= 2.5 \cdot 10^{-5}$, (c) $A= 1.03 \cdot 10^{-2}$ and $B= 0.65 \cdot 10^{-5}$,
(d) $A= 1.5 \cdot 10^{-2}$ and $B= 1.9 \cdot 10^{-5}$. Experimental data are shifted by
$R= -10$.

Figure 6.   Comparison of the evolution of $u_{2D}'_{max}$ and $u_S'_{max}$ with the experi-
ments of Corke & Mangano (1987, figure 65). Second-order results
for the subharmonic mode at $F= 82.7$, $b= 0.129$, and $\varepsilon= 0.05$. Ini-
tial values are $A= 4.5 \cdot 10^{-3}$ and $B= 1.1 \cdot 10^{-3}$ at $R= 750$.

Figure 7.   Evolution of the total two-dimensional velocity function u_{2D} over
$R= 630 - 680$. Second-order results for the subharmonic mode at
$F= 124$, $b= 0.33$, and $\varepsilon= 0.05$, with initial values $A= 7.82 \cdot 10^{-3}$ and
$B= 5.3 \cdot 10^{-5}$ at $R= 510$.

Figure 8.   Evolution of the total two-dimensional velocity function u_{2D} in the experiments of Kachanov et al. (1977). Results for the subharmonic mode at $F = 88$.

Figure 9.   Evolution of the total subharmonic velocity function u_S over $R = 630 - 680$. Second-order results for the subharmonic mode at $F = 124$, $b = 0.33$, and $\varepsilon = 0.05$, with initial values $A = 7.82 \cdot 10^{-3}$ and $B = 5.3 \cdot 10^{-5}$ at $R = 510$.
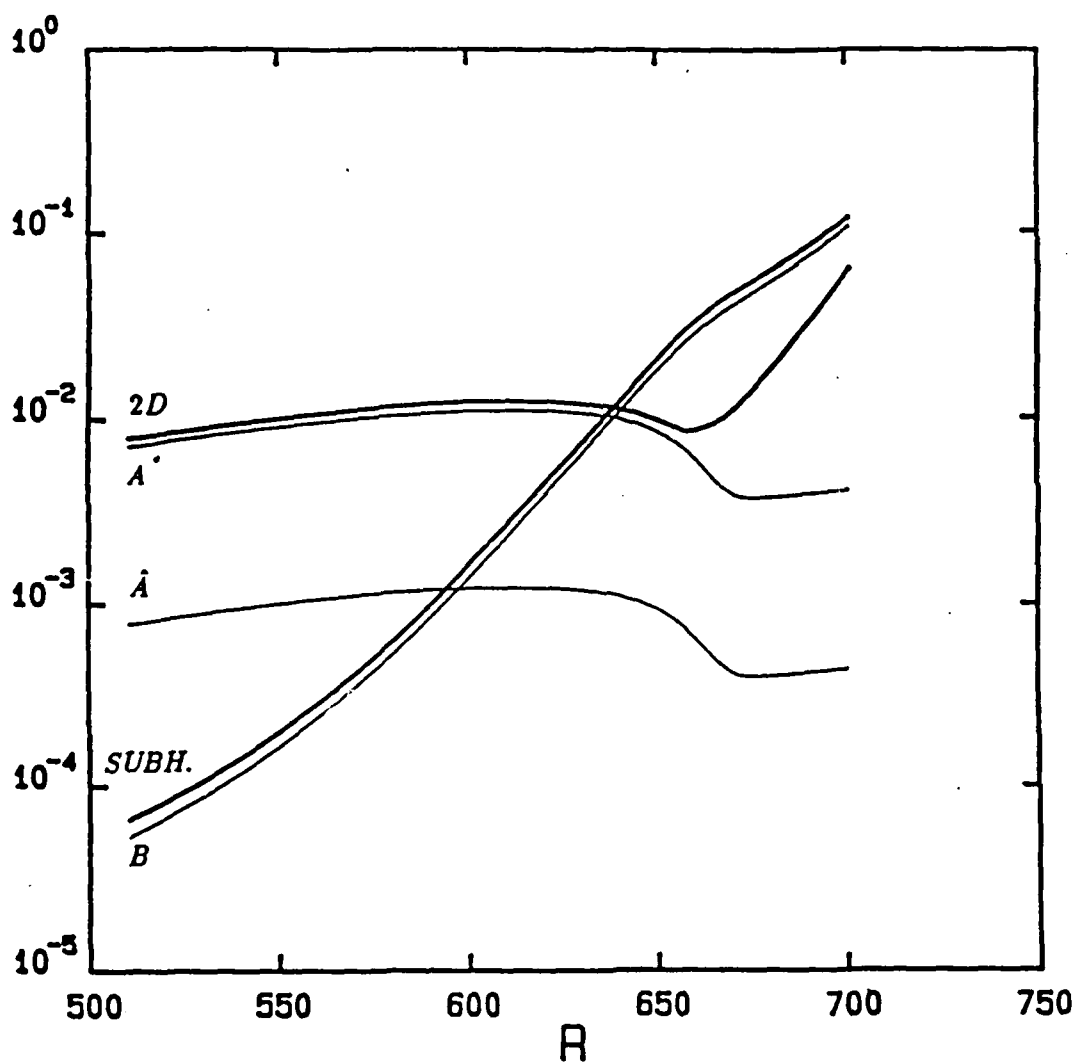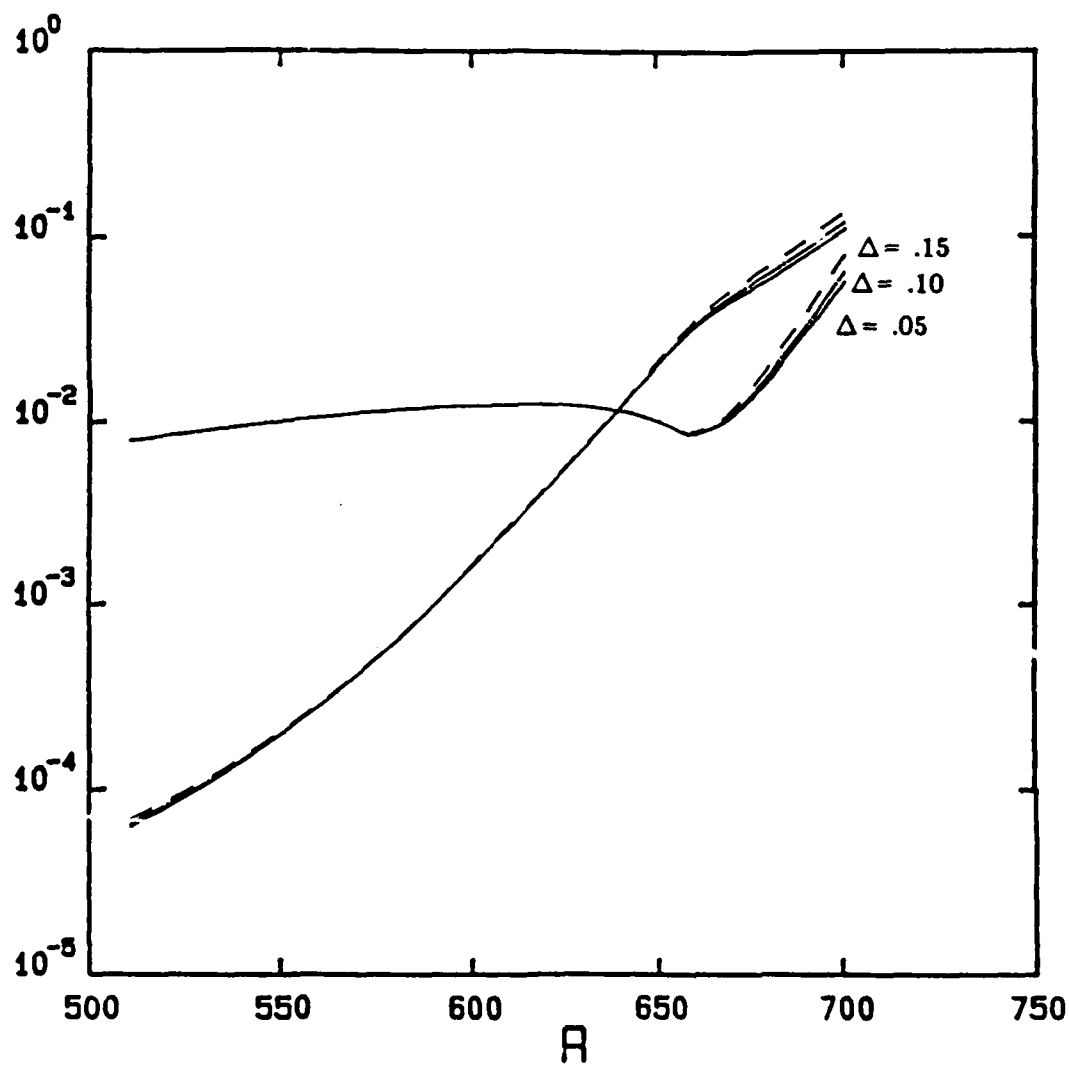
Figure 10.   Evolution of the different amplitude components, A^*, $\hat{A}$, B, $u_{2D}'_{max}$, and $u_F'_{max}$. Third-order results for the fundamental mode at $F = 64.4$, $b = 0.44$, and $\varepsilon = 0.01$. Initial values are $A = 1.6 \cdot 10^{-2}$ and $B = 7 \cdot 10^{-4}$ at $R = 675$.

Figure 11.   Evolution of $u_P'_{max}$ and $u_V'_{max}$ for first- and third-order results at $F = 64.4$, $b = 0.44$, and $\varepsilon = 0.01$. Initial values are $A = 1.6 \cdot 10^{-2}$ and $B = 7 \cdot 10^{-4}$ at $R = 675$.

Figure 12.   Comparison of the evolution of $u_P'_{max}$ and $u_V'_{max}$ with the experiments of Cornelius (1985, figures 16, 17). Third-order results for the fundamental mode at $F = 64.4$, $b = 0.44$, and $\varepsilon = 0.01$. Initial values are $A = 1.6 \cdot 10^{-2}$ and $B = 7 \cdot 10^{-4}$ at $R = 675$.

Figure 13.   Evolution of the total velocity profile u_P at the peak position for $R = 730 - 780$. Third-order results for the fundamental mode at $F = 64.4$, $b = 0.44$, and $\varepsilon = 0.01$, with initial values $A = 1.6 \cdot 10^{-2}$ and $B = 7 \cdot 10^{-4}$ at $R = 675$.

Figure 14.   Evolution of the total velocity profile u_V at the valley position for $R = 730 - 780$. Third-order results for the fundamental mode at $F = 64.4$, $b = 0.44$, and $\varepsilon = 0.01$, with initial values $A = 1.6 \cdot 10^{-2}$ and $B = 7 \cdot 10^{-4}$ at $R = 675$.

Figure 15.   Comparison of the total velocity profile u_P at the peak position with the experiments of Cornelius (1985, figure 16). Normalized function at (a) $R = 716$; (b) $R = 735$; (c) $R = 755$. Third-order results for the fundamental mode at $F = 64.4$, $b = 0.44$, and $\varepsilon = 0.01$, with initial values $A = 1.6 \cdot 10^{-2}$ and $B = 7 \cdot 10^{-4}$ at $R = 675$.

Figure 16.   Comparison of the total velocity profile, u_V at the valley position with the experiments of Cornelius (1985, figure 17). Normalized

function at (a) $R = 716$; (b) $R = 735$; (c) $R = 755$. Third-order results for the fundamental mode at $F = 64.4$, $b = 0.44$, and $\varepsilon = 0.01$, with initial values $A = 1.6 \cdot 10^{-2}$ and $B = 7 \cdot 10^{-4}$ at $R = 675$.

Figure 1.   Schematic of energy transfer between the mean flow and the two-
and three-dimensional waves. The dashed line signifies the 'cata-
lytic' parametric excitation (Herbert 1988a).

Figure 2. Evolution of the different amplitude components A^*, $\hat{A}$, B, $u_{2D}{}'_{max}$, and $u_S{}'_{max}$. Second-order results for the subharmonic mode at $F = 124$, $b = 0.33$, and $\varepsilon = 0.1$. Initial values are $A = 7.82 \cdot 10^{-3}$ and $B = 5.3 \cdot 10^{-5}$ at $R = 510$.
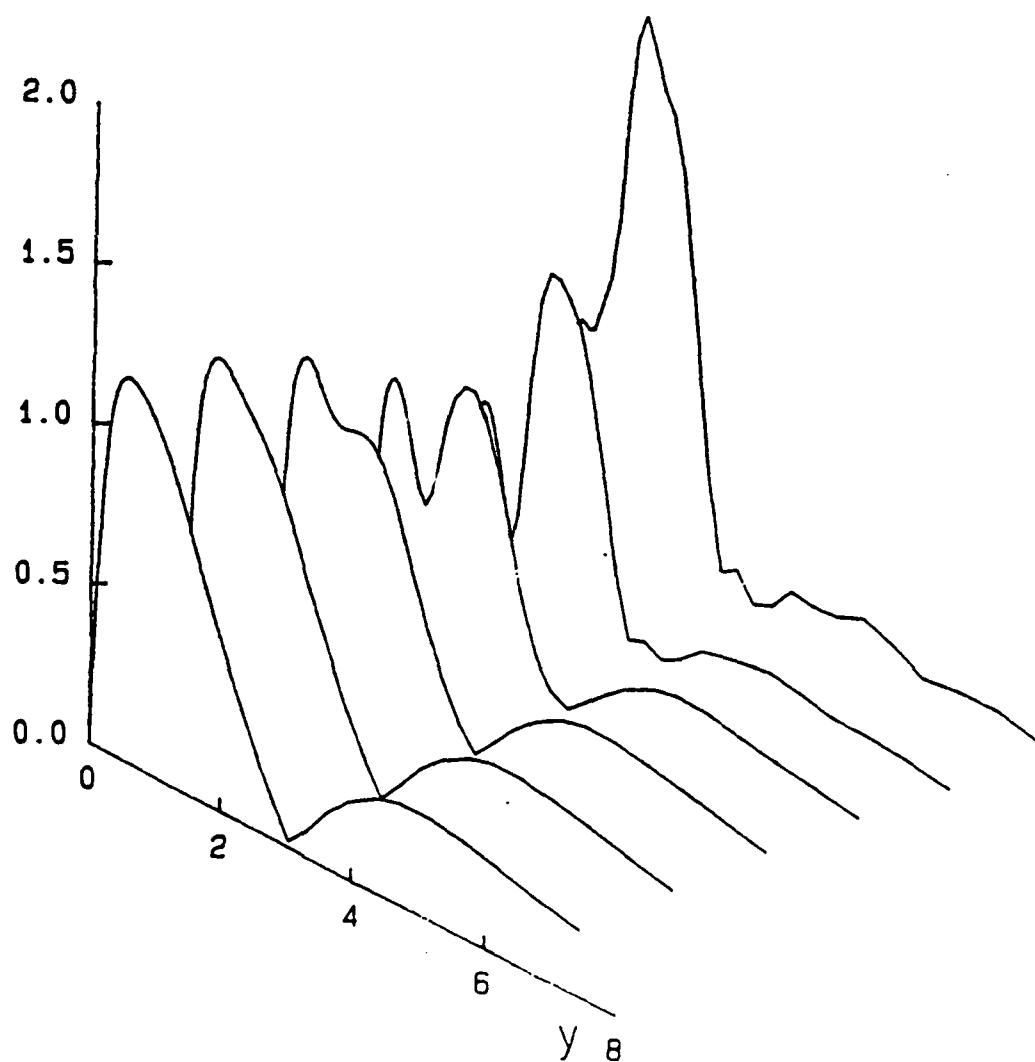
Figure 3. Comparison of the first-, second-, and third-order evolutions of $u_{2D}{}'_{max}$ and $u_S{}'_{max}$. Results for the subharmonic mode at $F = 124$, $b = 0.33$, and $\varepsilon = 0.005$. Initial values are $A = 5 \cdot 10^{-3}$ and $B = 10^{-4}$ at $R = 510$.

Figure 4.   Effect of the value of ε on the amplitude evolution of $u_{2D}'_{max}$ and $u_S'_{max}$ for a second-order interaction. Results for the subharmonic mode at $F= 124$, $b= 0.33$, and ε= 0.05, 0.1, 0.15. Initial values are $A= 7.82 \cdot 10^{-3}$ and $B= 5.3 \cdot 10^{-5}$ at $R= 510$.
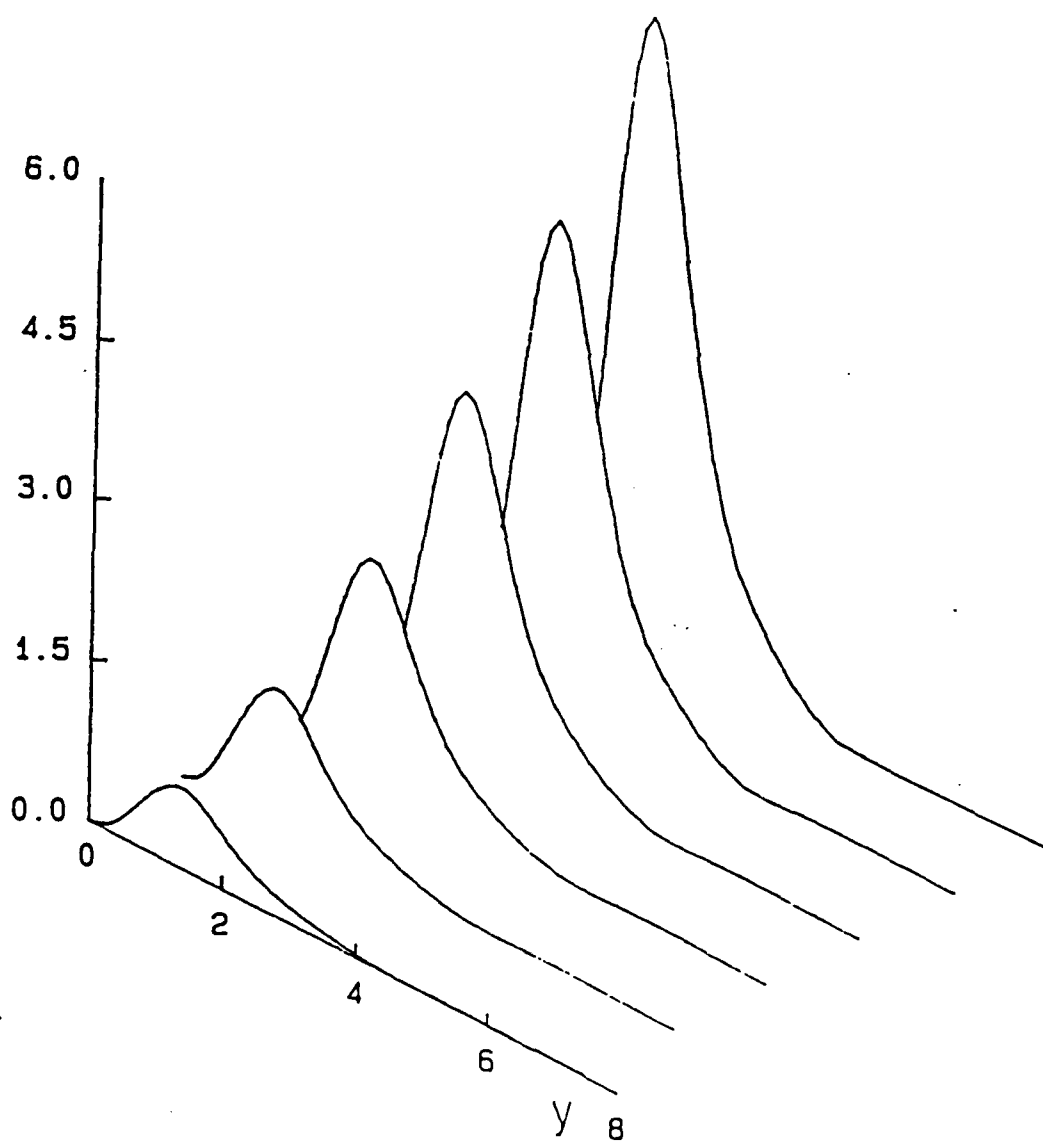
Figure 5.   Comparison of the evolution of $u_{2D}'_{max}$ and $u_S'_{max}$ with the experiments of Kachanov & Levchenko (1984, figure 2). Second-order results for the subharmonic mode at $F= 137$, $b= 0.40$, and $\varepsilon= 0.05$. (a) The TS wave with initial values $A= 5.2 \cdot 10^{-4}$ at $R= 500$ in the absence of the secondary mode. Initial values at $R= 510$ are (b) $A= 0.4 \cdot 10^{-2}$ and $B= 2.5 \cdot 10^{-5}$, (c) $A= 1.03 \cdot 10^{-2}$ and $B= 0.65 \cdot 10^{-5}$, (d) $A= 1.5 \cdot 10^{-2}$ and $B= 1.9 \cdot 10^{-5}$. Experimental data are shifted by $R= -10$.

(a)

Figure 5 (b)
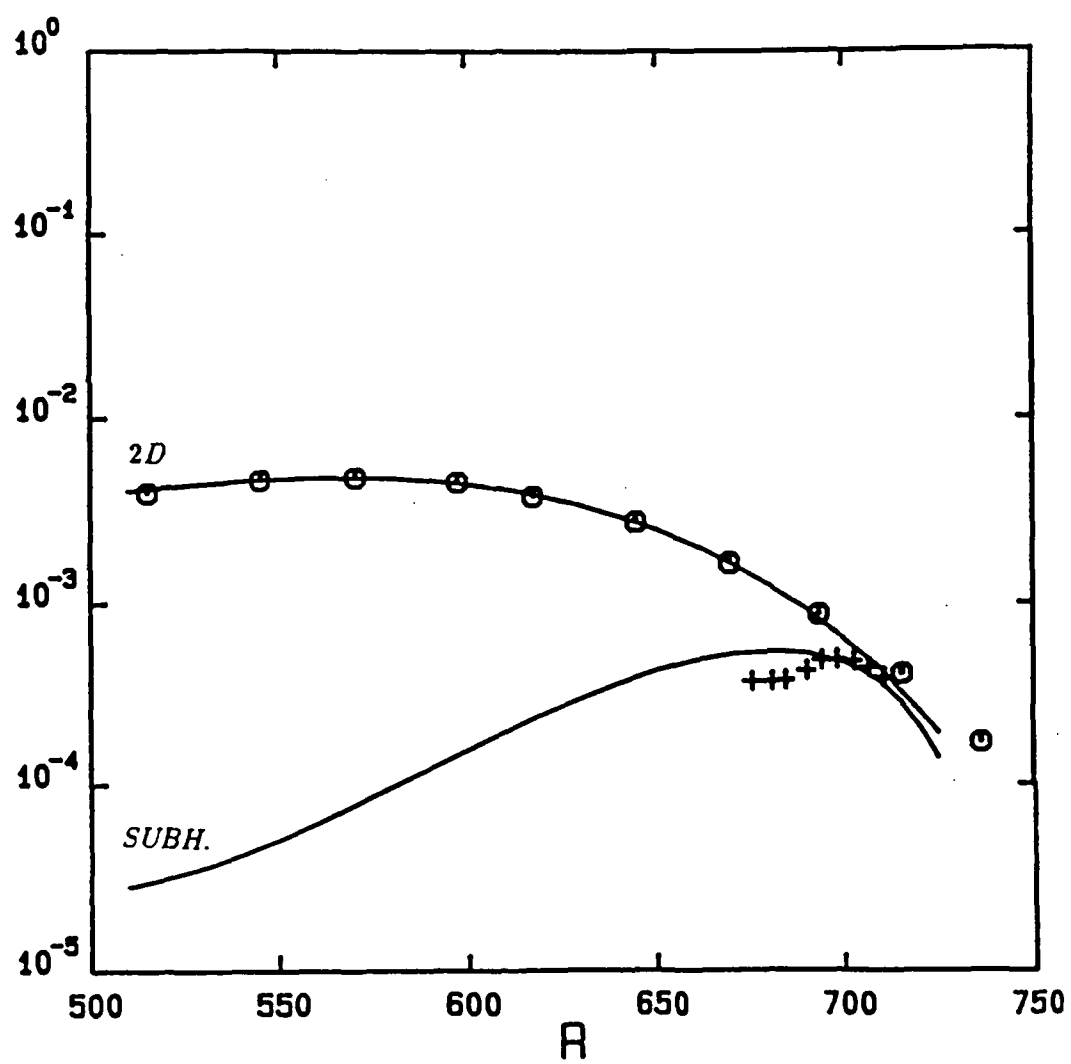
Figure 5 (c)
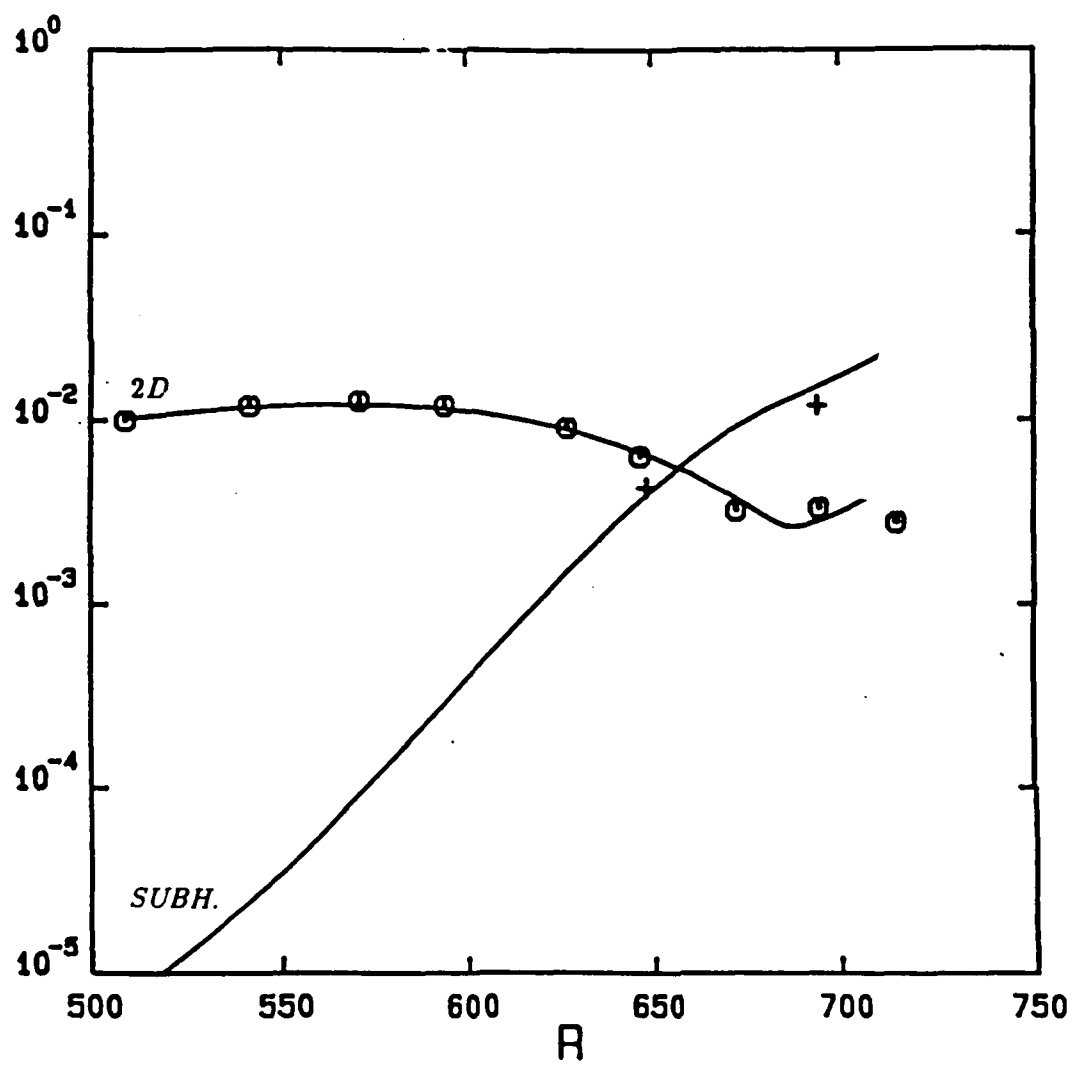
Figure 5 (d)

Figure 6. Comparison of the evolution of $u_{2D}'_{max}$ and $u_{S}'_{max}$ with the experiments of Corke & Mangano (1987, figure 65). Second-order results for the subharmonic mode at $F = 82.7$, $b = 0.129$, and $\varepsilon = 0.05$. Initial values are $A = 4.5 \cdot 10^{-3}$ and $B = 1.1 \cdot 10^{-3}$ at $R = 750$.

Figure 7.   Evolution of the total two-dimensional velocity function u_{2D} over $R = 630 - 680$. Second-order results for the subharmonic mode at $F = 124$, $b = 0.33$, and $\varepsilon = 0.05$, with initial values $A = 7.82 \cdot 10^{-3}$ and $B = 5.3 \cdot 10^{-5}$ at $R = 510$.

Figure 8.   Evolution of the total two-dimensional velocity function u_{2D} in the experiments of Kachanov et al. (1977). Results for the subharmonic mode at $F = 88$.

Figure 9.   Evolution of the total subharmonic velocity function u_S over $R = 630 - 680$. Second-order results for the subharmonic mode at $F = 124$, $b = 0.33$, and $\varepsilon = 0.05$, with initial values $A = 7.82 \cdot 10^{-3}$ and $B = 5.3 \cdot 10^{-5}$ at $R = 510$.

Figure 10. Evolution of the different amplitude components, A^*, $\hat{A}$, B, $u_{2D}'_{max}$, and $u_F'_{max}$. Third-order results for the fundamental mode at $F = 64.4$, $b = 0.44$, and $\varepsilon = 0.01$. Initial values are $A = 1.6 \cdot 10^{-2}$ and $B = 7 \cdot 10^{-4}$ at $R = 675$.
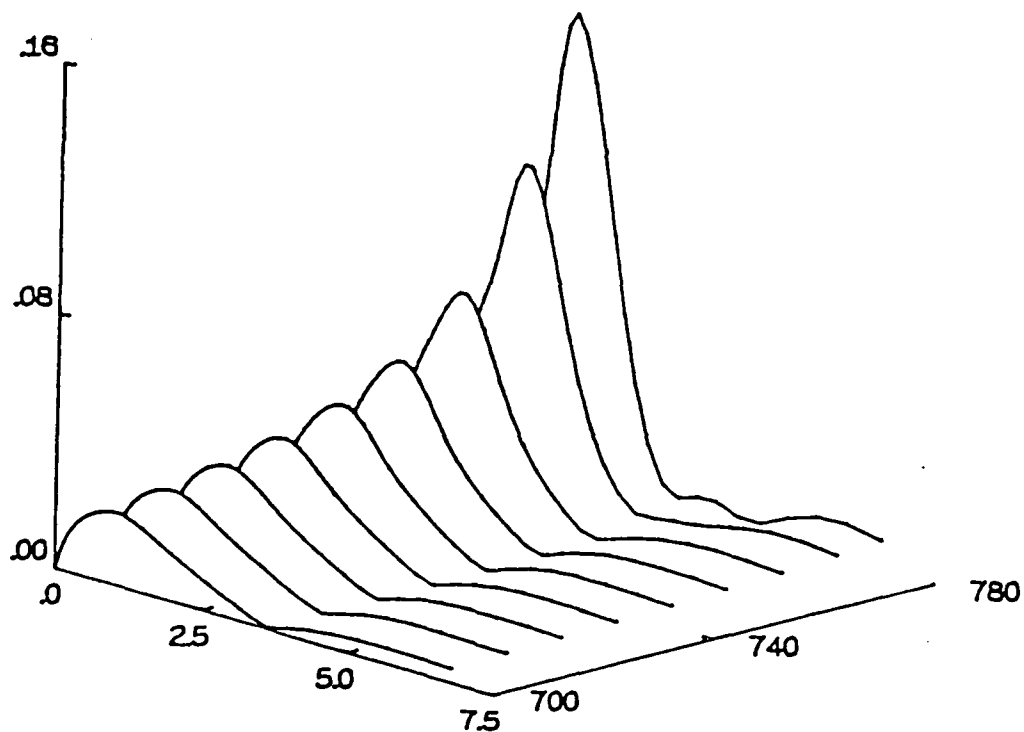
Figure 11. Evolution of $u_P'_{max}$ and $u_V'_{max}$ for first- and third-order results at $F = 64.4$, $b = 0.44$, and $\varepsilon = 0.01$. Initial values are $A = 1.6 \cdot 10^{-2}$ and $B = 7 \cdot 10^{-4}$ at $R = 675$.

Figure 12. Comparison of the evolution of $u_P{'}_{max}$ and $u_V{'}_{max}$ with the experiments of Cornelius (1985, figures 16, 17). Third-order results for the fundamental mode at $F = 64.4$, $b = 0.44$, and $\varepsilon = 0.01$. Initial values are $A \simeq 1.6 \cdot 10^{-2}$ and $B = 7 \cdot 10^{-4}$ at $R = 675$.

Figure 13. Evolution of the total velocity profile u_P at the peak position for $R = 730 - 780$. Third-order results for the fundamental mode at $F = 64.4$, $b = 0.44$, and $\varepsilon = 0.01$, with initial values $A = 1.6 \cdot 10^{-2}$ and $B = 7 \cdot 10^{-4}$ at $R = 675$.
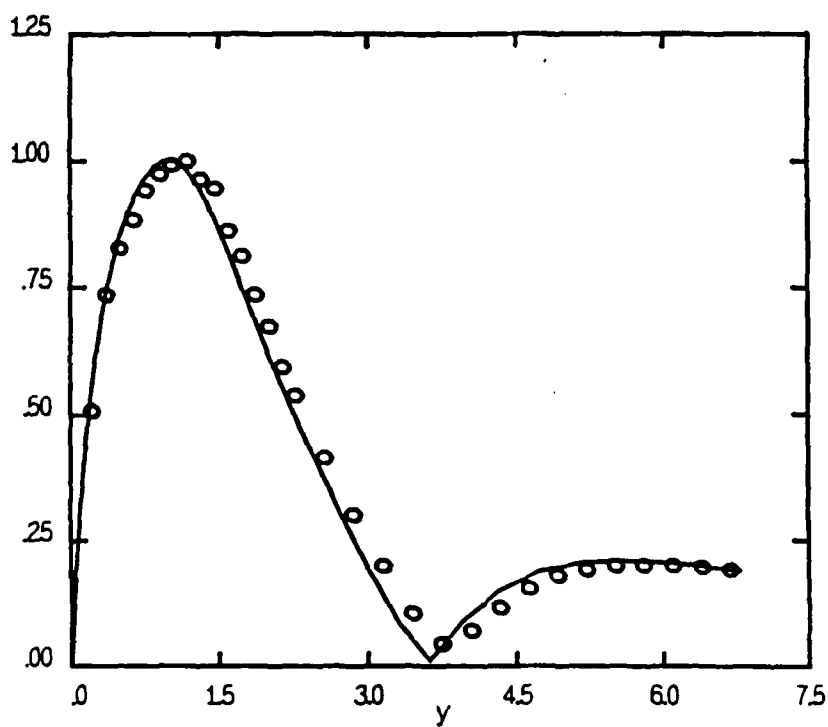
Figure 14.   Evolution of the total velocity profile u_V at the valley position for $R = 730 - 780$. Third-order results for the fundamental mode at $F = 64.4$, $b = 0.44$, and $\varepsilon = 0.01$, with initial values $A = 1.6 \cdot 10^{-2}$ and $B = 7 \cdot 10^{-4}$ at $R = 675$.
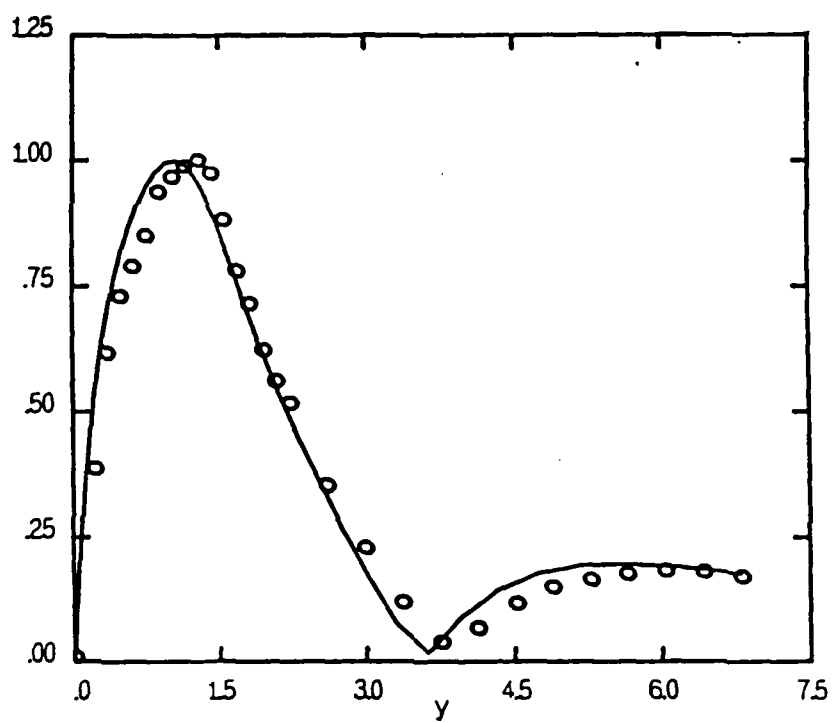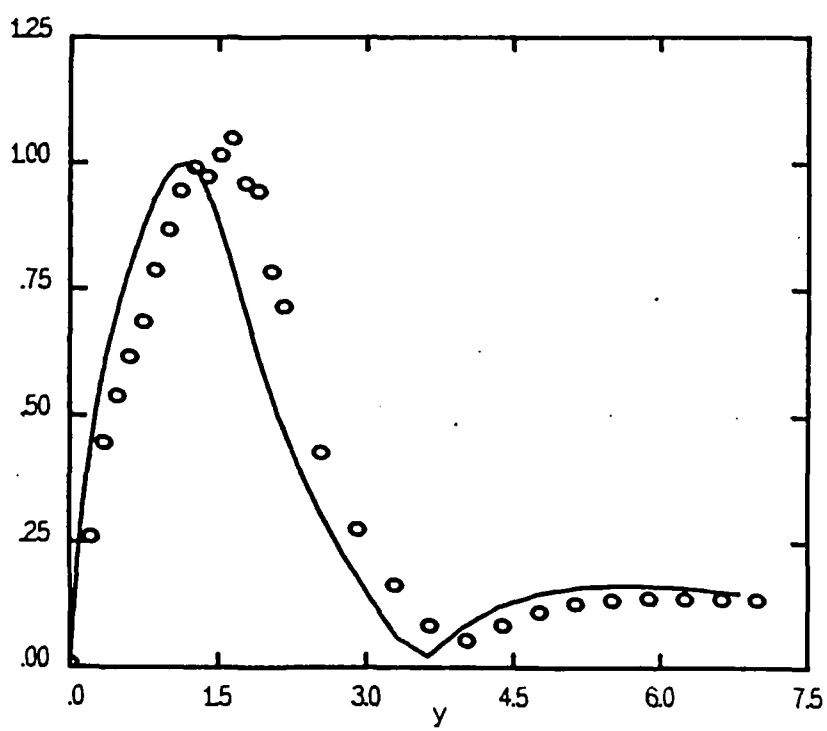
Figure 15. Comparison of the total velocity profile u_P at the peak position with the experiments of Cornelius (1985, figure 16). Normalized function at (a) $R = 716$; (b) $R = 735$; (c) $R = 755$. Third-order results for the fundamental mode at $F = 64.4$, $b = 0.44$, and $\varepsilon = 0.01$, with initial values $A = 1.6 \cdot 10^{-2}$ and $B = 7 \cdot 10^{-4}$ at $R = 675$.

(a)

Figure 15 (b)

Figure 15 (c)

Figure 16. Comparison of the total velocity profile, u_v at the valley position with the experiments of Cornelius (1985, figure 17). Normalized function at (a) $R=716$; (b) $R=735$; (c) $R=755$. Third-order results for the fundamental mode at $F=64.4$, $b=0.44$, and $\varepsilon=0.01$, with initial values $A=1.6\cdot10^{-2}$ and $B=7\cdot10^{-4}$ at $R=675$.
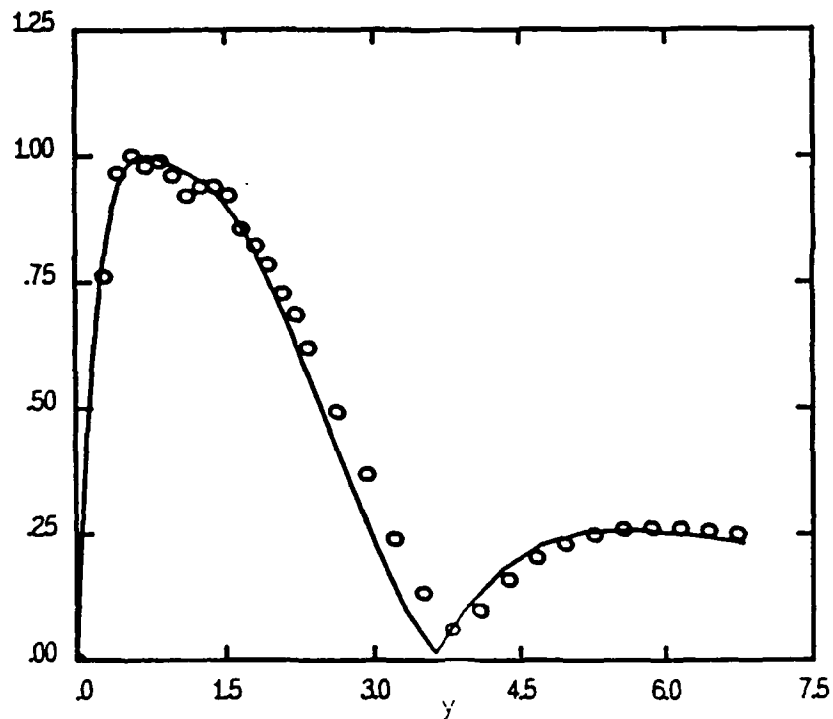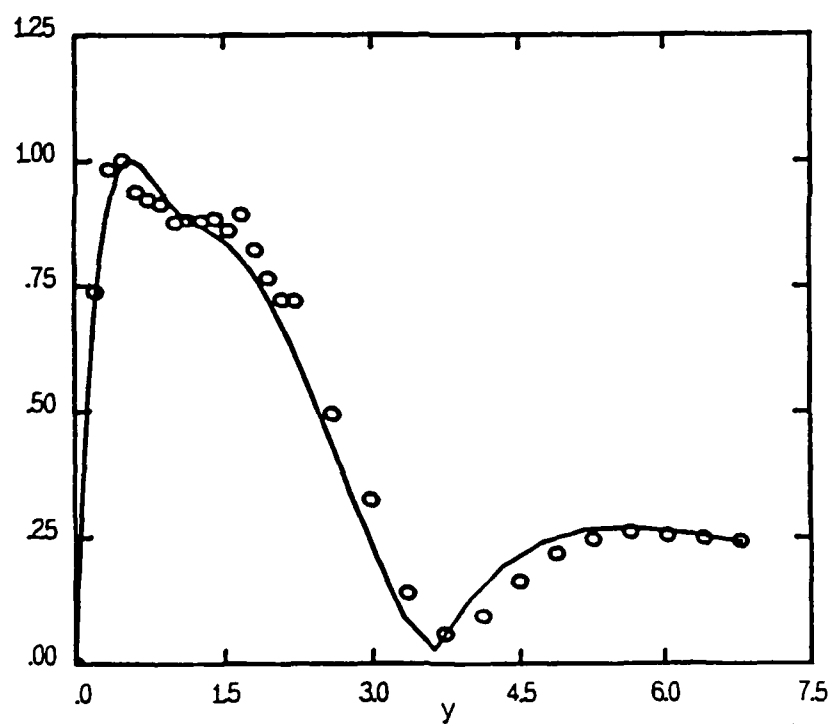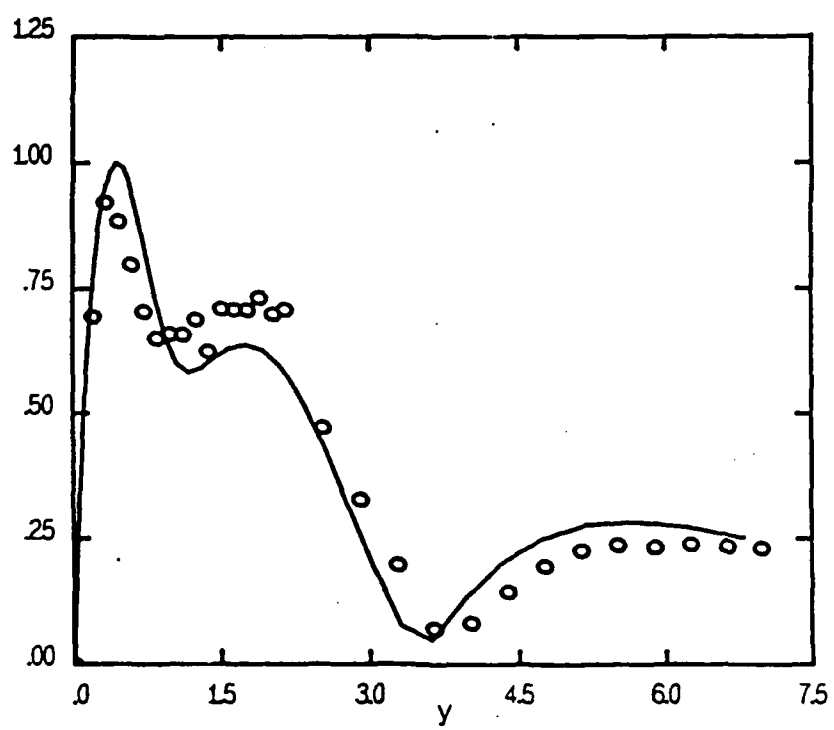
(a)

Figure 16 (b)

Figure 16 (c)

Appendix E

Appendix E

"Linear and Nonlinear Stability of the Blasius Boundary Layer,"

(Draft)

by F. P. Bertolotti, Th. Herbert, and P. R. Spalart

to be submitted to J. Fluid Mech.

Abstract

Two new techniques for the study of the linear and nonlinear instability in growing boundary layers are presented. The first technique employs partial differential equations of parabolic type exploiting the slow change of the mean flow, disturbance velocity profiles, wavelengths, and growth rates in the streamwise direction. The second technique solves the Navier-Stokes equation for spatially evolving disturbances using buffer zones adjacent to the inflow and outflow boundaries. Results of both techniques are in excellent agreement. The linear and nonlinear development of small amplitude Tollmien-Schlichting waves in the Blasius boundary layer is investigated with both techniques and with a local procedure based on a system of ordinary differential equations. The results are compared with previous work and the effects of nonparallelism and nonlinearity are clarified. The effect of nonparallelism is confirmed to be weak and consequently, not responsible for the discrepancies between measurements and theoretical results for parallel flow. Experimental uncertainties, the adopted definition of the growth rate, and the transient initial evolution of the TS wave in vibrating-ribbon experiments likely cause the discrepancies. The effect of nonlinearity is consistent with previous weakly nonlinear theories. While nonlinear effects are small near branch I of the neutral curve, they are significant near branch II and delay or even prevent the decay of the wave.

1 Introduction

The breakthrough in the analysis of the viscous instability of shear flows was achieved by Tollmien (1929) and Schlichting (1933) for the Blasius boundary layer which, owing to its streamwise growth, does not satisfy the basic assumption of a parallel flow in the Orr-Sommerfeld theory. The results of Tollmien and Schlichting were experimentally confirmed by Schubauer & Skramstad (1947). This confirmation is remarkable since Schubauer & Skramstad recorded spatial growth rates and converted these by use of the phase velocity to the temporal growth rates calculated by Schlichting (1933). Moreover, the disturbances were certainly of finite, observable amplitude. Gaster (1965) suggested the direct solution of the Orr-Sommerfeld equation for spatial growth rates and clarified the relation between spatial and temporal growth rates. Although access to powerful computers has eased, the less demanding temporal approach and the a posteriori conversion to spatial growth is still preferred.

The increasing accuracy in solving the Orr-Sommerfeld equation made clear that a discrepancy remained between theoretical and experimental results on the neutral curve for two-dimensional TS waves. Since these discrepancies are strongest at high frequency and low Reynolds number, the neglect of the boundary-layer growth was considered the most likely cause. Numerous efforts have been made to avoid the approximations - parallel mean flow and linearization - in the stability analysis of boundary layers. The most direct attempt to obtain stability results for two-dimensional disturbances has been made by Fasel (1976) by directly solving the Navier-Stokes equations numerically. The key to this success was the formulation of non-reflective artificial outflow-boundary conditions, a problem that is still unsolved for more general disturbances. In a similar approach, Bayliss et al. (1985) obtained results for the streamwise evolution of linear and nonlinear TS waves. These numerical studies, however, did not resolve the discrepancies between experiment and theory.

Other efforts aimed at avoiding only one of the crucial approximations. Itoh (1974) and Herbert (1974) applied perturbation methods to incorporate the effect of nonlinearity on the growth of two-dimensional waves and partially overcame the problem in representing the mean-flow distortion within the parallel-flow approximation. Within a strictly parallel framework, no mean-flow solution to the Navier-Stokes or boundary-layer equations exists

in a semi-infinite domain.

The effect of nonparallelism in the Blasius boundary layer has been studied with the method of multiple scales by Bouthier (1972), Saric & Nayfeh (1977), Van Stijn & Van de Vooren (1983), and Bridges & Morris (1984), with an iterative method by Gaster (1974), and with an asymptotic expansion in the frequency by Itoh (1986). Bouthier concluded that, in contrast to the parallel case, the growth rate of disturbances in nonparallel flows depends on the distance from the plate and on the flow quantity considered and thus requires careful definition. Although this conclusion was confirmed in the subsequent studies, their results are different and puzzling. In terms of the preferred experimental measure u'_{max}, the maximum streamwise rms fluctuation, Gaster found a neutral curve close to the parallel-flow result. While his findings were confirmed by Van Stijn & Van de Vooren and Bridges & Morris, Saric & Nayfeh presented a different neutral curve in better agreement with the experimental data. Moreover, their results were confirmed with new measurements by Kachanov & Levchenko (1977), leaving the truth hard to find.

Clarification of the nonparallel effect and of the combined effects of nonparallelism and nonlinearity would be highly desirable. The attempt to incorporate nonlinear effects in the multiple-scales approach fails, however, since the crucial solvability condition determines only one correction, either for nonparallelism or nonlinearity. This failure is likely caused by accounting for small terms of the same order at different levels of approximation, a procedure that is not rational in the sense of Van Dyke (1975). More recently, asymptotic theories valid in the limit of infinite Reynolds number have incorporated the effects of nonparallelism (Smith 1979a, 1979b) and nonparallelism and nonlinearity simultaneously (Goldstein & Durbin 1986). Smith finds the lower branch of the neutral curve similar to Saric & Nayfeh (1977) and that accounting for nonparallelism improves the agreement with the experimental data. However, the accuracy of the asymptotic results at the relatively low Reynolds numbers of concern is not verified.

Here, we apply three different methods for analyzing the stability of boundary layers based on ordinary, parabolic partial, and elliptic partial differential equations. The latter two methods account for both nonparallel and nonlinear effects. The method based on differential equations of parabolic type exploits the facts that the mean flow is governed by the boundary-layer approximation and, moreover, the second derivatives of the

disturbance growth rate, wavelength, and velocity profile with respect to the streamwise direction are sufficiently small to be neglected. While these facts have been used in previous multiple-scale analyses and the parabolic nature of the resulting intermediate equations has been mentioned by Gaster (1965), their potential for solving the stability problem has not been recognized. These parabolic equations, which we denote as parabolized stability equations (PSE), describe the evolution of linear or nonlinear two- or three-dimensional disturbances in boundary-layer flows with combined slowly changing streamwise properties such as nonparallelism, real-gas effects, or dissociation, although we restrict the formulation here to the Blasius boundary layer. The PSE can be applied as well in parallel flows to study the temporal or spatial nonlinear evolution of initial data. The initial-boundary-value problem associated with the parabolic equations can be solved with a marching procedure. Initial conditions can be arbitrarily chosen or can be obtained from a local procedure. This procedure solves a homogeneous linear system of ordinary differential equations for local eigensolutions similar to previous studies. These eigensolutions agree with the solution of the linearized PSE within negligible terms. Given arbitrary initial conditions, the PSE solution will exhibit a transient behavior.

The use of parabolic differential equations in the analysis of problems of basically elliptic nature with small feedback is successful in some other areas, e.g. the analysis of acoustic wave propagation (McAninch 1986). In the field of weakly nonparallel flow stability, Hall (1983) suggested solving parabolic equations for steady Görtler vortices describing the evolution within terms of order $O(R_x^{-1})$, where R_x is the Reynolds number based on the streamwise variable. In essence, this approach considers Görtler vortices a three-dimensional solution of the boundary-layer equations. For steady, spanwise periodic disturbances, Hall's equations are a special case of the PSE formulated in curvilinear coordinates. Itoh (1986) derived a parabolic equation for small-amplitude TS waves identical with the linearized PSE for two-dimensional disturbances. Itoh observed that his equation contains both the unsteady boundary-layer equation and the Orr-Sommerfeld equation as limits, hence its solutions can directly describe the matching of solutions shown with asymptotic methods by Goldstein (1983). Since separation of variables is inapplicable, Itoh choose an asymptotic expansion in frequency to reduce the problem to a sequence of ordinary differential equations.

An alternative approach for studying the spatial evolution of disturbances

in boundary layers including nonlinear and nonparallel effects is the direct numerical solution of the Navier-Stokes equations (DNS). Special attention must be paid to the non-physical outflow-boundary conditions to avoid the upstream reflection of energy of outflowing disturbances. Here we present a spectral method for solving the Navier-Stokes equations that avoids reflections by fringe regions adjacent to the inflow and outflow boundaries, yet maintains the benefits of using Fourier series in the streamwise and spanwise direction. The DNS approach takes no advantage of the essentially parabolic character of the disturbance evolution except in the fringe regions. Provided the fringe regions and streamwise periodic boundary conditions do not bias the solution, the DNS yield the benchmark for other approaches involving the one or other approximation.

Both PSE and DNS approach have trade-offs. The DNS solution remains accurate through transition into turbulent flow if the resolution is sufficient. The disadvantage is the enormous demand in computer time and memory. The validity of the PSE may restrict their use in the late stages of transition that are characterized by tertiary instabilities and the occurrence of spikes. In the earlier stages, however, solving the PSE is very efficient, more efficient than solving the traditional eigenvalue problems, and therefore the PSE are an attractive tool for studies on nonlinear wave interactions as well as for practical applications.

This paper consists of three major parts. Chapter 2 describes the parabolic stability equations and the associated eigenvalue problem for local solutions. Chapter 3 discusses the approch to solving the Navier-Stokes equations. Results of the various methods are presented in Chapter 4 for a comparison between each other and with previous work. Although the development of the PSE approach by Herbert & Bertolotti and of the DNS approach by Spalart occurred independently, we consider the side by side presentation of the two approaches and their results beneficial to both the verification of the new tools and the establishment of an accurate set of benchmark data for the nonparallel and nonlinear stability of the Blasius boundary layer.

2 The Parabolic Stability Equations

Without loss of generality, we consider two-dimensional disturbances in the Blasius boundary layer. The extension to three-dimensional disturbances and nonsimilar boundary-layer flows is straightforward. We use Cartesian coordinates x, y, where x is the streamwise direction and y is normal to the plate. The Navier-Stokes equations are written in terms of the stream function Ψ to satisfy continuity identically,

$$(\frac{\partial}{\partial t} - \frac{1}{R_0}\nabla^2 + \frac{\partial \Psi}{\partial y}\frac{\partial}{\partial x} - \frac{\partial \Psi}{\partial x}\frac{\partial}{\partial y})\nabla^2\Psi = 0 \tag{1}$$

All quantities are nondimensionalized using the velocity U_∞ and the fixed length $\delta_0 = \sqrt{\nu \tilde{x}_0/U_\infty}$, where $\tilde{x}_0$ is a fixed dimensional distance from the leading edge and ν the kinematic viscosity. $R_0 = U_\infty \delta_0/\nu$ is the Reynolds number based on δ_0 and $R_0 = (U_\infty \tilde{x}_0/\nu)^{1/2}$. We further note the relation $x_0 = \tilde{x}_0/\delta_0 = R_0$.

We decompose the streamfunction into the basic flow, $\Psi_0(x,y)$, and the disturbance, $\psi(x,y,t)$. Within the boundary layer approximation, the basic flow is given by $\Psi_0 = f(\eta)(x/x_0) + O(R_0^{-2})$ where f satisfies the Blasius equation,

$$f''' + \frac{1}{2}ff'' = 0 \tag{2}$$

$$f = f' = 0 \text{ at } \eta = 0,\ f' \to 1 \text{ as } \eta \to \infty$$

with $\eta = \tilde{y}/\delta(\tilde{x})$ and $\tilde{y}$ is the dimensional coordinate normal to the plate. The nonlinear equation governing the disturbance ψ is obtained by introducing the combined flow into the Navier-Stokes equation and subtracting the equation satisfied by the basic flow:

$$(\frac{\partial}{\partial t} - \frac{1}{R_0}\nabla^2 + \frac{\partial \Psi_0}{\partial y}\frac{\partial}{\partial x} - \frac{\partial \Psi_0}{\partial x}\frac{\partial}{\partial y})\nabla^2\psi \tag{3}$$

$$+\frac{\partial \psi}{\partial y}\frac{\partial^3 \Psi_0}{\partial x \partial y^2} - \frac{\partial \psi}{\partial x}\frac{\partial^3 \Psi_0}{\partial y^3} = (\frac{\partial \psi}{\partial x}\frac{\partial}{\partial y} - \frac{\partial \psi}{\partial y}\frac{\partial}{\partial x})\nabla^2\psi + O(R_0^{-2})$$

where the errors of order $O(R_0^{-2})$ are introduced by the boundary-layer approximation to the mean flow.

Owing to its elliptic nature, this equation supports solutions in the form of waves. Applying the boundary-layer approximation directly to this equation and thereby changing the character from elliptic to parabolic would be incorrect since the relatively short wavelength of instability waves causes streamwise changes too large to be neglected (Herbert & Morkovin 1980). Parabolic equations for the slowly varying components of the solution can be obtained, however, when accounting separately for the wavelike nature of the disturbance.

A spatially evolving wave of constant frequency ω (and spanwise wavenumber β) is fully described by specifying the streamwise wave number $\alpha(x)$, the streamwise growth rate $\gamma(x)$, and the velocity profiles as derivatives of the streamfunction $\phi(x, y)$. The disturbance streamfunction can be written in the form

$$\psi(x, y, t) = \phi(x, y) \exp \left[\int_{x_0}^{x} a(\zeta) d\zeta - i\omega t \right] + c.c. \qquad (4)$$

where $a(x) = \gamma(x) + i\alpha(x)$. When considering solutions ψ of the linearized version of equation (3), the dependence of a and ϕ on x results from the nonparallelism of the mean flow that renders equation (3) non-separable in x and y. In general, the dependence on x can result from nonparallelism or nonlinearity. The weak divergence of the mean flow with x suggested to previous investigators a perturbation expansion in a slow streamwise variable. Such expansions are used in the method of multiple scales as well as in Gaster's iterative technique, and will be applied in our local procedure to produce ordinary differential equations in y. The derivation of the PSE rests on two assumptions shared with these expansion techniques:

(A1) The variation of γ, α, and ϕ in x is sufficiently small to neglect second derivatives $\partial^2/\partial x^2$ and products of first derivatives ∂/∂ of these quantities.

(A2) Within the order of approximation (A1), the disturbance is independent on the downstream conditions yet exhibits elliptic characteristics at higher order.

Assumption (A2) was first discussed by Gaster (1965) and he questioned whether it would be meaningful to proceed with a rational multiple-scales approach indefinitely to higher orders. Support for assumption (A2) can

be derived from an observation reported by Morkovin (19??): The evolution of disturbances up to the onset of secondary instability is a viscous phenomenon. The maximum amplification occurs when a positive feedback loop exists between the two viscosity-dominated regions, the viscous critical layer and the Stokes layer at the wall. Morkovin observed that the ratio of the Stokes-layer thickness to the distance of the critical layer from the wall remains practically constant along the ridge of maximum TS wave amplification in the range $1.22 \cdot 10^5 < R_x < 8.44 \cdot 10^8$. Since the growth of the boundary layer is the agent that tunes and detunes the feedback loop, it is plausible to expect changes in the wavenumber and growth rate to occur on the same scale as the divergence of the basic flow.

With assumption (A1), the derivatives of ψ with respect to x are linear in $\partial\phi/\partial x$ and da/dx, and take the simple form

$$\frac{\partial^m \psi}{\partial x^m} = [a^m \phi + m a^{m-1}\frac{\partial\phi}{\partial x} + \frac{m}{2}(m-1)a^{m-2}\frac{da}{dx}\phi]\chi \qquad (5)$$

Introducing this result in the disturbance equation (3) yields a partial differential equation of parabolic type that is the first of two equations which compose the PSE. The parabolic character is clearly exhibited when the linearized equation for two-dimensional disturbances is written in operator form,

$$(L_0 + L_1)\phi + L_2\frac{\partial\phi}{\partial x} + \frac{da}{dx}L_3\phi = 0 \qquad (6)$$

with boundary conditions

$$\phi(x,0) = \frac{\partial}{\partial y}\phi(x,0) = 0, \; \phi(x,y) = \frac{\partial}{\partial y}\phi(x,y) = 0 \text{ as } y \to \infty \qquad (6a)$$

and initial conditions

$$\phi(x_0,y) = f(y), a(x_0) = a_0 \qquad (6b)$$

The operators L_0 to L_3 operate only in y and are

$$L_0 = -\frac{1}{R}(D^2 + a^2)^2 + (\frac{\partial\Psi_0}{\partial y}a - i\omega)(D^2 + a^2) - \frac{\partial^3\Psi_0}{\partial y^3}a \qquad (7a)$$

$$L_1 = \frac{\partial^3\Psi_0}{\partial x \partial y^2}D - \frac{\partial\Psi_0}{\partial x}(D^2 + a^2)D \qquad (7b)$$

$$L_2 = -\frac{4a}{R}(D^2 + a^2) + \frac{\partial \Psi_0}{\partial}(D^2 + 3a^2) - 2i\omega a - \frac{\partial^3 \Psi_0}{\partial^3} \qquad (7c)$$

$$L_3 = -\frac{2}{R}(D^2 + 3a^2) - i\omega + \frac{\partial \Psi_0}{\partial y}3a \qquad (7d)$$

with $D = \partial/\partial y$. L_0 is the Orr-Sommerfeld operator and L_1 accounts for the transverse velocity component of the basic flow.

A second equation is required to resolve the ambiguity in the partition of Ψ in eq. (4). This ambiguity arises because both ϕ and the exponential term depend on x, and thus, the growth and phase variation of the disturbance may be represented either by the exponential term or by the streamwise changing ϕ. To complete the specification of the PSE we remove the ambiguity commonly by specifying the normalization condition

$$\frac{\partial \phi(x, y^*)}{\partial x} = 0, x \geq x_0 \qquad (8)$$

where y^* is some appropriate location. Equations (6) and (8) comprise the linearized parabolic stability equations governing the evolution of the unknow functions a and ϕ. The nonlinear PSE will be discussed below. Alternative normalizations, e.g. $da/dx = 0$, can be locally utilized whenever convenient, provided ϕ maintains property (A1).

The simplicity of deriving the PSE under the assumptions (A1) and (A2) underlines their ability to capture a wide range of linear and nonlinear phenomena. No hierarchical ordering of terms based on length scales or amplitudes is required, eliminating the need for deeper insight prior to the analysis. The nonlinear problem can be easily treated when the parabolic equation is solved with a marching procedure. In special limits, the PSE represent the equations used in previous studies ranging from receptivity to secondary instabilities. At high Reynolds numbers, when the nonparallel effects are very small, the linearized PSE approache the Orr-Sommerfeld equation. At low Reynolds numbers and low frequencies, the wavenumber becomes small and powers of a become negligible. In this limit, the linearized PSE (6) approaches the unforced unsteady boundary layer equation used in receptivity analysis. Itoh (1986) used this fact to verify the matched asymptotic expansions of Goldstein (1983). Preliminary results indicate that using the three-dimensional, nonlinear version of the PSE to analyze the evolution of a finite amplitude TS wave and a small amplitude three-dimensional wave,

one captures both the weakly non-linear Craik mechanism and the parametric secondary instability mechanisms usually unvealed by Floquet analysis (Herbert 1988).

2.1 Measures of Growth

In the parallel-flow approximation, all physical quantities grow or decay according to the eigenvalue of the Orr-Sommerfeld equation in exactly the same way. In a nonparallel mean flow, the growth and phase variation of some physical quantity Q depends on a, ϕ, and possibly its derivatives in y. The growth rate of Q is defined as the logarithmic derivative

$$\bar{\gamma}(x) = \frac{1}{Q}\frac{\partial Q}{\partial x}$$

where the division by Q renders the growth independent of the magnitude of Q. As observed by Bouthier, the dependence of ϕ on y makes the growth rate at each streamwise location ambiguous since different rates are obtained at different distance from the wall. Furthermore, as discussed by Schubauer & Skramstad (1947) and later by Gaster (1965) and Saric & Nayfeh (1977), the growth rate is affected by the direction, say $Y = Y(x)$, along which the streamwise derivative of Q is taken. Van Stijn & Van de Vooren (1983) further noted that if growth is based on the u component of the disturbance velocity at the location $y = y_m$ corresponding to the maximum u_{max} of u, the growth rate is independent of the direction $Y(x)$.

Measurements of u_{max} are a good indicator for the growth of disturbances. The experimental measurements of the u component are more accurate than those of the v component. Measured growth data based on u_{max} are independent of the traversed path of the sensor and avoid the need to determine the exact height of the location above the plate. In addition, the amplitude based on u_{max} is proportional to the strength of the vorticity at the critical layer that plays a central role in the evolution of secondary instabilities. The growth rate and wavenumber based on u_{max} are given by:

$$\bar{\gamma}(x) = \gamma(x) + Re[(\frac{\partial \phi(x, y_m)}{\partial y})^{-1}\frac{\partial^2 \phi(x, y_m)}{\partial y \partial x}] \qquad (10a)$$

$$\bar{\alpha}(x) = \alpha(x) + Im[(\frac{\partial \phi(x, y_m)}{\partial y})^{-1}\frac{\partial^2 \phi(x, y_m)}{\partial y \partial x}] \qquad (10b)$$

Other quantities, such as the disturbance energy, can be monitored for growth, and growth rates can be defined locally at some point y or integrated across the boundary layer. With some exceptions, such as measuring the growth of u at the point where u reverse the phase, growth rates and wavenumbers based on different quantities agree within $O(R_x^{-1/2})$. However, neutral stability curves can differ widely at the higher frequencies where the growth rate is of this order.

Having presented a definition of growth, eq (10) we can expand the discussion on the normalization condition, eq (8). Let the function $\bar{a}(x)$, based on u_{max}, or other quantity, be known. Equation (8) imposes $\partial^2 \phi / \partial x^2 = 0$ for all x at y_s. At other y locations the second derivative is small since the profile does not distort rapidly in x. Hence, because the growth of ϕ is restricted by the normalization, it follows that $|\bar{a} - a| \ll 1$. Conversely, the normalization $a = const.$ may be used in the neighborhood of a location, say x_1, if the constant is chosen close to $\bar{a}(x_1)$, thus forcing $\partial^2 \phi / \partial x^2 \ll 1$ at x_1. For example, the a obtained with the parallel flow approximation is sufficiently close to $\bar{a}$. However, integrating the PSE over an extended downstream distance keeping a constant will violate assumption (A1) due to the variation of $\bar{a}$ with x. Normalization conditions based on quantities other than u_{max} may be used provided condition (A1) is not violated.

2.2 Local Solutions

To obtain pointwise results on stability and to generate the initial conditions (6b) for stability analysis with the PSE, we apply a local procedure that uses only the basic flow and the disturbance parameters at some streamwise location x_0, say. If the amplitude of the TS wave is sufficiently small for linearization, this local procedure is similar to that introduced by Bouthier (1972) and later applied by others, yet our derivation appears much simpler and provides a more consistent formal approach. In particular, this approach permits accounting for both nonparallelism and nonlinearity. Therefore, for finite-amplitude TS waves, the local procedure can be coupled with a Landau expansion in the amplitude. In any case, the local procedure rests on ordinary differential equations that govern the properties of the solution in the neighborhood of x_0. Here, we present only the linear procedure to obtain the unknown quantities ϕ, $\partial \phi / \partial x$, a, and da/dx in equation (6) for given parameters ω, R_0, and the basic flow Ψ_0.

We introduce a Taylor expansion for ϕ, a and the basic flow Ψ_0 with respect to the variable $\xi = x - x_o$ and note that higher derivatives can be neglected within assumption (A1) and the boundary-layer approximation to the basic flow. We thus obtain

$$\phi(x, y) = \phi_0 + \xi\phi_1, \ a(x) = a_o + \xi a_1$$

and a similar expansion for the basic flow, where

$$\phi_0 = \phi(x_0, y), \ \phi_1 = \frac{\partial\phi(x_0, y)}{\partial x}, \ a_0 = a(x_0), \ a_1 = \frac{da(x_0)}{dx}$$

The disturbance streamfunction takes the form

$$\psi(x, y, t) = (\phi_0 + \xi\phi_1)exp[\int_0^\xi (a_0 + \zeta a_1)d\zeta - i\omega t] \tag{11}$$

Introducing this expression into eq. (6) and requiring the equation to be valid for varying ξ provides two equations,

$$(L_0 + L_1 + a_1 L_3)\phi_0 + L_2\phi_1 = 0 \tag{12a}$$

$$(L_4 + a_1 L_2)\phi_0 + L_0\phi_1 = 0 \tag{12b}$$

where

$$L_4 = \frac{\partial^2 \Psi_0}{\partial x \partial y}(D^2 + a^2)a - \frac{\partial^4 \Psi_0}{\partial y^3 \partial x}a.$$

Together with the homogeneous boundary conditions on ϕ_0 and ϕ_1 from eqs. (6a), equations (12) represent a coupled system of equations for the unknown quantities a_0, $\phi_0(y)$, a_1, $\phi_1(y)$. In contrast to previous formulations, this system simultaneously determines all quantities up to order $O(R^{-1})$ in one step. Moreover, solving this system does not require the usual solvability condition and thus eqs. (12) provide a suitable zeroth-order approximation in a Landau expansion for finite amplitudes.

The solution of eqs. (12) can be obtained in different ways depending on the choice of normalization and numerical approach. We can directly impose the normalization (8) such that ϕ_0 and ϕ_1 are subject to the conditions

$$\frac{d\phi_0(y^*)}{dy} = 1, \ \frac{d\phi_1(y^*)}{dy} = 0 \tag{13}$$

and solve the nonlinear system (12), e.g. by use of Newton's method.

An interesting alternative uses the normalization $a = $ const. and hence implies $a_1 = 0$. Then the equations (12a,b) form an eigenvalue problem for the single eigenvalue a_0 and eigenvector (ϕ_0, ϕ_1),

$$\begin{bmatrix} L_0 + L_1 & L_2 \\ L_4 & L_0 \end{bmatrix} \begin{Bmatrix} \phi_0 \\ \phi_1 \end{Bmatrix} = \begin{Bmatrix} 0 \\ 0 \end{Bmatrix} \tag{14}$$

This formulation allows to easily determine the asymptotic form of the function $\phi(x, y)$ outside the boundary layer,

$$\phi(x, y \gg 1) = (x + iy)e^{i a y} \tag{15}$$

This asymptotic behavior is different from that of Orr-Sommerfeld solutions in parallel flows. Accordingly, a small error has been introduced in previous analyses that exploit the asymptotic behaviour to replace the boundary conditions at infinity by conditions at finite y.

Finally, an iterative procedure can be utilized to solve the eigenvalue problem subject to conditions (13). This procedure starts with solving the Orr-Sommerfeld problem $L_0 \phi_0 = 0$ to obtain an approximation to a_0 and ϕ_0. The next step solves eq. (12b) together with the norm (13) on ϕ_1 for a_1 and ϕ_1 by using a solvability condition or solving the augmented system. The third step serves to find a new approximation to a_0 and ϕ_0 using the inhomogeneous equation (12a) and a second solvability condition. Up to this point, the iterative procedure leads to equations identical with those derived with the method of multiple scales (e.g. Saric & Nayfeh 1977). While the iterative procedure can be continued until the results converge to the solution of the simultaneous equations, it is consistent with the order of approximation to truncate after the third step.

The local procedure breaks down when $|a|$ tends to zero because the operator L_4 becomes of the order $O(R^{-2})$ of the neglected terms when a is of order $O(R^{-1})$. This situation occurs at low Reynolds numbers, hence in the receptivity range. The marching procedure does not suffer from this limitation since no ordering between a and da/dx is required. Without the local procedure, the initial conditions must be given by some other means.

2.3 The Eigenvalue Spectrum

The eigenvalue a appears up to fourth power in the matrix of the local procedure. The spectrum is accessible through standard software packages, such a EISPACK, provided the equations are reformulated into a larger system that contains the eigenvalue linearly or by using the linear companion matrix (Bridges & Morris 1984). Figure 1 shows the spectrum for $R = 500$ and $F = 100$ together with the spectrum of the Orr-Sommerfeld equation (OSE). Our local formulation has the perturbing effect of splitting each OSE eigenvalue into two neighboring pairs.

The split is due to the perturbing effect of the operators L_1 and L_4 that are of order $\epsilon = O(R^{-1})$, on the eigenvalues of the Orr-Sommerfeld operator, L_0. Let $(\mu_1, \mu_2, \ldots, \mu_N)$ be the eigenvalues of L_0, with associated eigenvectors $(\phi_1, \phi_2, \ldots, \phi_N)$. Set L_1 and L_4 to zero and call the resulting matrix M. This matrix has the eigenvalues of L_0 with multiplicity two. However, there is only the eigenvector of the form $(\phi_j, 0)^T$ associated with the eigenvalue μ_j of double multiplicity, consequently M is defective. It can be shown that the index of each eigenvalue is 2, so the eigenvalues of (14) with L_1 and L_4 of $O(\epsilon)$ has a Puiseux series representation,

$$a_{a,b}(\epsilon) = \mu_j + c_{a,b}\epsilon^{1/l} + d_{a,b}\epsilon^{2/l} + O(|\epsilon|^{3/l}) \tag{16}$$

where the subscripts a and b refer to the two perturbed eigenvalues. We conclude that the variation of the eigenvalues of (14) from the eigenvalues of the Orr-Sommerfeld equation is of order $O(R_x^{-1/4})$.

If $2N$ Chebyshev polynomials are used to approximate the eigenvector $(\phi, \partial\phi/\partial x)$, the linear companion matrix is of size $7N \times 7N$. By employing the known asymptotic form of ϕ outside the boundary layer, (15), the appearance of the eigenvalue is reduced from fourth order to second order, and the linear companion matrix reduces to $4N \times 4N$. In addition to the saving of computational effort, gains in accuracy are obtained (Haj-Hariri, 1989).

2.4 The Nonlinear Problem

We now consider the streamwise evolution of a wave of frequency ω and finite amplitude. In this case, the flow field is composed of the basic flow,

the distorted TS wave, and its harmonics:

$$\psi(x,y,t) = \psi(x,y) + \sum_{n=-\infty}^{\infty} \phi_n(x,y) exp[\int_{x_o}^{x} a_n(\zeta)d\zeta - in\omega t] \qquad (17)$$

where $a_n = \gamma_n + in\alpha$ and $|\bar{a} - a| \ll 1$ holds for all n. Inserting the expansion (17) into the disturbance equation (3), using eq. (5), and performing harmonic balance in the frequency yields a set of coupled nonlinear equations of the form:

$$[(L_0 + L_1)\phi_n + L_2 \frac{\partial \phi_n}{\partial x}] exp[\int_{x_o}^{x} a_n(\zeta)d\zeta] \qquad (18a)$$

$$= \sum_{m=-\infty}^{\infty} N[\phi_m(x,y), \phi_{n-m}(x,y)] exp[\int_{x_0}^{x} (a_m + a_{n-m})d\zeta]$$

where the linear operators L depend on $\alpha(x)$ and $\gamma_n(x)$ while the nonlinear operator N depends on $\alpha(x)$, $\gamma_m(x)$, and $\gamma_{n-m}(x)$. For simplicity we use in eq. (18) the normalization $da_n/dx = 0$. To avoid violation of assuption (A1), we use a_n = const. during each marching step and implement the normalization (8) by updating the value of a after each step.

The boundary conditions for the Fourier components in eq. (17) are:

$$\phi_n = \frac{\partial \phi_n}{\partial y} = 0, \quad \text{at} \quad y = 0, y \to \infty \quad \text{for} \quad n = 1, 2, 3, \ldots \qquad (18b)$$

$$\phi_0 = \frac{\partial \phi_0}{\partial y} = \frac{\partial^3 \phi_0}{\partial y_3} = 0, \quad \text{at} \quad y = 0, \frac{\partial \phi_0}{\partial y} = 0 \quad \text{as} \quad y \to \infty \qquad (18c)$$

The boundary conditions for the oscillatory Fourier components correspond to u and v velocity vanishing at the wall and infinity. The boundary conditions for the mean flow distortion omit the condition $v = 0$ at infinity to allow for the variation in the displacement thickness, as required by the boundary layer approximation.

2.5   Numerical Formulation

The semi-infinite domain above the plate is mapped algebraically to $(0, 1]$ and the differential operators in y are converted into algebraic form using a spectral collocation method. If not otherwise stated, the results presented here have been obtained using forty Chebyshev polynomials. The streamwise

derivative, $\partial\phi/\partial x$ is approximated by the first order finite difference form $(\phi_{n,j+1} - \phi_{n,j})/\Delta x_j$. Iteration is employed to solve the nonlinear algebraic system exactly at the midpoint of the interval, where the finite difference form of $\partial/\partial x$ is second-order accurate. The iteration employs a predictor-corrector approach that corrects the values a_n until the normalization condition is satisfied. In this way the governing equation is simplified since the terms da_n/dx are set to zero. We note that since convergence of the iteration is monitored during every step, marching stops if the equation fails to be exactly satisfied.

The trapezoidal procedure leads to a coupled nonlinear algebraic system of the form:

$$(L_0 + L_1)[\phi_n^*] + L_2[\phi_{n,j+1} - \phi_{n,j}]/\Delta x$$

$$= \sum_{m=-\infty}^{\infty} N(\phi_m^*, \phi_{n-m}^*) A_{m,j}^* A_{n-m,j}^* / A_{n,j}^* \qquad (19)$$

where the asterisk denotes quantities evaluated at the midpoint of the step,

$$A_{n,j}^* = A_n(0) exp[\gamma_n^* \frac{\Delta x}{2} + \int_{x_0}^x \gamma_n(\zeta)d\zeta],$$

and the operators are evaluated with the parameter values at the midpoint.

The initial condition is provided by solving the nonlinear local problem using a Landau expansion in amplitude. Such an expansion is possible since no solvability condition is used to treat the nonparallelism of the flow.

2.6 Properties of the Global, Local, and Marching Schemes

We have seen that the matrix (13) has pairs of neighboring eigenvalues, so, in particular, it can have a pair of unstable eigenvalues. The eigenvalues are purely an algebraic quantity, and we asked ourselves whether the associated growth rate based on u_{max}, as in (10), displayed the same "neighboring pair" character as found in the spectrum. Figure 3 shows the variation of the algebraic eigenvalue pair (a) and (b) with Reynolds number as a dotted line, and the physical growth rate associated with each one of them as a solid line. While the algebraic eigenvalues differ noticeably, the maximum difference in physical growth rates is negligible, being of the order of 10^{-4}. The physical

growth rates given by the local and marching procedures agree well. The solid circles denote the marching results for the case of the initial profile and physical growth rate given by eigenvalue (a), and the open circles for eigenvalue (b).

The marching procedure is computationally more efficient than the local procedure by an order of magnitude. We have performed our calculations on a Cray-XMP/24. The marching procedure, using 40 Chebyshev polynomials, employs 0.06 seconds per step, regardless of the step size. In contrast, the local procedure, using Newton iteration, converges in 0.38 seconds on a Cray-XMP/24 following a change in the Reynolds number.

An important property of the marching code is the variation of accuracy with streamwise step size. We tested the accuracy by comparing the quantity $H = [\bar{\gamma}^2 + \bar{\alpha}^2]^{1/2}$, based on u_{max}, at $R = 1000$ obtained by marching from $R = 400$ with different steps sizes. The most accurate value was assumed to be given by the smallest step size, $\Delta R = 2$, and was used as reference. Nonlinear effects were neglected. The step sizes ranging from 2 to 100 where used. For step sizes larger than 100 the marching procedure may diverge. We note that using a step size of $\Delta R = 100$ one marches from branch I to branch II at this frequency in only 4 steps. The difference $H - H_{\Delta R=2}$ stays at order 10^{-5} up to a step size of 50, and increases afterwards to 10^{-3} at a step size of 100.

3   The Direct Navier-Stokes Solution

The numerical method used here evolved from that presented by Spalart (1984) and applied since to a variety of transitional and turbulent boundary layers. The algorithm, spectral in space and second-order accurate in time, was designed to solve the incompressible Navier-Stokes equations over a flat plate (at $y = 0$) with periodic conditions in the directions (x and z) parallel to the plate. Because of the periodicity the studies of spatially-evolving flows could not be exact, and had to involve assumptions of slow growth of the boundary-layer thickness and disturbance energy, similar to those presented in part 1 of this paper but more rudimentary (see the use of the group velocity by Spalart & Yang 1987). The streamwise evolution of the laminar flow was accounted for to a reasonable approximation, but the non-parallel effects (nonzero v component) were not.

The new ingredient is a procedure, first applied to the Hiemenz flow (Spalart 1988), which allows the treatment of some truly spatially-evolving, nonparallel flows with the same algorithm. Effectively the equations are solved with inflow and outflow conditions, so that the range of applications of the method is close to that of Fasel (1976). The procedure is justified only for shallow domains such as boundary layers, or long pipes and channels. There is a moderate waste of grid points, which is more than offset by the many advantages of using Fourier series; the outflow condition has been shown to accept infinitesimal waves or strongly nonlinear disturbances with no evidence of reflection or numerical instabilities. This new method will be useful to explore nonparallel effects and the early stages of transition, but will not supersede the short-period "temporal" calculations for the later stages, because of the expense involved with treating a large domain at once.

Let x be the direction in which the flow is not uniform, but for which the numerical method requires periodicity. The periodic domain $[0, \lambda]$ is divided into a "useful region" $[L, \lambda - L]$ and two "fringe regions" $[0, L]$ and $[\lambda - L, \lambda]$ at either end of the interval (by periodicity, these two regions can be regarded as one). The useful region is intended to cover the whole spatial history of a wave whereas earlier work with this code contained only one or a few wavelengths. Let $U_B(x, y)$ be the laminar velocity field; it satisfies the Navier-Stokes equations, in conjunction with a pressure field p_B. Split the velocity field $U(x, y, t)$ into a prescribed part $U_0(x, y)$ and a disturbance part $U_1(x, y, t)$;

$$U = U_0 + U_1 \tag{20}$$

The first step is to define a field U_0 that is periodic and smooth in x (at least two continuous derivatives) but coincides with the laminar flow in the useful region:

$$U_0(x, y) = U_B(x + x_0, y) \quad \text{for} \quad L < x < \lambda - L \tag{21}$$

Here x_0 is a parameter which allows us to locate the useful region in different parts of the laminar flow (for Blasius flow, the domain must start some distance downstream of the leading edge). A simple way to construct U_0 is to define a function $\hat{x}(x)$ which equals x on $[L, \lambda - L]$ but is periodic with period λ, and to write $U_0 = (u_0, v_0)$ with $u_0(x, y) = u_l(\hat{x} + x_0, y)$, $v_0(x, y) = (d\hat{x}/dx) \, v_l(\hat{x} + x_0, y)$. Naturally in the fringe U_0 is not a Navier-Stokes solution. It is not even essential to make it divergence-free.

The equations governing U_1 are the following:

$$\nabla \cdot U_1 = 0, \qquad\qquad (22a)$$

$$U_{1t}+U_0\cdot\nabla U_1+U_1\cdot\nabla U_0+U_1\cdot\nabla U_1 = -\nabla p_1+\nu\nabla^2 U_1-d(x)U_1+F(x,y,t). \quad (22b)$$

In the useful region, U_0 is a Navier-Stokes solution (i.e., $U_0 \cdot \nabla U_0 = -\nabla p_0 + \nu\nabla^2 U_0$), and d and F are both zero. A simple manipulation of (22a) then shows that it reduces to (3) and that $U = U_0 + U_1$ satisfies the Navier-Stokes equations within that region, which was the objective.

The key assumption is that the nonphysical phenomena occurring in the fringe do not invalidate the solution in the useful region. In general, the incompressible Navier-Stokes equations include long-range pressure interactions; however in a shallow domain this range is only of the order of the smaller dimension, here the boundary-layer thickness δ. This is why the assumption $\delta \ll \lambda$ is essential here, as it probably is for any numerical inflow-outflow strategy, or in a wind tunnel for that matter (defining λ loosely as the streamwise extent of the flow).

The role of the $-d(x)U_1$ term in (22b) is to damp the disturbances while they are in the fringe. d is a positive scalar function that rises smoothly from 0 in the useful region to a finite value in the fringe. Assuming that the laminar flow is in the positive x direction, the disturbances (i.e., U_1) are convected by U_0 into the fringe and their amplitude is reduced by orders of magnitude by the $-dU_1$ term. As a result the fluid that enters the useful region from the fringe, at $x = L$, is essentially free of disturbances, which amounts to the "inflow condition" $U = U_0 = U_B$. We assume that the useful region and the fringe communicate only by convection of disturbances, and that information cannot travel upstream more than a few δ. In other words, on the scale of L and λ, the equations have a parabolic behavior.

The last term in (22b) is a prescribed body force $F(x,y,t)$, periodic in time and confined to a short region in x, that is used to generate waves in the flow (the analog of a vibrating ribbon). With the present setup, adding a body force within the domain is more convenient than explicitly adding the perturbation to the inflow condition. In either case, there is no shape for the perturbation that is more justified than others. However, some shapes do generate waves in a smoother manner, resulting in a shorter transient in x before the wave is "well developed" in the sense of exhibiting a smooth growth rate (there is no rigorous concept of a "pure" TS wave since the

solution is fully two-dimensional). A fair choice is of the form $F_x = \partial\psi/\partial y$, $F_y = -\partial\psi/\partial x$, with

$$\psi = \epsilon \; \exp\left(-\frac{(x-x_r)^2}{\sigma_x^2} - \frac{y^2}{\sigma_y^2}\right) \; y^2 \; \cos(\omega t - kx). \qquad (23)$$

Here, ϵ is the amplitude of the force; σ_x and σ_y are length scales in x and y; x_r is the position of the "ribbon"; ω is the frequency of the wave; k is a wave-number. The primary parameters are ω and $x_r + x_0$, and ϵ becomes important for nonlinear waves. The other parameters are chosen empirically to obtain a smooth transient; k is an estimate of the wave-number of the wave, σ_x is of the order of the wave-length, and σ_y of the order of δ.

The function in (23) was constructed from a Gaussian factor, to make it fall rapidly but smoothly to 0; a y^2 factor, to impose the boundary conditions at the wall; and a time-periodic wave-like dependence on t and x. The couple (F_x, F_y) is divergence-free. The boundary and divergence conditions are not indispensable in a body force, but if the divergence-free projection of F does not satisfy the no-slip condition thin shear layers will appear at the wall, and may degrade the numerical accuracy.

In the algorithm that solves (22b) for U_1 the terms not found in the Navier-Stokes equations (two cross terms with U_0 and the d and F terms) are treated like the nonlinear term $U_1 \nabla U_1$, by an explicit Runge-Kutta scheme. This limits the magnitude of d, for numerical stability; a typical peak value for $d(x)$ is $0.5/\Delta t$ (Δt being the time step). In a typical situation U_1 is reduced by three orders of magnitude while passing through the fringe (for our purpose there is no need to reset U_1 exactly to 0). This can be achieved with $L \approx \lambda/9$; thus, less than 25% of the domain is wasted.

In practice the functions d, $\hat{x} - x$, and F are not exactly zero in the useful region, since Gaussians are used. However, the parameters such as σ_x are chosen small enough (relative to λ) that the residual values are negligible. Note also that since U_B is given by the Blasius equations, it is not exactly a Navier-Stokes solution. A higher-order approximation would require further assumptions about the outer flow, and not be unique; and its stability properties would presumably differ very little from those of the basic Blasius solution.

The system given by (22) was programmed and tested, and the parameters such as L/λ or σ_y/δ chosen, mostly empirically. One basic requirement

is that the homogeneous system ($F = 0$) be stable, which is not granted because of the streamwise amplification of the wave and depends primarily on the d term and the width of the fringe. When this is true, we can start at $t = 0$ with $U_1 = 0$ and activate F. After a sufficient time (a few times λ/U_∞) a time-periodic solution is obtained for U_1. With infinitesimal amplitudes ϵ the nonlinear term $U_1 \nabla U_1$ is inactive and the system behaves linearly; in particular, the periodic solution is accurately harmonic with frequency ω. Resolution tests, tests in which x_0 was varied, and moderate alterations of the ribbon parameters were all satisfactory. Another test is to use for U_B a parallel flow with Blasius profile. In that case exponential growth in x is obtained, with a growth rate close to that given by the Orr-Sommerfeld equation. Furthermore the growth rate is maintained up to the edge of the fringe at $\lambda - L$, demonstrating that there is very little upstream influence of the extra terms in the fringe. This test also allows us to estimate the extent of the transient needed to the right of x_r to obtain a well-developed wave. Even with well-chosen parameters in (23), this extent is about $5 \ 10^4 \nu/U_\infty$ in x; as a result, it is impossible to firmly define the leftmost part of the neutral curve, which is around $x = 9 \ 10^4 \nu/U_\infty$. In addition, it is much more difficult to obtain smooth and reproducible growth rates for decaying waves than for growing waves (this was to be expected, considering the existence of continuous-spectrum modes with arbitrarily small decay rates in the Orr-Sommerfeld equation).

Amplitude ratios (for the wave amplitude from Branch I to Branch II) of the order of e^5 have been obtained (with $F = 50$). Much larger ratios, such as e^{10}, will eventually cause problems because even small numerical errors in the large-amplitude region will degrade the accuracy in the low-amplitude region. This would be true with almost all numerical methods, whether the errors propagate due to the global character of a spectral method, or to an implicit time integration scheme, or to the Poisson solver for the pressure. This numerical difficulty is absent in all the "temporal" calculations, or in the parabolic theory presented in this paper.

Two cases were chosen to compare the theory and the numerical results. One is linear and at relatively low frequency ($F = 50$), see Fig. 6; the emphasis is on nonparallel effects. The other is nonlinear, at $F = 86$, see Fig. 11 and 12.

4 Results

4.1 Nonparallel Effects

Experimental measurements have shown the occurrence of instability at lower Reynolds numbers and at higher frequencies than predicted by the parallel theory. The discrepancy has often been attributed to the effect of basic flow nonparallelism, and the consensus was, and still is amongst some researchers, that nonparallelism is always and strongly a destabilizing agent. This belief is incorrect, and stems from a misinterpretation of the results. Herein we duplicate the analysis of previous researchers using the linear PSE. By using the same code for the comparison we remove the 'computational' differences and highlight the role played by the interpretation of results.

As described above, the choice of reference length δ_o for nondimensionalization is the value of $\delta(\tilde{x}_0)$ at the initial location of the marching calculations. Since this location varies from run to run we remove this variation from the output data by redimensionalizing all results with the local length scale, $\delta(\tilde{x})$.

The first published study of nonparallelism dates back to 1972, by Bouthier. Gaster published his results in 1974, and Saric & Nayfeh published theirs in 1974, 1975, and 1977. The results of Gaster where confirmed by Van Stijn & Van de Vooren in 1982, and the results of Saric & Nayfeh where confirmed by Bridges & Morris. All investigators used the method of multiple scales, except Gaster who used a W.K.B.J. technique. Both approaches are equivalent to first order, however Gaster noted that the ability of the method of multiple scales to proceed to higher order side-steps the elliptic nature of the disturbance equation (3), possibly leading to nonphysical results.

We have applied Bouthier's and Gaster's definition of growth to the results given by the linearized PSE and compared the resulting neutral stability curves. Bouthier chose to measure growth by monitoring the disturbance's kinetic energy, $\epsilon = u^2 + v^2$, and defined instability on a pointwise basis, Gaster chosed the integral of the kinetic energy, the integral of the u component of velocity, and the quantity u_{max}. Figure 3 shows the comparison, the symbols denote data from Bouthier and Gaster, the lines denote our calculations. The good agreement shows the reproducibility of their results, and shows the sensitivity of the neutral stability curve to the chosen definition of growth.

Bouthier performed his study in parabolic coordinates. Perhaps for this

reason he was biased in considering measuring rates of streamwise change along lines of constant η,

$$\bar{\gamma}\bar{B}(x,\eta) = \frac{1}{2\epsilon}\frac{\partial\epsilon}{\partial x}\Big|_{\eta} \qquad (24)$$

The differentiation along lines of constant η misleadingly distorts the growth rate. Most of the effects Bouthier attributed to nonparallelism are really due to the direction of differentiation. To illustrate this point we have applied definition (24) to data furnished from the Orr-Sommerfeld equation (OSE), since differentiating along lines of constant $\eta(x)$ renders the growth rate of the OSE a function of x and y. The results are shown in figure 4 in the form of lines in the R, η plane on which the growth rate is constant, i.e. iso-amplification contours. Both the contours from nonparallel calculations, figure 4a, and the ones from the OSE, figure 4b, show similar structure. Note in particular that near the wall both plots show maximum instability. Bouthier's neutral stability curve shown in figure 3 is based on the stability at the wall. For the parallel results one can show that at the wall, i.e. in the limit of $y \to 0$, definition (24) yields the growth rate $\alpha_{OSE} - 1/(2R)$, showing clearly how (24) leads to misleading values. The dots in figure 4a,b mark the position of u_{max}. In figure 4b they also mark the branch I and II as given by the parallel theory, since at this point the direction of differentiation does not affect the growth rate.

Saric & Nayfeh intended to use u_{max} as the indicator of growth in order to compare directly with experimental measurements but instead published a neutral stability curve based only on the eigenvalue of the Orr-Sommerfeld equation plus its nonparallel correction. Bridges and Morris have shown that the corresponding physical quantity is the v component of velocity measured at approximately $y = 2$. At this location the contribution by the profile, $(1/v)(\partial v/\partial x)$ is zero. The usefulness of such definition is limited, since in experiment the v component of velocity is too small to measure. Saric & Nayfeh displayed also growth rates based on u, differentiated along lines of constant η. These results are in agreement with ours, and the comparison is shown in figure 7.

Among the analysis of the above investigators, the analysis of Gaster was the most accurate and complete. He compared growth rates based on u_{max} with experimental data, and concluded that the discrepancy at the high frequencies could not be explained. In figure 3 we compared results for the

kinetic energy definition:

$$E(x) = \int_0^\infty (u^2 + v^2)dy$$

$$\bar{\gamma}_G = \frac{1}{E}\frac{dE}{dx} \qquad (25)$$

The effect of nonparallelism on the neutral curve is visible at the higher frequencies. A direct comparison with experimental data is not possible because, to the authors' knowledge, no experimental growth rates of integrated data is available. Saric & Nayfeh argued that both Bouthier's and Gaster's definition of energy is incomplete, missing the product between the disturbance and the basic flow. This quantity is measured in experiment. We comput the neutral stability curve based on their definition of energy (no results where given by Saric & Nayfeh),

$$\hat{\epsilon} = 2U_0 u + u^2 + v^2$$

$$\hat{E}(x) = \int_0^T \int_0^\infty \hat{\epsilon}^2 dy dt$$

$$\bar{\gamma}_S = \frac{1}{\hat{E}}\frac{d\hat{E}}{dx}$$

where * denotes complex conjugate, T is one period of the TS wave, and time integration is used to obtain an rms value. Obtaining an rms value in time rather than in space, as chosen by Saric & Nayfeh, is simpler. The neutral stability curve is shown in figure 3 as a solid line with a dot at its peak. The difference in growth rates $\gamma\bar{G}$ and $\bar{\gamma}\bar{S}$ is negligible.

Figure 5 shows the neutral stability curve based on the growth rate of u_{max}, as defined by (10a). Gaster's neutral curve based on this quantity is not shown, but it agrees very well with our results. The u velocity profile exhibits two local maximums (see figure 12b) and Gaster computed the growth rate at both the lower and the upper maximum. Our calculations show that the labels for the lower and upper maximum in Gaster's figure 2 are switched, an unfortunate typographical error since the two curves are noticeably different.

Comparison of the neutral curve based on u_{max} with the curve given by the parallel calculations shows the effect of nonparallelism to be small. The critical Reynolds numbers remains unchanged, and the overall effect of nonparallelism on the neutral stability curve is a slight extension to higher

frequencies, and a streamwise shift of branch one and two. More importantly the maximum growth rate in the nonparallel flow, again based on u_{max}, is close to the value given by parallel theory. Figure 6a and 6b show amplitude variation, based on u_{max}, of a TS wave at frequency of 220 and 50, respectively, calculated by the parallel theory (dashed), the u_{max}, and the integral of the kinetic energy. The circles denote data given by the full Navier-Stokes solution using an maximal TS amplitude of $10sup-8$ to ensure linearity. At the lower frequency all three curves have similar values. This is noteworthy since TS waves may reach the amplitudes needed to generate secondary instability at these lower frequencies, while at the higher frequencies, where advance stages of transition are unlikely to occur, the difference between them increases.

The experimental data of Ross, Barnes, Burns & Ross, and of Schubauer & Skramstad, is shown in figure 5, along with the experimental data of Strazisar & Reshotko (the only ones to show error bars), Kachanov & Levchenko and Wortmann as reported in figure 1 of Saric & Nayfeh. The neutral curve given by the PSE using (10) and given by the OSE are also shown. The discrepancy between calculated and measured neutral curves is significant at frequencies above 200. Measurement of the weak amplification at these high frequencies and low Reynolds numbers is plagued with difficulties, as mentioned to us by Saric in a private communication. To name some; a) The region of accelerated flow at the leading edge makes difficult to relate the position of measurement to Blasius coordinates, b) Measurements too close to the ribbon cannot be trusted, while the finite span of the ribbon affects measurements downstream, c) The zero pressure gradient required for Blasius flow is very tough to achieve, and small variations of C_p have large effects on stability, d) At high frequencies the combination of small amplitude changes and experimental error makes the measurement of growth difficult.

In conjunction with b), our numerical results indicate that altering the initial condition results in a transient region which can display higher growth rates than the unperturbed case. These results are discussed below. Moreover, *part* of the discrepancy between measured and calculated data shown in figure 5 can be attributed to the experimental procedure. Ross et al. measured the growth of the u component of velocity along lines of constant η at points $.I$ off $.R$ the maximum of u, thus altering the growth rate in the same way as Bouthier. Figure 7a shows the iso-amplification lines in the R eta plane at a frequency of 200 based on the u component of velocity and

differentiation along lines of constant η. Figure 7b shows the lines obtained by differentiating along lines of constant y. The square in 7a denotes the location of measurement of Ross et al. Note that at this height branch one is about 20 R upstream of the value based on u_{max}, whose position is marked with the circle. This observation helps explain the 'systematic error of -20 R' mentioned in their paper.

Measurement of growth below the position of u_{max} also extends the neutral curve to higher frequencies. Figure 8 shows the calculated neutral curve based on the growth of u along lines of constant *eta* at the location of measurement of Ross et al., $\eta = 0.7$, at $\eta = 0.4$ and at $\eta = 0$. This last curve corresponds to Bouthier's neutral curve in figure 5. The increase of the maximum unstable amplitude as the point of measurement moves towards the wall demonstrates how the the neutral curve can be extended to higher frequencies by the measuring technique.

Schubauer & Skramstad measured growth along lines parallel to the plate at a location below the maximum of u. Figure 7b shows the iso-amplification lines obtained with this procedure. While the investigators believed that measuring below the maximum introduced an apparent damping, in reality it introduced a destabilizing action. Note that, below $y = 3$, the left neutral line, which corresponds to branch one, reaches the highest Reynolds number at u_{max} and the right neutral line, which corresponds to Branch two, reaches the lowest Reynolds number also at u_{max}. Thus differentiating at constant y misleadingly shows amplification anywhere off the maximum of u (for $y < 3$).

At the height corresponding to u_{max} the measurement of growth is independent of direction. Conversely, we investigated the growth rate along a family of lines of the form $y = x^c$, with c varying from zero to one half, to see if the growth rate is constant across the boundary layer along a particular direction. No such direction was found.

5   Transient Analysis

We studied the sensitivity of growth rates to changes in the initial conditions. The correct initial profile, *phi*$_o$, as given by the local procedure, was perturbed with a profile satisfying the b.c. but otherwise arbitrarily chosen of the form

$$\phi_D = Ay^2 e^{-y-\zeta y^2}$$

where the amplitude A is such that the maximum of the u component of the perturbation is one and one-half times the maximum of the undisturbed TS wave, and the value of ζ is chosen so that no singularity exists at the initial location of marching (Hall 1983).

$$\zeta = 1/2 + a^{2/6} + i\omega R/12$$

As shown in figure 9a, the TS wave u component of velocity is perturbed mainly in the region below the point of phase reversal, the region most likely influenced by the vibrating ribbon at the critical layer ($y \approx 1/3$) used in the experiments. No claim is made, however, of capturing the true events at the ribbon. The initial value of the growth rate and wavenumber, a_0 was perturbed by increasing its value by 50 percent. The complete initial disturbance streamfunction was

$$\psi_0 = (\phi_0 + \phi_D)e^{(1+1/2)a_0 x}e^{-i\omega t}$$

The recovery to the unperturbed TS profile was found to occur within one wavelength, λ_0. To be consistent with the parabolic approximation, very small step sizes where taken in the initial stages of marching. Two step sizes were used; (S1) $0.003125\lambda_0$ and (S2) $0.00625\lambda_0$. After marching half a wavelength downstream the step size was increased to $0.025\lambda_0$ and $0.05\lambda_0$, respectively.

Figure 9b shows the transient growth rate, based on u_{max}, at $F = 50$. The initial location x_0 is at $R = 550$, which is one wavelength upstream of branch 1. The close agreement between the solid and dashed lines, corresponding respectively to step sizes S1 and S2, shows that the numerical effects are not strong. The transient growth rate shifts branch 1 upstream by the modest amount of $\approx 5\Delta R$. The velocity profile half a wavelength downstream of x_0 was found to closely follows the undisturbed TS profile. This fast recovery indicates that, within our choice of perturbation, the evolution of the TS wave depends weakly on different initial conditions, much unlike the case of Goertler vortices, as discussed by Hall.

At higher frequencies, where the growth rates are weak, the growth rate oscillates about the unperturbed value for a longer downstream distance. Figure 9c shows the transient growth rates at $F = 270$. The oscillations are strong enough to display a branch 1 and a branch 2 at a frequency well above the neutral curve. This could explain, in part, the experimentally measured

neutral curve at the higher frequencies. The neutral stability curve given by our choice of perturbation function is shown in figure 10.

5.1 Nonlinear Analysis

One may also suspect the neglect of nonlinearity in the theory to contribute to the discrepancy between results and measured data. To the best of our understanding, the experimental measurements of Ross et al. at the higher frequencies have been performed at a TS wave amplitude of about 1.4 percent rms. A previous study (Herbert, 1975) employing the parallel flow approximation has shown that the effect of nonlinearity on the stability of the Blasius boundary layer at the higher frequencies is destabilizing. Our nonlinear nonparallel calculation based on a Landau expansion in amplitude confirm this, but the shift from the linear calculation is small. The circles in figure 10 show neutral stability points for a u_{max} amplitude of 1.4 percent, where growth rate is based on u_{max} of the TS wave. We conclude that in the Blasius boundary layer the discrepancy between experiment and theory still exist, and cannot be attributed to nonparallel and nonlinear effects.

The nonlinear evolution of a 2 dimensional TS wave of frequency $F = 86$ was studied starting form $R = 400$ and marching downstream. Six Fourier components were used, with wavenumbers 0α, α ..., 5α. Three initial amplitudes where selected; $A_0 = 0.20\%$, 0.25%, and 0.30% (based on u_{max} rms). The results show that the effects on nonlinearity increase strongly with amplitude. When $A_0 = 0.25\%$, the disturbance reaches a maximum amplitude of 2.44% at $R = 877$, and then decays, but when $A_0 = 0.30\%$, the disturbance keeps growing even past $R = 950$. We believe that eventually the disturbance will reach an quasi equilibrium state where the amplitude will vary slowly (if at all) with streamwise position at amplitude levels of the order of 10 percent. Three dimensional disturbances, i.e. secondary instability, will develop at much lower amplitudes, so these equilibrium states are mostly of academic interest.

Amplitude curves are shown in figure 11. The upper heavy line is the amplitude of the TS wave for the 0.25 percent initial amplitude level, the lower heavy line is the amplitude of the 2α harmonic. The upper and lower thin lines show the corresponding quantities for an initial TS amplitude of 0.30 percent. The dashed curve is given by linear analysis with a 0.25 percent initial amplitude. The circles and squares denote the values given by the full

Navier-Stokes simulation, and show good agreement with our results. The velocity profiles for the 0.25 percent initial amplitude case, at $R = 800$ are shown in figure 12. For the u velocity profiles of the TS wave and the 2α and 3α harmonics the abscissa is the rms amplitude. The abbreviation MFD stands for mean flow distortion, which is the zero wavenumber harmonic. The squares denote the values given by full Navier Stokes simulation.

The effect of nonlinearity on growth rate is readily seen in figure 13, where growth rates are plotted vs. amplitude at various Reynolds numbers ($F = 86$). The lines are from the Landau amplitude expansion of order A^5, A^7, and A^9, and the circles are given by the the marching code with various runs with increasing initial amplitude. The error in the marching procedure is of order of the amplitude of the last term in the Fourier series, which can be easily monitored.

The good agreement between the nonlinear solutions to the PSE and full Navier-Stokes solutions reinforces the correct ordering of the neglected terms to $O(R^2)$. We ran the marching code on a Cray XMP/24. Even though no special effort was made to optimize the code, and ϕ for each Fourier component was approximated by 40 Chebyshev polynomials, run times remained short: the two runs needed to generate the data shown in figure 11 took 162 seconds of CPU time each, while the data for figure 8 (linear calculation) was obtained in less than 4 seconds.

6   Concluding Remarks

In view of the diverse results of previous studies, we have used the PSE to investigate the effect of nonparallelism in the Blasius boundary layer. Our results show that this an effect is small, in agreement with the results of Gaster (1974) and Van Stijn & Van de Vooren (198?). The numerical results of Bouthier (1973) and Saric & Nayfeh (1977) can be reproduced but our analysis shows that their definitions of growth rates are not based on relevant physical quantities, hence should not be compared with the existing experimental measurements.

The effect of finite amplitudes on growth rates is considered. Our nonlinear investigations show that the maximum unstable frequency is higher than predicted by linear theory, but not high enough to explain the experimentally observed amplifications. The effect of initial transients on the evolution of

TS waves is also considered. By arbitrarily distorting the initial conditions we observe a region of transient growth which can alter the curve of neutral stability, suggesting a possible reason for the discrepancy at high frequencies between experiments that use a vibrating ribbon to excite the boundary layer and stability theory.

An alternative approach for studying the spatial evolution of disturbances in boundary layers including nonlinear and nonparallel effects is the direct numerical solution to the Navier-Stokes equation. Special care must be taken to avoid using outflow boundary conditions which reflect upstream part of the energy of an outgoing disturbance. Herein we present a method for solving the full Navier-Stokes equation which uses buffer zones adjacent to the inflow and outflow boundaries, but still maintains the benefits of using Fourier series in the streamwise and spanwise direction.

The direct Navier-Stokes approach does not take advantage of the essentially parabolic character of the evolution of the disturbances, except in the fringe regions. This approach has an advantage and a disadvantage when compared to solving the PSE. The advantage is that the solution remains accurate all the way into turbulent flow, provided there is sufficient resolution, while the validity of the PSE may become questionable at the tertiary stages of transition, characterized by the appearance of spikes. The disadvantage is the enormous increase of memory and computational time needed. For this reason the PSE has practical applications.

Results from the two approaches are compared as a first step in validation, and the agreement is found to be excellent. We plan to extend the comparisons to the evolution of three-dimensional disturbances, and to flows with adverse pressure gradients. We divided this paper into three parts, the first of which describes the Parabolic Stability Equation, the second the full Navier-Stokes solution, and the third the results. Although the development of the parabolic stability equation by Herbert & Bertolotti and of the direct Navier-Stokes solver by Spalart was done independently, the authors feel that the reader will benefit from the side by side presentation of the two approaches and associated results which describe the same physical phenomena.

Acknowledgment
REFERENCES

Figure 1. Eigenvalue spectrum at $R = 500$, $F = 100$. Triangles denote values obtained with expansion of ϕ, $\partial\phi/\partial x$ in 25 Chebychev polynomials, circles denote values obtained with 40 polynomials. Solid dots denote values from Orr-Sommerfeld equation calculated with 40 polynomials, solid line with 80 polynomials.
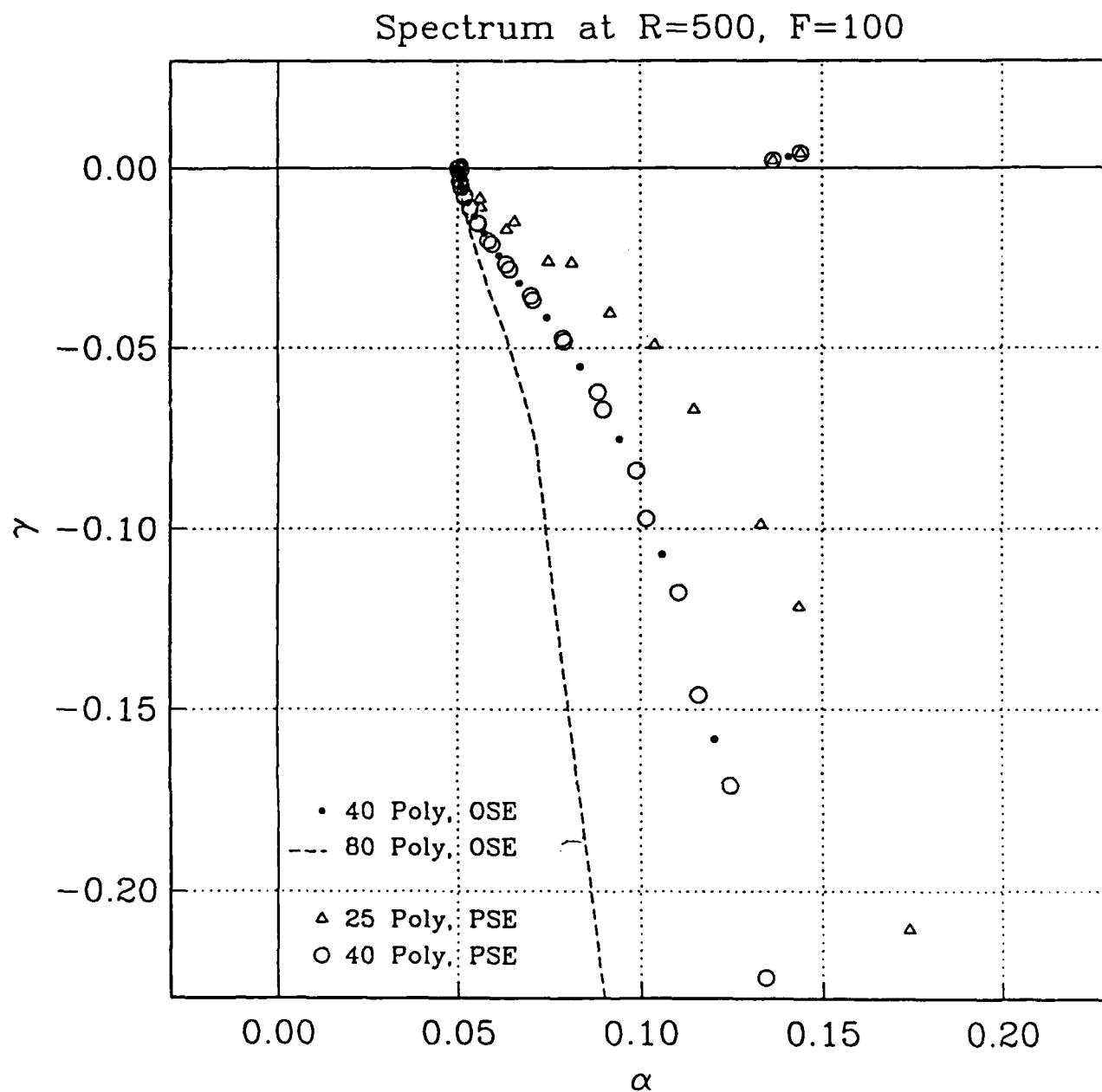

Spectrum at R=500, F=100

Figure 2. Variation of $\gamma = real\,(a)$ of the eigenvalue-pair (a) and (b) with Reynolds number at a frequency of 86. Dash lines denote values of the eigenvalue γ, solid lines denote the growth rate based on u_{max} associated with the eigenvalue. Symbols denote the growth rate given by the marching procedure employing as initial condition the eigenvector associated with eigenvalue (a), solid dots, and eigenvalue (b), circles.

Algebraic and Physical Growth rates, F=86
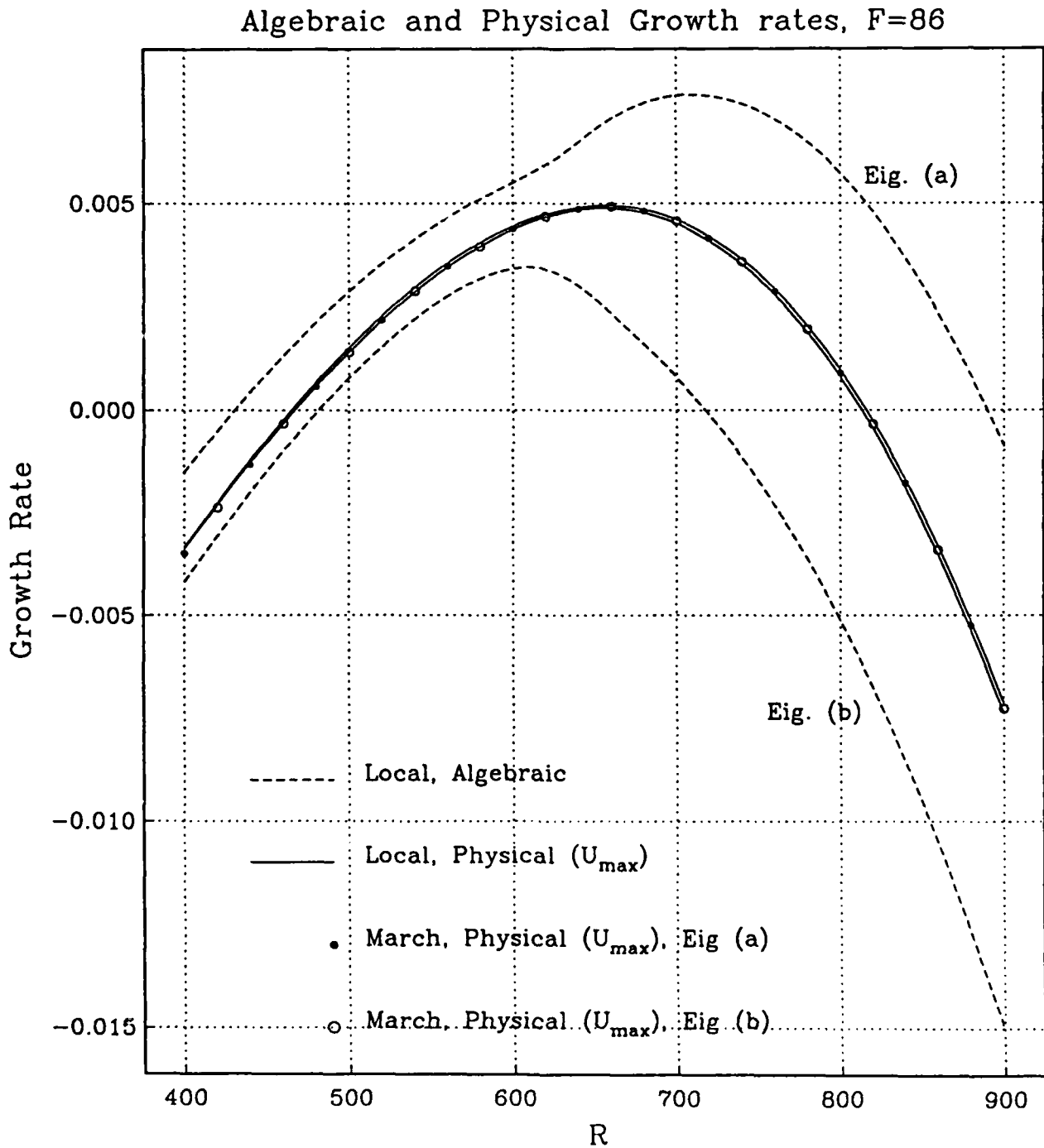
Figure 3. Reproduction of the neutral stability curves of Bouthier and Gaster with the PSE (solid lines). Circles denote the original results of Bouthier, squares those of Gaster. The dash curve is given by Orr-Sommerfeld equation.
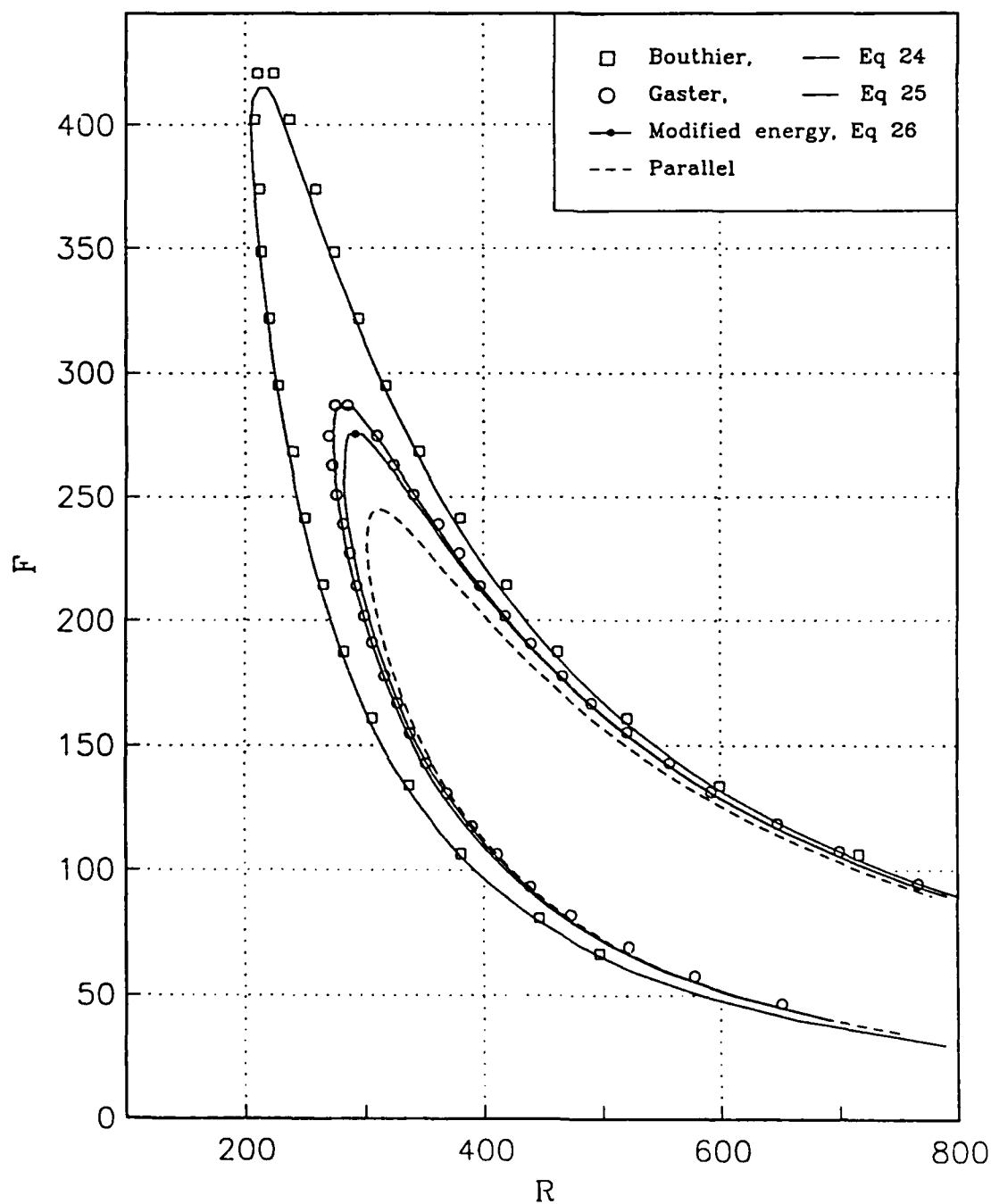
Figure 4. Lines of constant amplification in the R, η plane at a frequency of $F = 200$. Growth rate based on energy, eq (24). (a) results from present formulation, (b) results from Orr-Sommerfeld equation. Circles denote position of u_{max}.
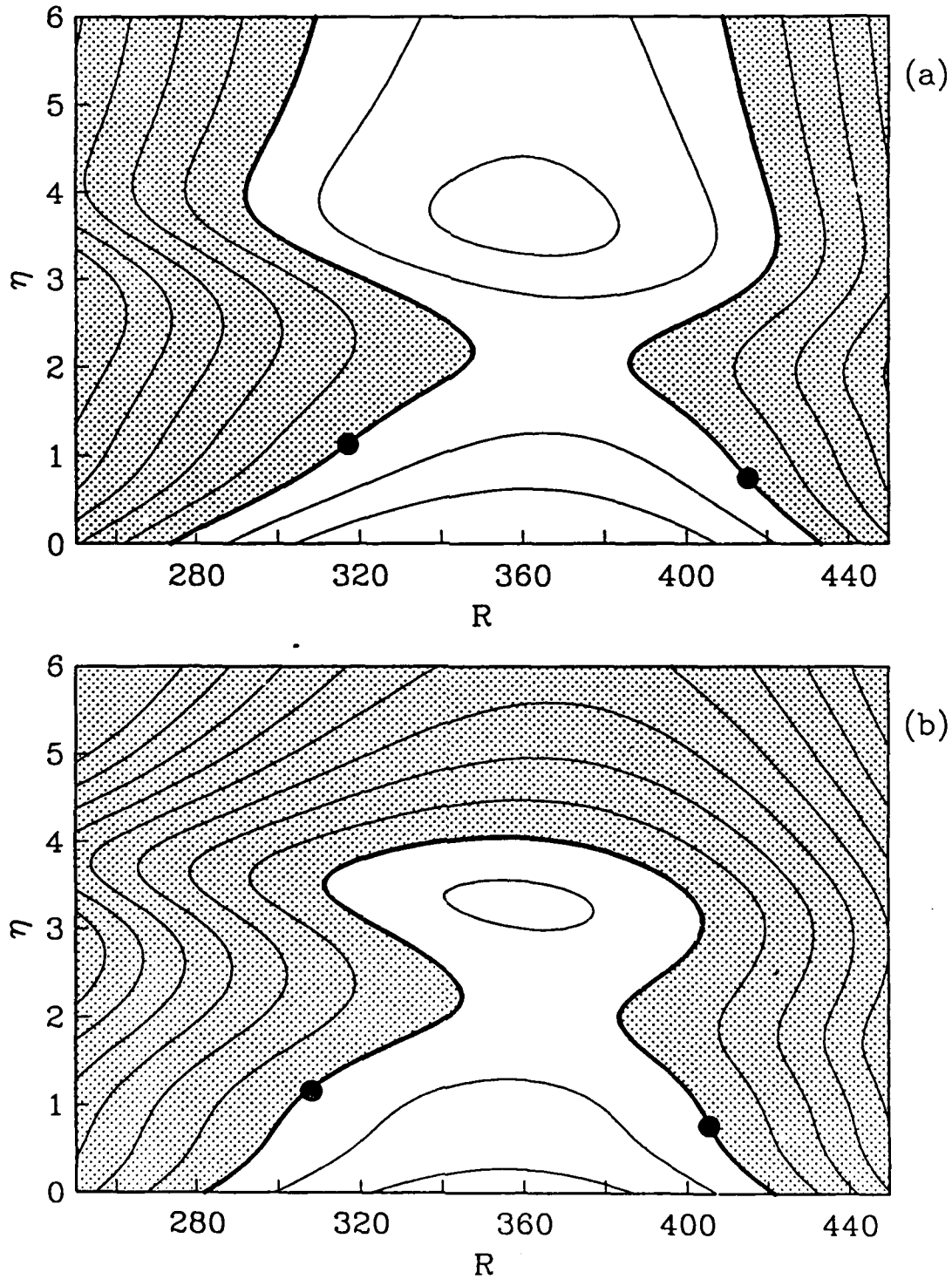
Figure 5. Comparison of neutral stability curve based on growth of u_{max} with the curve given with the Orr-Sommerfeld equation (parallel flow) and with experimental data (from figure 1 of Saric & Nayfeh).
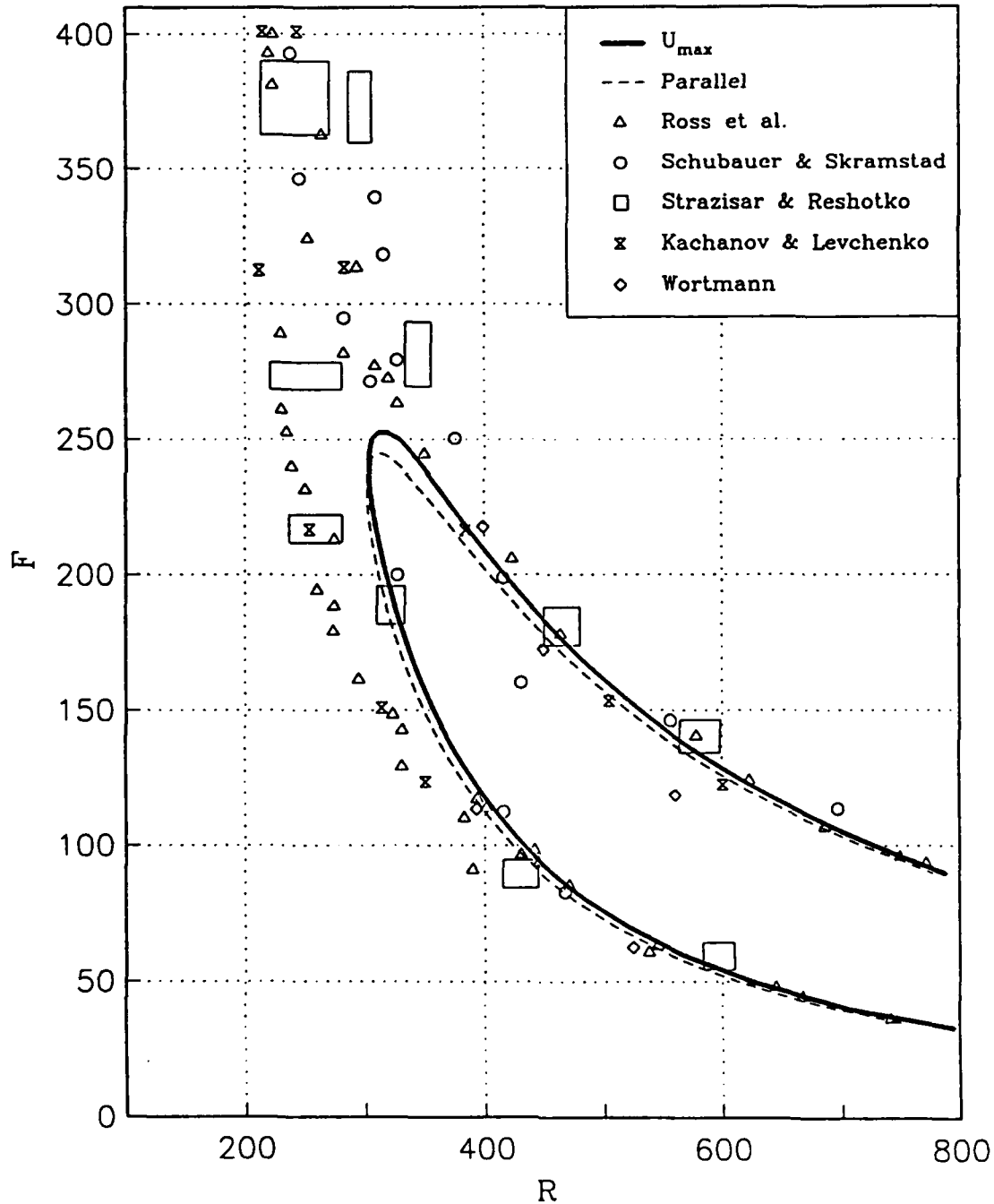
Figure 6. Amplitude of the disturbance based on the quantities $\int(u^2 + vsuo2)\,dy$ and u_{max} at a frequency of 220 (a) and 50 (b). Growth rates nondimensionalized with the local value of $\delta(x)$. Circles denote results from the full Navier-Stokes calculation using a maximum TS amplitude of 10^{-8}. Dashed line given by Orr-Sommerfeld equation (parallel flow).

$F = 220$

$F = 50$
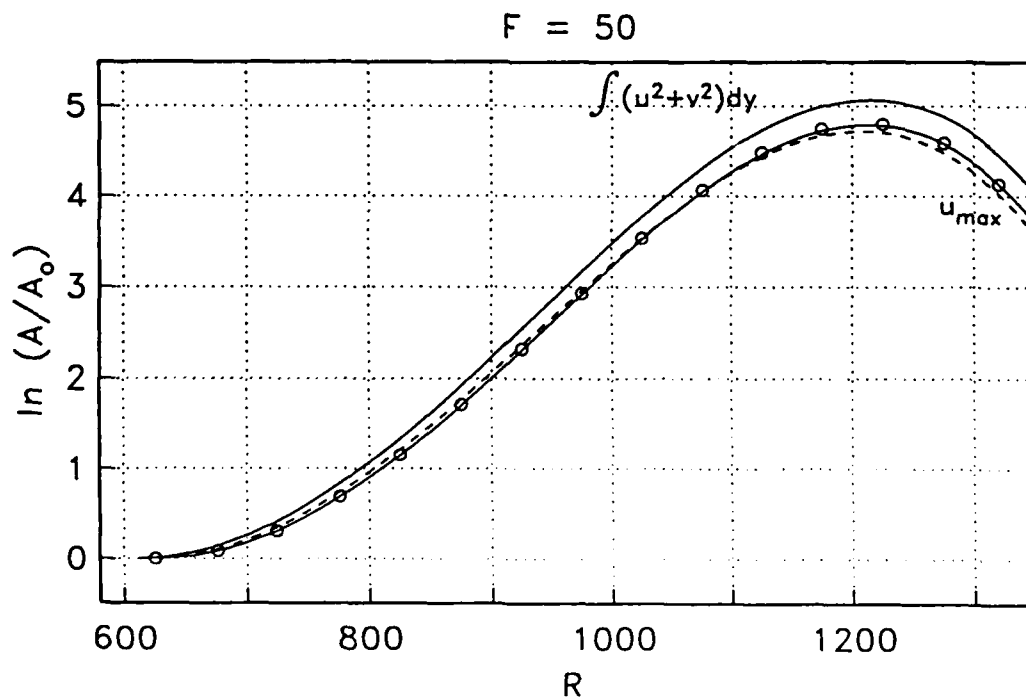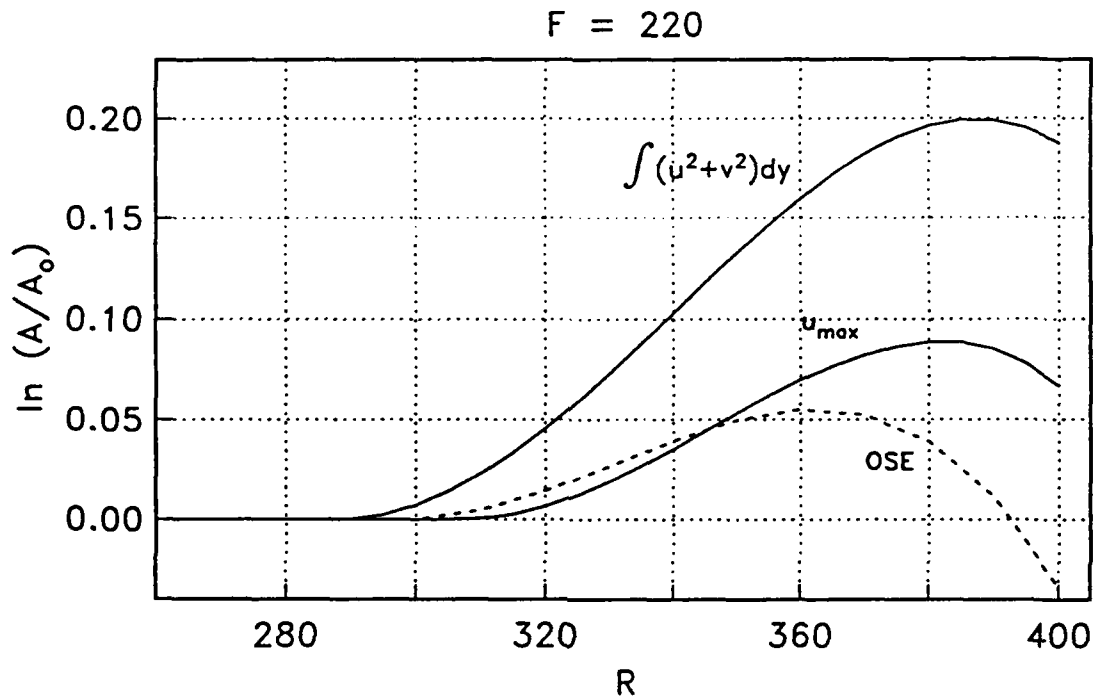
Figure 7. Lines of constant amplification in the R, η plane at a frequency of $F = 200$. Growth rate based on the u component of velocity. (a) Differentiation along lines of constant η, (b) differentiation along lines of constant y. Circles denote the location of u_{max}. Square denotes location of measurement used by Ross et al. Triangles denote results given by Saric & Nayfeh.
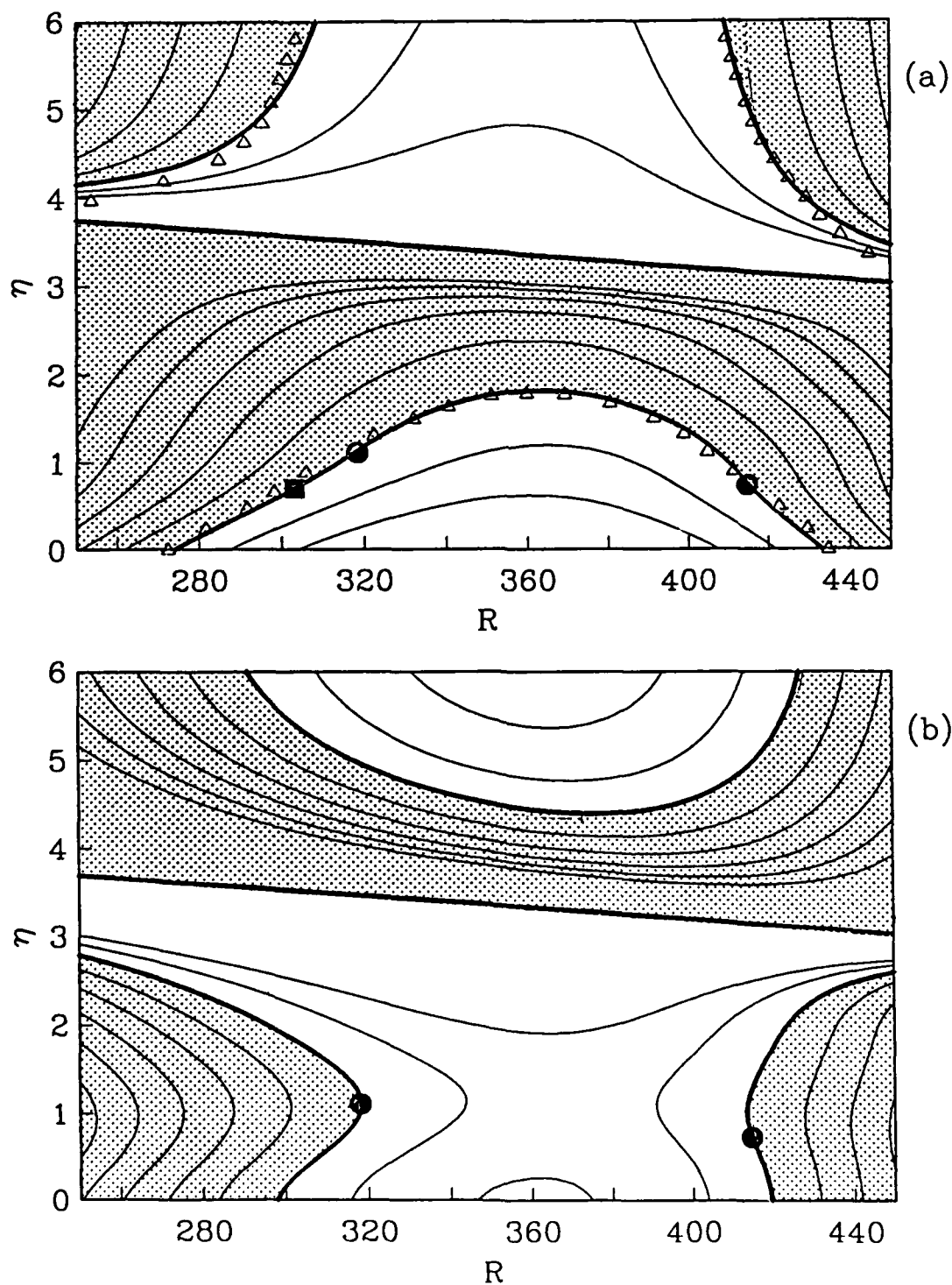
Figure 8. Neutral stability curves of growth rate based on u component of velocity obtained by performing the measurement at different distances from the wall. Differentiation along lines of constant η. Comparison with the experimental data of Ross et al. (squares) and Schubauer & Skramstad (circles).
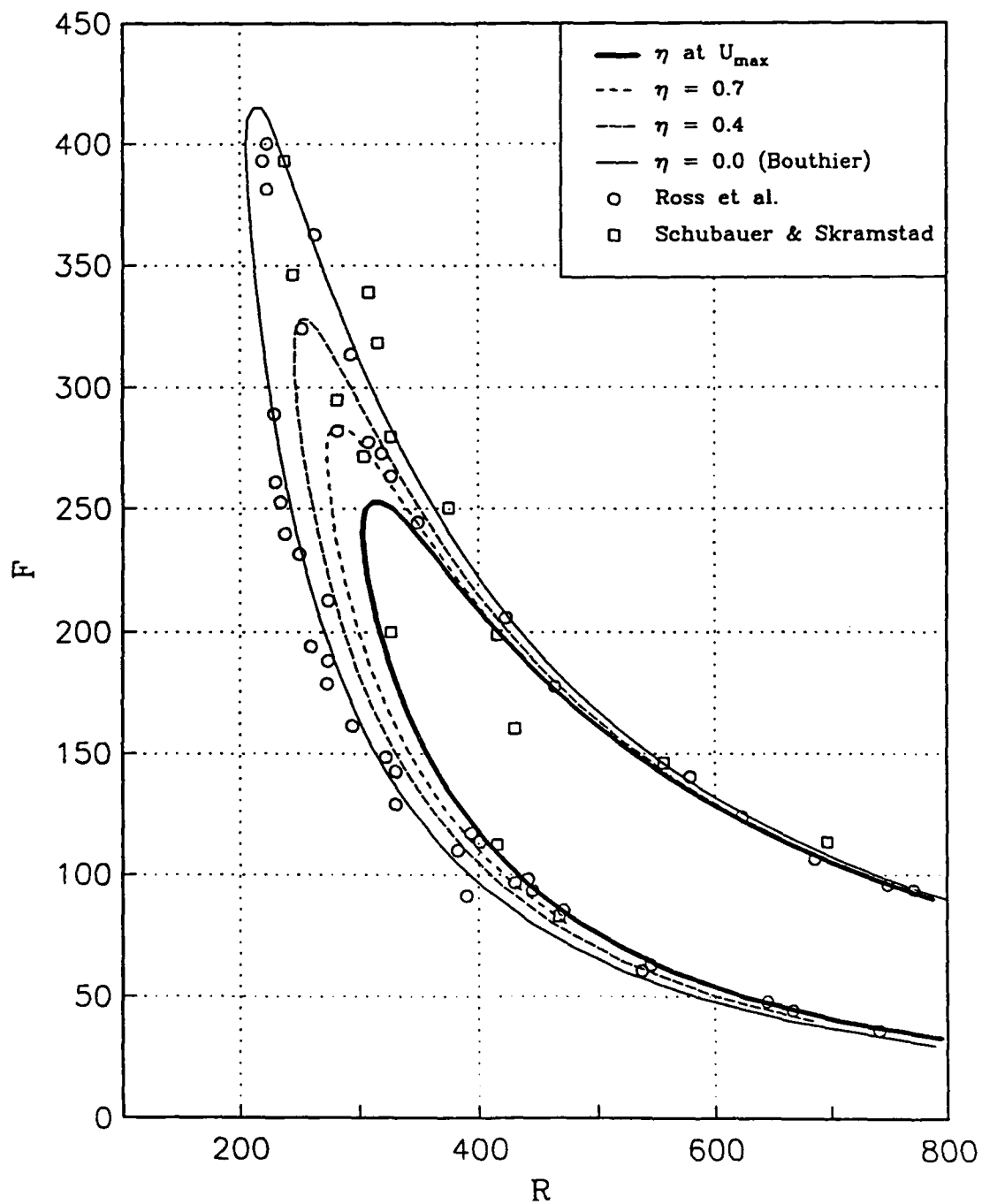
Figure 9. Transient response of TS wave to perturbed I.C. (a) Initial perturbed u velocity profile. Dots represent unperturbed values. (b) Growth rate given with step size S1 (solid line) and S2 (dashed line) at $F = 50$ (b), and $F = 270$ (c).
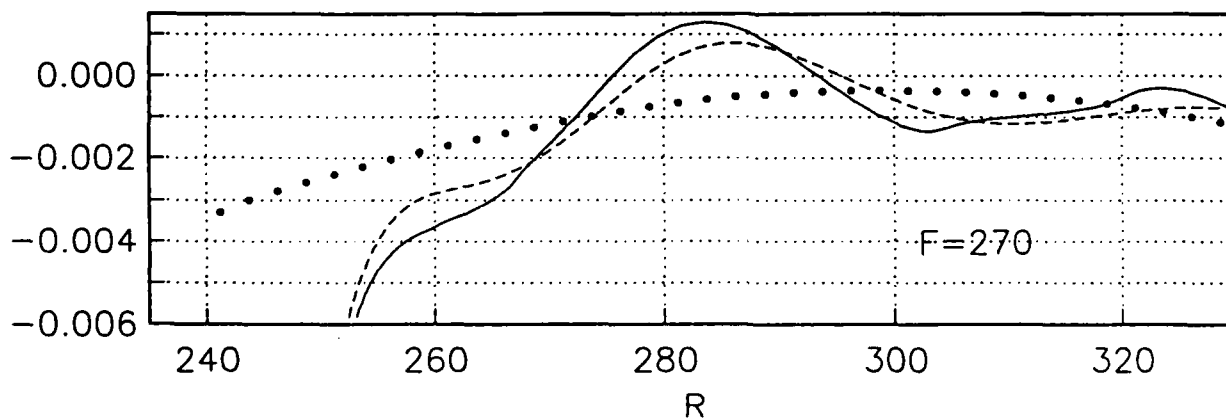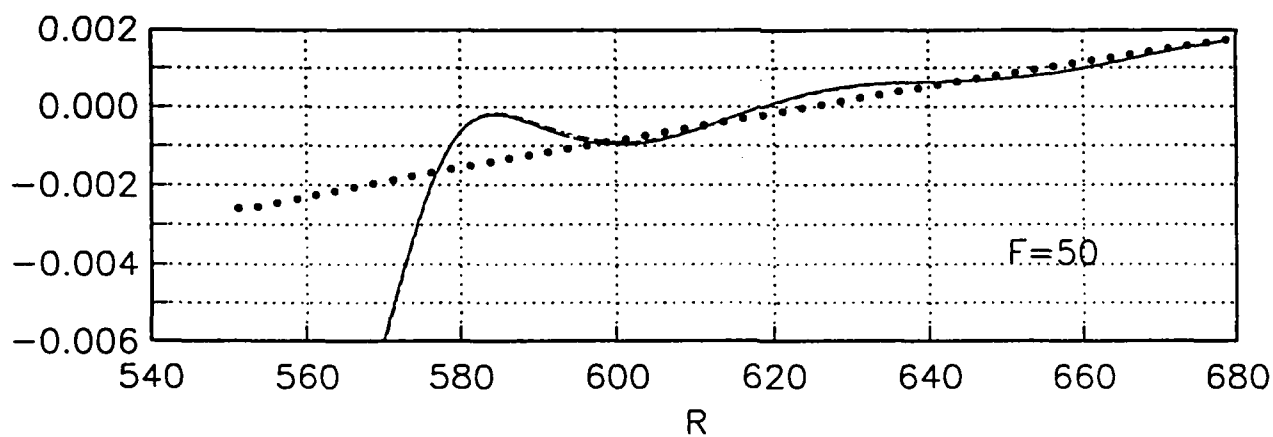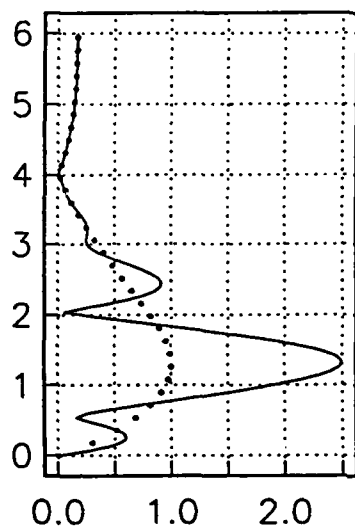
Figure 10. Particular of the neutral stability curve based on the growth rate of u_{max}. Solid line given by linearized PSE, circles given by Landau expansion in amplitude at an amplitude of 1.4% rms based on u_{max} of the TS wave. Dashed line from Orr-Sommerfeld equation. Triangles given by linear PSE with perturbed initial conditions, as in fig 9.
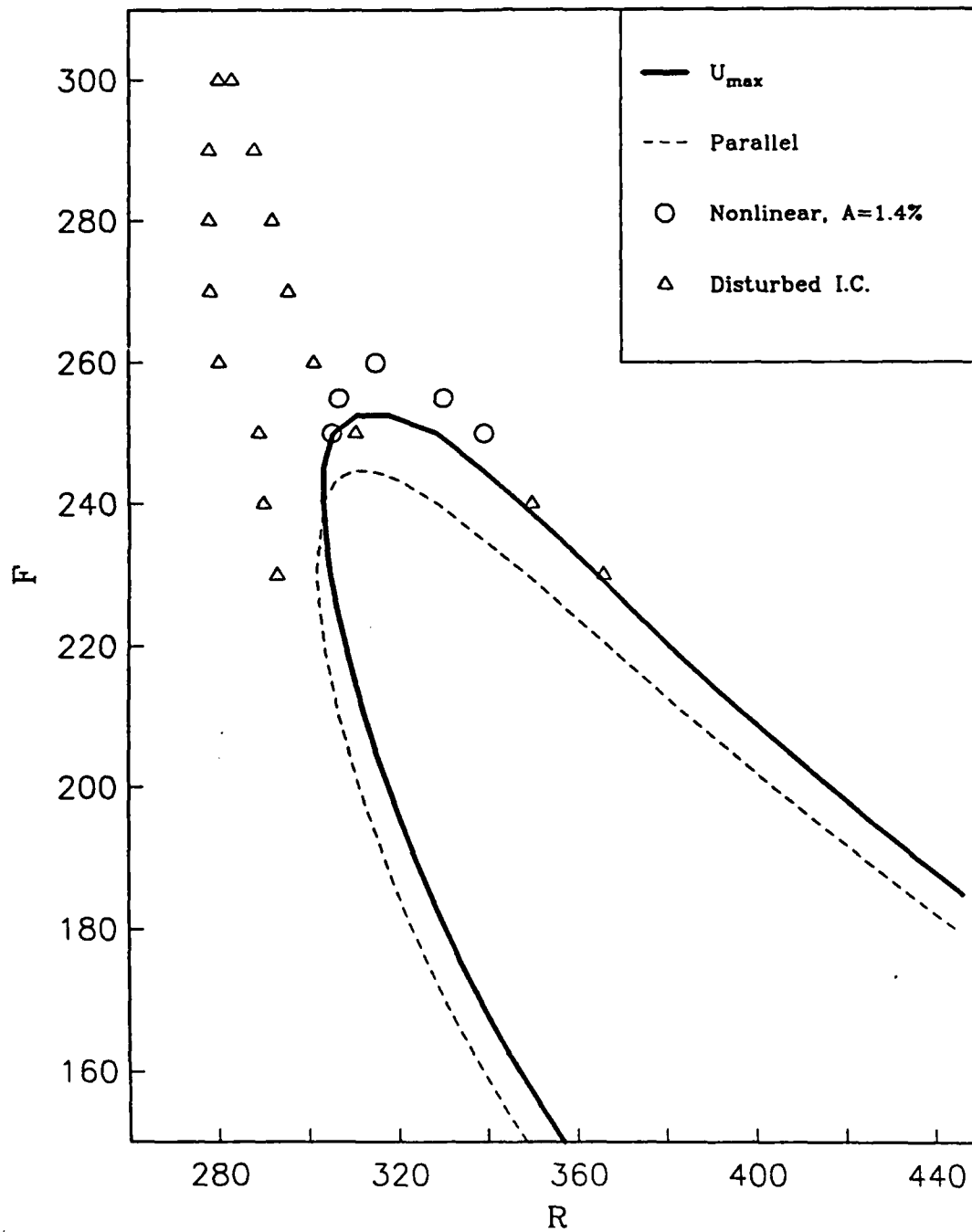
Figure 11. Comparison of amplitude growth, based on u_{max} from nonlinear calculation employing 6 Fourier modes (solid) and full Navier-Stokes solution (symbols) Top heavy line denotes amplitude of TS wave with initial amplitude of 0.25%. Bottom heavy line is amplitude of 2α harmonic. Light line denote corresponding results for initial TS wave amplitude of 0.30%. $F = 86$. Dashed line from linear PSE calculation

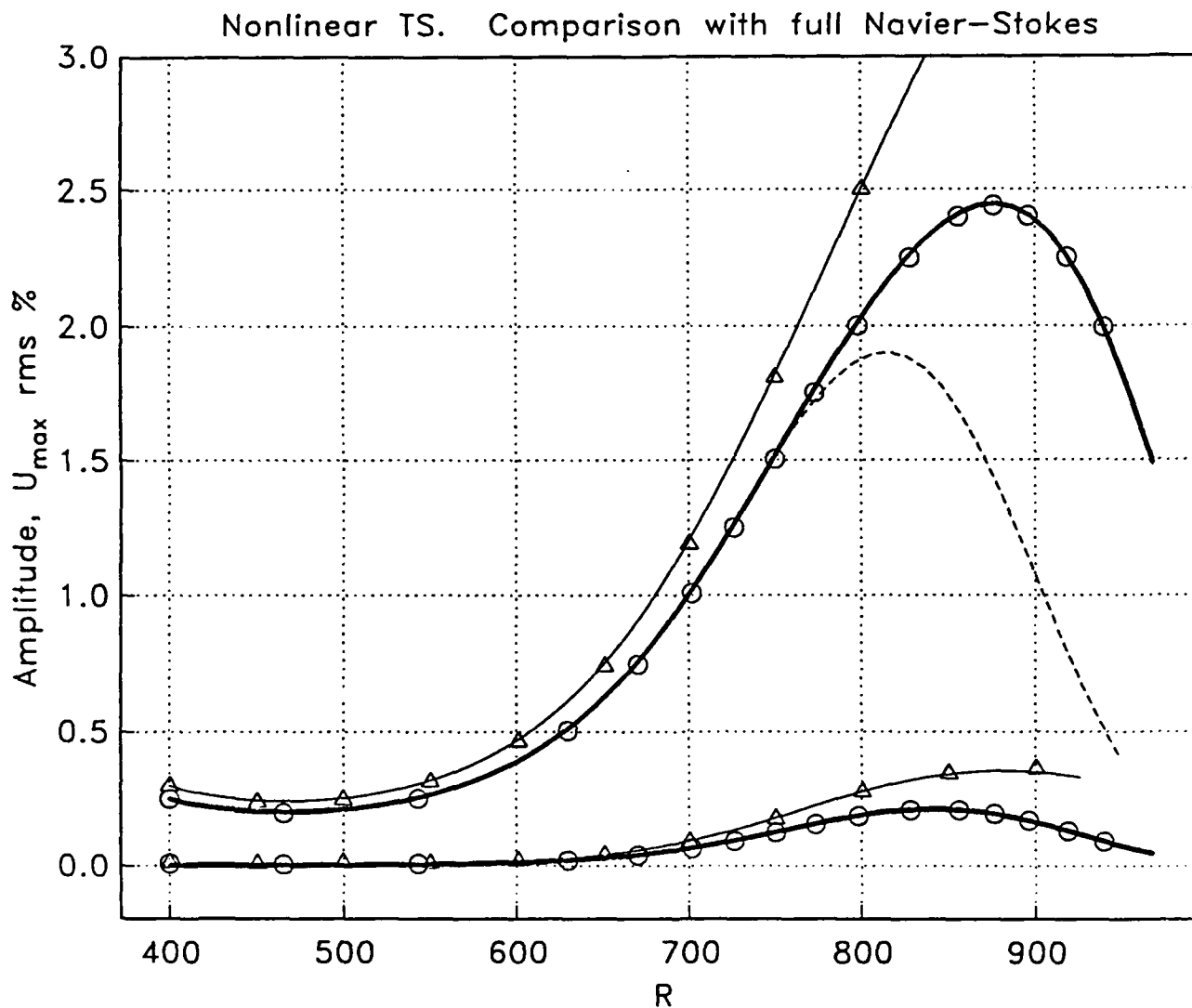Nonlinear TS. Comparison with full Navier–Stokes

Figure 12 Profiles for the $0F$, $F = 86$ (TS wave), $2F$, and $3F$ Fourier components at $R = 800$, from the calculation using 0.25% initial amplitude, shown in figure 13. Symbols denote values given by full Navier-Stokes solution.
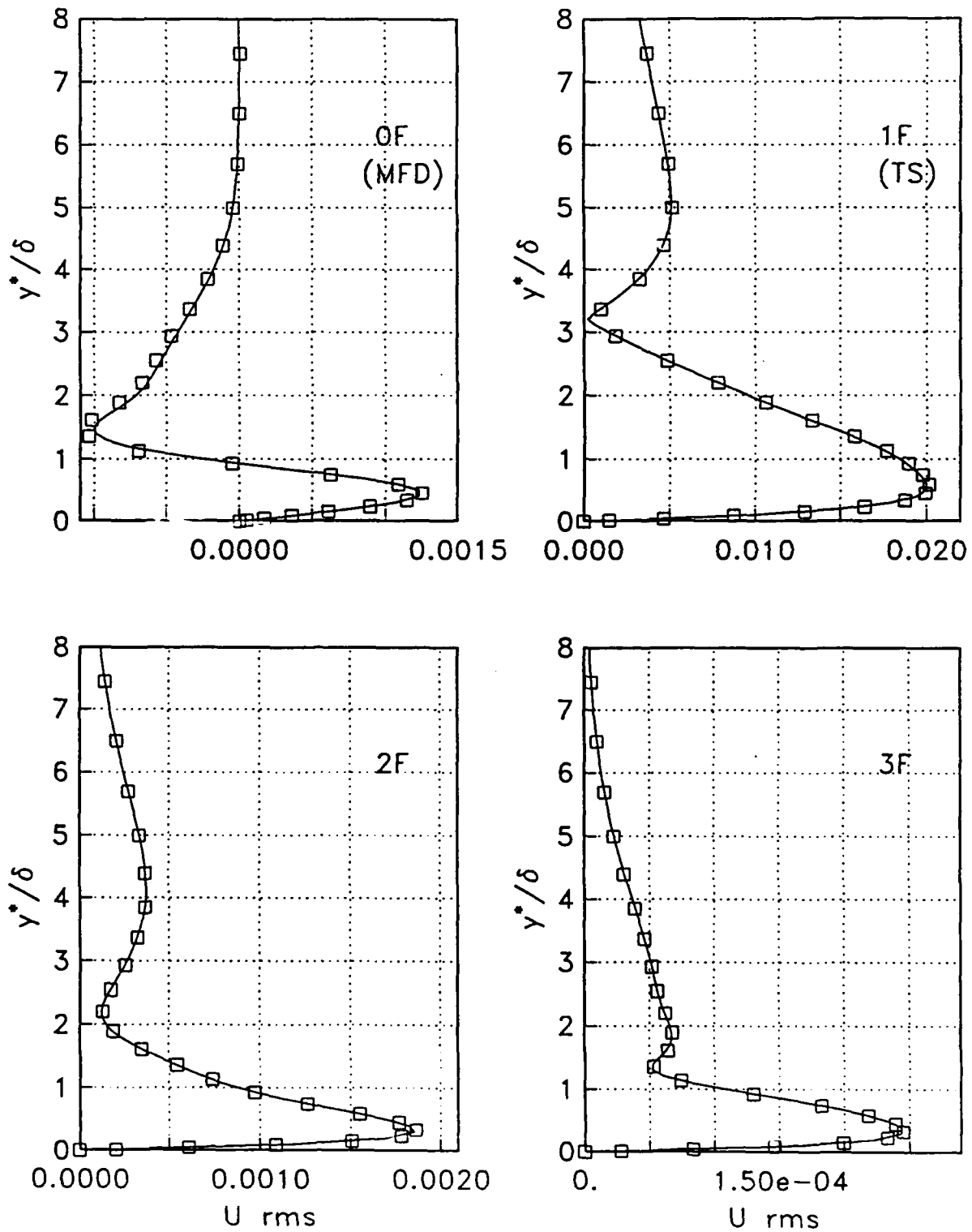
- 40 -

Figure 13. Amplitude vs. growth rate at $F = 86$ at selected Reynolds numbers. Lines from Landau expansion with terms up to order A^5, A^7, and A^9, circles from marching solutions with initial amplitudes 0.02%, 0.2%, 0.25%, and 0.3%, at $R = 400$.

F=86. Landau $A^{5,7,9}$ and Marching (5 harmonics)